Incorporation of functionalized halloysite nanotubes (HNTs) into thin film nanocomposite (TFN) nanofiltration membranes for heavy metal removal from wastewaters

Amirsajad Atashgar

Thesis submitted to the University of Ottawa
in partial Fulfillment of the requirements for the
Master of Applied Science

Department of Chemical and Biological Engineering
Faculty of Engineering
University of Ottawa

To My Parents

Abstract

Global water scarcity is an enormous and yet imminent challenge for our time. Industries such as machinery manufacturing, metallurgy, etc., generate increasing volumes of wastewaters containing heavy metals. These wastewaters are often directly or indirectly discharged into the environment. Heavy metals are not biodegradable; therefore, they can accumulate in the body, creating severe health problems such as cancer, nausea, or even death. It is necessary to remove heavy metals from wastewaters before their discharge to the environment. There are different methods to do that. Among them, membrane separation technology is a promising method for wastewater treatment. In particular, nanofiltration (NF) membranes, due to their rejection mechanism (size exclusion and charge repulsion), are most suitable to remove s heavy metals from wastewater. A new class of high-performance semipermeable membranes for reverse osmosis (RO), nanofiltration (NF), and forward osmosis (FO) applications are thin-film nanocomposite (TFN) membranes.

In this work, novel NF TFN membranes were fabricated by incorporating the functionalized halloysite nanotubes (HNTs) with the first generation of poly(amidoamine) (PAMAM) dendrimers (G1). Also, the same membranes were used for the removal of heavy metals in FO separation. The combination of FO and NF processes represents the novel two-stage FO-NF hybrid process for heavy metal removal.

The membranes showed high rejections of Na_2SO_4 (97%-98%) and $MgCl_2$ (82%-90%) in NF tests. Although lower than Na_2SO_4, the rejections of $MgCl_2$ are much greater than those reported in the literature. The remarkable rejections of $MgCl_2$ are attributed to positively charged HNTs-G1 nanoparticles incorporated in the selective polyamide (PA) layer of TFN membranes. The FO experiments using $MgCl_2$ as a draw solution revealed excellent rejections of Cu^{2+} and Pb^{2+} by TFN membranes ranging from 95% to 98%. The presence of heavy metal in the feed solution enhanced the FO performance of the membranes. In particular, the reverse flux of draw solute ($MgCl_2$) decreased by at least 2.5 times compared to the experiments with pure water as a feed. Simultaneously, the water flux also increased. The improved FO performance in the presence of heavy metals is attributed to their adsorption by the membranes.

Résumé

La pénurie mondiale d'eau est un défi énorme et pourtant imminent pour notre époque. Des industries telles que la fabrication de machines, la métallurgie, etc., génèrent des volumes croissants d'eaux usées contenant des métaux lourds. Ces eaux usées sont souvent rejetées directement ou indirectement dans l'environnement. Les métaux lourds ne sont pas biodégradables; par conséquent, ils peuvent s'accumuler dans le corps, créant de graves problèmes de santé tels que le cancer, des nausées ou même la mort. Il est nécessaire d'éliminer les métaux lourds des eaux usées avant leur rejet dans l'environnement. Il existe différentes méthodes pour y parvenir. Parmi elles, la technologie de séparation par membrane est une méthode prometteuse pour le traitement des eaux usées. En particulier, les membranes de nanofiltration (NF), en raison de leur mécanisme de rejet (exclusion de taille et répulsion de charge), sont les plus appropriées pour éliminer les contaminants tels que les métaux lourds ou les sels des eaux usées. Une nouvelle classe de membranes semi-perméables hautes performances pour les applications d'osmose inverse (RO), de nanofiltration (NF) et d'osmose directe (FO) sont les membranes nanocomposites à couches minces (TFN).

Dans ce travail, de nouvelles membranes NF TFN ont été fabriquées en incorporant des nanotubes d'halloysite (HNT) fonctionnalisés avec la première génération de dendrimères de poly (amidoamine) (PAMAM) (G1) pour améliorer les performances des membranes NF pour l'adoucissement de l'eau. En outre, les mêmes membranes ont été utilisées pour l'élimination des métaux lourds lors de la séparation par osmose directe (FO).. La combinaison des procédés FO et NF représente le nouveau procédé hybride FO-NF en deux étapes pour l'élimination des métaux lourds.

Les membranes ont montré des rejets élevés de Na_2SO_4 (97% -98%) et $MgCl_2$ (82% -90%) dans les tests NF. Bien que inférieurs à Na_2SO_4, les rejets de $MgCl_2$ sont beaucoup plus importants que ceux rapportés dans la littérature. Les rejets remarquables de $MgCl_2$ sont attribués à des nanoparticules HNTs-G1 chargées positivement incorporées dans la couche de polyamide sélectif (PA) des membranes TFN. Les expériences FO utilisant $MgCl_2$ comme solution de tirage ont révélé d'excellents rejets de Cu^{2+} et Pb^{2+} par les membranes TFN allant de 95% à 98%. La présence de métaux lourds dans la solution d'alimentation a amélioré les performances FO des membranes.

En particulier, le flux inverse du soluté de tirage ($MgCl_2$) a diminué d'au moins 2,5 fois par rapport aux expériences avec de l'eau pure comme alimentation. Simultanément, le flux d'eau a également augmenté. L'amélioration des performances des FO en présence de métaux lourds est attribuée à leur adsorption par les membranes.

Statement of Contributions

I hereby declare that this work has not been submitted or accepted for any other degree. Dr. Boguslaw Kruczek and Dr. Daryoush Emadzadeh supervised the research performed in this thesis.

Chapter 2: Incorporation of functionalized halloysite nanotubes (HNTs) into thin film nanocomposite (TFN) nanofiltration membranes for water softening

Fabrication of all membranes, testing them with an NF system, and physicochemical characterizations of membranes were carried out by Amirsajad Atashgar. The NF setup was initially built by Mr. David Carter and modified by Farhad Asempour. The idea of incorporating modified HNTs in NF TFN membranes for NF applications was first proposed by Dr. D. Emadzadeh, and developed by Amirsajad Atashgar. Surface functionalized HNT were synthesized and provided by Dr. Somaye Akbari. SEM and TEM images of the HNT and zeta potentials of the HNT were provided by Dr. S. Akbari. FTIR characterizations were conducted with the help of Dr. S. Akbari. The article was written by Amirsajad Atashgar. Finally, Dr. D. Emadzadeh, Dr. S. Akbrai, and Dr. B. Kruczek critically reviewed and revised the article.

Chapter 3: Incorporation of functionalized halloysite nanotubes (HNTs) into thin-film nanocomposite (TFN) nanofiltration membranes for water softening

Fabrication of TFC and modified TFN membranes, testing them with an FO system, and physicochemical characterizations of membranes were carried out by Amirsajad Atashgar. The FO setup was built by Mr. Du Bai. The idea of incorporating modified HNTs in NF TFN membranes for FO applications was first proposed by Dr. D. Emadzadeh, and developed by Amirsajad Atashgar. The article was written by Amirsajad Atashgar. Finally, Dr. D. Emadzadeh, and Dr. B. Kruczek critically reviewed and revised the article.

Acknowledgments

At first, I would like to express my deepest gratitude to my supervisor Dr. Boguslaw Kruczek for his support, funding, guidance, and patience through these two wonderful years of my study at the University of Ottawa. Whenever I needed help or have a question, the door to Prof. Kruczek's office was open to me. From Prof. Kruczek, I learned not only the knowledge of the membranes technology but also the dedicating spirit for work. I could not have imagined having a better mentor and supervisor for my M.A.Sc study.

I would also like to extend my most profound appreciation to Dr. Daryoush Emadzadeh for his mentorship and his valuable support and guidance. He guided me and introduced me to the amazing world of membrane technology, and taught me membrane fabrication and characterization. I like to thank Dr. Somaye Akbrai for introducing me to the dendritic polymers, the surface modification of nanoparticles, and helping me with membrane characterization. I would also like to thank Farhad Asempour. He introduced me to the amazing world of thin-film nanocomposite membranes and taught me through membrane fabrication and characterization. I want to thank my friends and colleagues in Kruczek's research group: Du Bai, Sofia Reyes Lombardo, and Fatemeh Abedi.

Finally, and most importantly, I owe hugely to my dear parents, Hossein Atashgar and Zahra Rasoulian, and my lovely sister Nazanin Atashgar. Without their endless love, support, and encouragement, I would not have come this far.

Table of content

Abstract ..... **III**

Résumé ..... **IV**

Statement of Contributions ..... **VI**

Acknowledgments ..... **VII**

Table of content ..... **VIII**

List of figures ..... **XI**

List of Tables ..... **XIII**

Nomenclature ..... **XIV**

Chapter 1. Introduction **1**

1.1. Overview of the thesis 1

1.2. Principles of the NF and FO processes 3

1.2.1. Rate equations 3

1.2.2. Separation mechanism of NF membranes 6

1.3. Research objectives 7

1.4. Thesis Structure 8

1.5. References 9

Chapter 2. Incorporation of functionalized halloysite nanotubes (HNTs) into thin-film nanocomposite (TFN) nanofiltration membranes for water softening **12**

Abstract 13

2.1. Introduction 14

2.2. Experimental 16

2.2.1. Material 16

2.2.2. Functionalization of HNTs 16

2.2.3. Synthesis of the TFC and TFN membranes 17

2.2.4. Nanofiltration performance 18

2.2.5. Membranes and nanoparticles characterization 20

2.3. Result and discussion 20

.2.3.1 **Characterization of the nanoparticles** 20

2.3.2. Characterization of the Membranes 23

2.3.3. Membranes separation performance 28

2.4. Conclusions 32

2.5. Acknowledgment 33

2.6. References 34

Chapter 3. Evaluation of heavy metal removal in forward osmosis process using functionalized HNTs-based TFN NF membranes **41**

Abstract **42**

3.1. Introduction 43

3.2. Experimental 46

3.2.1. Materials 46

3.2.2. Functionalization of HNTs 46

3.2.3. TFC and TFN membranes fabrication 47

3.2.4. Forward osmosis tests and data analysis 49

3.2.5. Rejection of heavy metals in NF process 53

3.2.6. Characterization of membrane and nanoparticles 54

3.3. Results and discussion 55

3.3.1. Nanoparticle characterization 55

3.3.2. Membrane Characterization 55

3.3.3. FO performance 56

3.3.4. Rejection of heavy metals in FO and NF processes 60

3.4. Conclusions and Recommendations 63

3.5. Acknowledgment 64

3.6. Appendix 65

3.7. References 66

Chapter 4. General Discussion, Conclusion, and Recommendations 68

Appendix 71

List of figures

Figure 1-1. The concept of the hybrid process (FO-NF) 3

Figure 2-1. Schematic structure of the HNTs-G1[20] 17

Figure 2-2. Schematic representation of fabrication of TFC membrane 18

Figure 2-3. Cross-flow NF membrane testing system, PI, FI and, TI stands for pressure, flow and temperature indicator, respectively[27] 19

Figure 2-4. TEM image of acid-washed HNTs[20] 21

Figure 2-5. SEM images of a) HNTs b) HNTs-G1[20] 21

Figure 2-6. ATR-FTIR spectra of HNTs and HNTs-G1. The arrow shows the presence of a new peak according to amid group 23

Figure 2-7. Top surface water contact angle of TFC and TFN membranes. 24

Figure 2-8. SEM images of the top surface of (A) TFC (B) TFN(0.025%) (C) TFN(0.05%) (D) TFN(0.1%) membranes. 25

Figure 2-9. FTIR spectra of the PS35 (support), TFC, and TFN membranes. 26

Figure 2-10. Surface zeta potential of TFC and TFN membranes. 27

Figure 2-11. Pure water flux performance of the TFC and TFN membranes at 20 bar and 25°C. 29

Figure 2-12. Rejection performance of different salts for the TFC and TFN with 3000 ppm feed aqueous solution 10 bar and 25 °C. 30

Figure 3-1. A hybrid two-stage FO-NF process for heavy metal removal from wastewater. 44

Figure 3-2. Schematic representation of the structure of HNTs-G1. 47

Figure 3-3. Schematic representation of fabrication of TFN membrane 48

Figure 3-4. Schematic diagram of FO experimental system.[13] 50

Figure 3-5. Cross-flow NF membrane testing system, PI, FI and, TI stands for pressure, flow and temperature indicator, respectively [14] 54

Figure 3-6. Progress of dynamic FO experiments using a TFC membrane in the AL-FS orientation; the mass of the feed and draw solutions as a function of time. Draw solution: 1 M $MgCl_2$. **A)** DI water as a feed; **B)** 200 ppm $CuSO_4.5H_2O$ solution as a feed. 57

Figure 3-7. Progress of dynamic FO experiments using a TFC membrane in the AL-FS orientation; the mass of $MgCl_2$ as a function of time. Draw solution: 1 M $MgCl_2$. **Blueline:** DI water as a feed; **Orangeline:** 200 ppm $CuSO_4.5H_2O$ solution as a feed. 57

Figure 3-8. The average water flux of TFC and TFN membranes using the different feed. **Orange:** DI water; **green:** 200 ppm $CuSO_4.5H_2O$ solution; **purple:** 200 ppm $Pb(NO_3)_2$ solution. Draw solution in all experiments: 1 mol. L^{-1} $MgCl_2$. 59

Figure 3-9. The average reverse flux of $MgCl_2$ TFC and TFN membranes using the different feeds. **Orange:** DI water; **green:** 200 ppm $CuSO_4.5H_2O$ solution; **purple:** 200 ppm $Pb(NO_3)_2$ solution. Draw solution in all experiments: 1 mol. L^{-1} $MgCl_2$. 60

Figure 3-10. The average rejections of Cu^{2+} and Pb^{2+} by TFC and TFN membranes in FO tests.62

List of Tables

Table 1-1. Types of the membranes based on their filtration class[14] 3

Table 2-1. Monomer concentration and HNTs-G1 loading for the fabrication of TFC and TFN membranes. 18

Table 2-2.Hydrated radius of different salts[28]..... 19

Table 2-3. TGA and Zeta potential results of modified HNTs 22

Table 2-4. Total peak area under 1618–1720 cm^{-1}(amideI), 1600–1620 cm^{-1}(aromatic amide), and various peaks in the 3120–3706 cm^{-1} range for the PS35 (support), TFC and TFN membranes. 26

Table 2-5. Performance comparison between TFN (HNTs-G1) membrane and other reported TFN membranes 31

Table 3-1. Monomer concentration and HNTs-G1 loading for the fabrication of TFC and TFN membranes. 48

Table 3-2. The calculated concentration of the heavy metals based on their molecular weight. . 51

Table 3-3. Summary rejection and adsorption of heavy metals TFC and TFN membranes in FO experiments. 61

Table A3-4. Summary of FO performance of TFC and TFN membranes in the experiments with pure water and 200 ppm solutions of $Pb(NO_3)_2$ and $CuSO_4.5H_2O$ as a feed. In all experiments, the draw was 1 $mol.L^{-1}$ $MgCl_2$ solution. 65

Nomenclature

Na_2SO_4	Sodium sulphate	**$Pb(NO_3)_2$**	Lead (II) nitrate
NF	Nanofiltration	**PIP**	Piperazine
ATR-FTIR	Attenuated total reflectance-Fourier transform infrared spectroscopy	**RO**	Reverse osmosis
		XPS	X-ray photoelectron spectroscopy
ppm	Parts per million	**APTES**	Aminopropyltriethoxysilane
TEM	Transmission electron microscopy	**C_f**	Salt concentrations in feed (g/l)
PSF	Poly (Sulfone)	**C_p**	Salt concentrations in permeate (g/l)
$CuSO_4$	Copper (II) sulphate	**HNT-COOH**	Carboxylic acid functionalized HNT
DI	Deionized distilled water	**HNT-G1**	First generation PAMAM functionalized HNT
DS	Draw solution	**Jw**	Permeate flux
FS	Feed solution	**Vp**	Collected permeate volume (L)
TMC	Trimesoyl chloride	**WHO**	World Health Organization
XRD	X-Ray diffraction	**t**	Time (h)
HNT	Halloysite nanotube	**R**	Salt rejection (%)
ICPMS	inductively coupled plasma-mass spectrometry	**NP**	Nanoparticles
$MgCl_2$	Magnesium chloride	**PA**	Polyamide
TFC	Thin film composite	**PAMAM**	poly(amidoamine) dendrimer
TFN	Thin film nanocomposite	**NaCl**	Sodium chloride
A	Water permeability coefficients ($L.m^{-2}.h^{-1}.bar^{-1}$)	**B**	Solute permeability coefficients ($L.m^{-2}.h^{-1}$)
SEM	Scanning electron microscopy	**COCl**	acyl chloride
COOH	Carboxylic acids		

Chapter 1. Introduction

1.1. Overview of the thesis

Water is the foundation of life. Water shortage is one of the most difficult challenges of our time. According to the world health organization (WHO), nearly 1 billion people have difficulty accessing safe water, resulting in various health problems worldwide. It has been estimated that 2 million people die each year due to the lack of safe and drinkable water[1,2]. Industries such as machinery manufacturing, metallurgy, etc., have developed much faster in the last decade. Heavy metals, i.e., elements with an atomic mass between 63.5 and 200.6 and a specific gravity greater than 5, are among the major contaminants in wastewater, which are therefore directly or indirectly discharged into the environment [3]. Many different approaches have been proposed to remove heavy metals from wastewater, of which membrane technology is one of the most promising approaches [1–10].

Membrane technology is unique because of its simplicity of operation, no need for chemical additives, etc. This technology is used in various water-related applications, such as drinking water treatment, wastewater treatment, and brackish water treatment. The heart of the membrane technology is a membrane, a thin and selective barrier that enables the transport of specific compounds between two media [11]. Although there is intensive research on inorganic membranes, organic polymer membranes dominate in practical applications. There are different materials to fabricate polymer membranes. They include polysulfone (PS), polyethersulfone (PES), cellulose acetate (CA), poly(vinylidene fluoride) (PVDF) [11–13]. Membranes are classified according to their specific application, Microfiltration (MF), Ultrafiltration (UF), Nanofiltration (NF), Reverse Osmosis (RO), and Forward Osmosis (FO)[14]. Table 1-1 shows the general information for different membrane types. The smaller the pore size, the smaller the solute that can be rejected by the membrane. Also, the smaller pores, the higher the operating pressure is required. Since the establishment of NF membranes in the 1970s, NF has been used in wastewater treatment such as water softening and other separation applications such as dairy products, pharmaceutical purifications, etc. [15,16].

This thesis focuses on the NF and FO processes and develops novel thin-film nanocomposite (TFN) membranes with enhanced separation performance for heavy metal removal. The selective layer properties determine the properties of high and medium-pressure membranes (e.g. NF membranes). The porous support layer is necessary for the NF membrane to provide mechanical support, and it does not affect membrane productivity. However, unlike the NF process, the support layer dramatically influences the productivity of the FO process. The porous sublayer is responsible for internal concentration polarization (ICP), unique to FO processes. The ICP reduces the osmotic pressure, thereby reducing the driving force for water transport. Therefore, unlike NF membranes, which only require the optimization of the selective layer, the FO membranes require the optimization of both the selective and porous sublayer. This thesis focuses only on optimizing the selective layer on the same support sublayer (a commercial UF membrane) for both processes. Our approach's primary assumption is that if a selective layer can reject a given solute (e.g. heavy metals) in the NF process, it will also reject it in the FO process. Moreover, if a designated draw solute is rejected in the NF process, its transport – reverse solute flux – will be minimized in the FO process. The latter is necessary to generate the osmotic pressure gradient for the water transport in the FO process.

Conventionally, heavy metals are removed from wastewater by using a single-stage NF or RO process. The main disadvantage of using these high-pressure processes is the high fouling tendency. To lower the fouling tendency, which is detrimental to membrane performance, we propose using a hybrid two-stage FO-NF process, shown in Figure 1-1. In the first stage (FO), the heavy metals are rejected absence of hydraulic pressure. At the same time, water permeates from the wastewater feed to a draw solution. Subsequently, the diluted draw solution is regenerated in the NF process (second stage) while producing the final product - pure water. The key to this concept is the membrane. The membrane should have an excellent rejection of the draw solute and heavy metals. At the same time, the membrane should be highly permeable to water. As stated above, we focus only on developing the selective layer, which will be assessed in the NF process and subsequently verified in the FO process. The optimization of the porous sublayer, which plays a critical role in FO processes' productivity, is not considered in this thesis.

Table 1-1. Types of the membranes based on their filtration class[14]

Membrane type	Pore size (nm)	Typical target removed	Operating pressure (bar)
MF	50-500	Yeast and bacteria	1-2
UF	2-50	Viruses and colloidal solids	2-10
NF	≤ 2	Viruses, divalent and multivalent ions	8-30
RO	0.3-0.6	Almost all impurities	10-80
FO	0.3-0.6	Almost all impurities	-

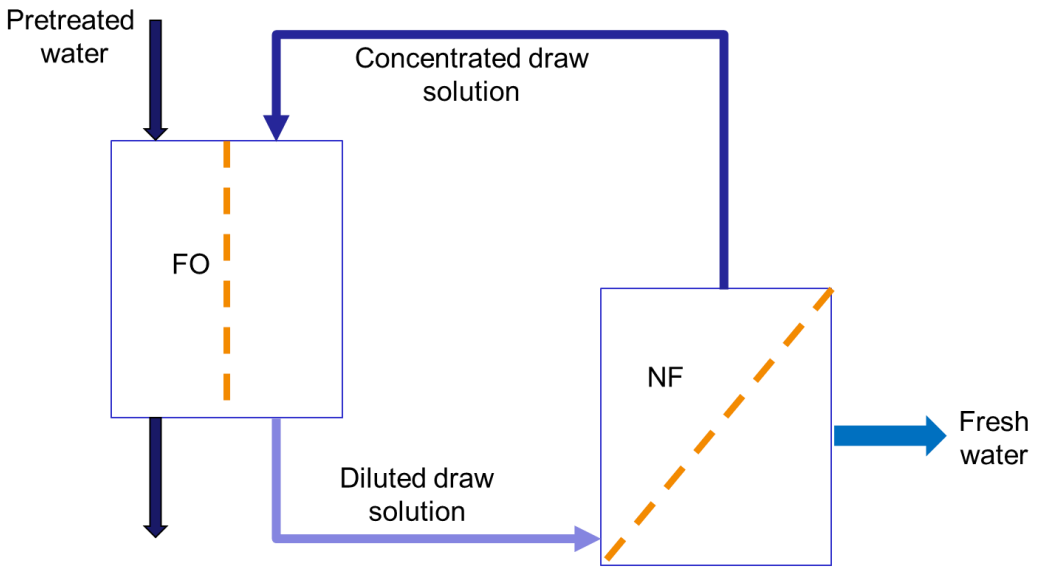

Figure 1-1. The concept of the hybrid process (FO-NF)

1.2. Principles of the NF and FO processes

1.2.1. Rate equations

It is generally assumed that transport in NF and FO processes follows a solution-diffusion (SD) model. According to the SD model, the rate equation for the water flux (J_w) in NF membranes is given by:

$$J_w = A(\Delta p - \Delta \pi) \quad (1)$$

where A is the water permeability coefficient, Δp and $\Delta \pi$ are the hydraulic and osmotic pressure gradients across the membrane, respectively. The osmotic pressure for a dilute solution of an electrolyte is given by (van't Hoff equation):

$$\pi = icRT \tag{2}$$

where: i is the number of ionic species each molecule will dissociate, and c is the molar concertation of solute. For concentrated electrolyte solutions, Eq. (2) is modified by multiplying it by a dimensionless osmotic pressure coefficient (ϕ). There is specialized software, for example, OLI Stream analyzer (OLI Systems, USA), which allows evaluation of the osmotic pressure of a wide variety of solutions.

The rate equation for the salt flux (J_s), on the other hand, is given by:

$$J_S = B(c_m - c_p) \tag{3}$$

where: B is the solute permeability coefficients, respectively, and c_m and c_p are the solute concentrations at the membrane surface at the feed and permeate sides, respectively. Typically, c_m is greater than c_f, the latter being the solute concentration in the bulk feed solution. The situation in which $c_m > c_f$ indicates an external concentration polarization (ECP), which is undesirable. First, the ECP increases the driving for the solute transport across the membrane and, secondly in increases the osmotic pressure gradient across the membrane, which leads to a decrease in the water flux. Typically, NF membranes are rated based on their water flux (productivity) and their apparent (observed) rejection (SR), which is defined as:

$$SR = \left(1 - \frac{c_p}{c_f}\right) \times 100\% \tag{4}$$

Consequently, the ECP leads to a simultaneous decrease in both membrane productivity and selectivity. Since $c_f >> c_p$, it is assumed that the concentration of solute in bulk permeate solution and that on the membrane surface are similar. In other words, there is no concentration polarization at the permeate side of the membrane.

The basis for transport and separation in FO processes is the difference between the osmotic pressure across a semi-permeable membrane resulting from the difference in solute concentration in draw solution (c_d) and feed solution (c_f). In FO processes, the solvent (water) is transported from the feed solution into the draw solution across the membrane, which implies $c_d >$

c_f. In the absence of hydraulic pressure gradient, assuming the applicability of the SD model, the rate of the water flux is given by:

$$J_W = A(\pi_{d,m} - \pi_{f,m}) \quad (5)$$

where A is the water permeability, the same as in Eq. (1), and the subscript m signifies that the osmotic pressures of the draw and feed solutions are based on the solute concentrations, $c_{d,m}$ and $c_{f,m}$, on the respective membrane surfaces. The osmotic pressures $\pi_{d,m}$ and $\pi_{f,m}$ could be significantly different from the respective bulk osmotic pressures $\pi_{d,b}$ and $\pi_{f,b}$.

Unlike NF processes, the solute flux (J_s) in FO processes moves in the opposite direction to the water flux. Assuming applicability of the SD model, the solute flux, which is also referred to as the reverse solute flux, is given by an equation similar to Eq. (3):

$$J_S = B(c_{d,m} - c_{f,m}) \quad (6)$$

The water and solute fluxes' opposite directions give rise to an inherent internal concentration polarization (ICP). Unlike the ECP, which can be significantly reduced by creating turbulence near the membrane surface to facilitate the transport of the rejected solute from the membrane surface back to the bulk solution, the ICP is not reduced by external turbulence because it occurs within the pores of the support layer of the membrane. On the other hand, since there is no applied hydraulic pressure, the ECP in FO processes is less severe than in pressure-driven NF processes.

Forward osmosis systems can be operated in two different membrane orientations, the Active Layer facing Draw Solution (AL-DS) and the Active Layer facing Feed Solution (AL-FS). The AL-DS orientation is also referred to as the Pressure Retarded Osmosis (PRO) mode, and the AL-FS orientation is the Forward Osmosis (FO) mode. In the PRO mode, $\pi_{f,m} > \pi_{f,b}$ and the resulting concentration polarization is referred to as a concentrative ICP. On the other hand, in the FO mode, $\pi_{d,m} < \pi_{d,b}$ and the resulting concentration polarization is referred to as dilutive ICP. The extent of the ICP, in either case, depends on the solute resistivity (R') in porous support [17–19]:

$$R' = \frac{L_s}{D_{eff}} \quad (7)$$

where L_s is the thickness of the porous support and D_{eff} is the diffusivity of solute in the porous sublayer. If L_s is very small and/or D_{eff} is very large, $\pi_{f,m} \rightarrow \pi_{f,b}$ in the PRO mode and $\pi_{d,m} \rightarrow \pi_{d,b}$ in the FO mode, which maximizes the water flux.

1.2.2. Separation mechanism of NF membranes

In the SD model, the membrane is treated as a "black box." In other words, the SD model does not provide information on the mechanism of separation in the membrane.

NF membranes have a pore size between UF and RO membranes. Consequently, the NF membranes have unique properties between the UF and RO membranes. The NF membranes require lower operating pressures and are associated with higher water flux than RO membranes. However, they are not suitable for the rejection of monovalent solutes such as NaCl. On the other hand, they can effectively reject multivalent ions, including heavy metals [20]. Although NF membranes are not as productive as the UF membranes, their ability to reject heavy metals often present in wastewaters makes them attractive for wastewater treatment[21].

The separation in NF membranes is based on the sieving (steric) and Donnan potential mechanisms. NF membranes' surface typically carries some electrical charge, and Donnan potential is created between charged ions in the NF membrane and the co-ions in the effluent. Repulsion will happen between the charged surface of the membrane and the ions of the same charge. Simultaneously, to maintain electroneutrality, the counter-ions of these co-ions will also be rejected [18]. Consequently, the rejection of neutral species in NF is solely based on size exclusion. On the other hand, ions' rejection is also possible by the electrostatic interactions [5,22]. The latter is typically more dominant than the former. This is why NF membranes are not suitable for rejecting monovalent ions, while most multivalent ions are retained [23]. For this reason, NF membranes are very attractive for the removal of heavy metals from water [19,24].

The two main challenges of NF membranes or membranes in water-related applications are the trade-off between selectivity and permeability and membrane fouling. Membranes with higher rejection usually possess lower water permeability and vice-versa. The membrane fouling accumulates the retained substance on the surface and/or inside the membrane pores. The membrane fouling leads to a significant decrease in membrane productivity, which can be irreversible. Consequently, fouling can decrease the lifetime of the membrane significantly. The

membrane fouling is accelerated in pressure-driven processes. Therefore, although not as severe as in RO processes, it is also a key obstacle in NF processes [11]. A pre-treatment of the feed stream can reduce fouling. However, a pre-treatment adds to the operating cost of the membrane process.

One common approach to address a trade-off and membrane fouling problems is adding nanoparticles into the membrane's selective layer. The resulting membranes, referred to as thin-film nanocomposite (TFN) membranes, have gained a lot of attention. The incorporation of nanoparticles affects the structure and physicochemical properties of the resulting TFN membranes compared to the base thin-film composite (TFC) membranes responsible for productivity and selectivity. Nanoparticles also affect the membranes' surface properties, directly improving their antifouling capabilities [25].

1.3. Research objectives

This research aims to develop a suitable membrane for a hybrid FO-NF process to remove heavy metals from wastewater. The membrane is to reject not only heavy metals but also low molecular weight divalent salts. The latter is to be a draw solution in the FO process. The same membrane will be utilized in both NF and FO processes, but the former will be used in the membrane development part to optimize membrane properties. This approach assumes that if solutes are rejected in the NF process, they will also be rejected in the FO process. This assumption will be verified experimentally.

A commonly used interfacial polymerization (IP) technique, in which the selective membrane layer is synthesized by polymerizing a water-soluble monomer with a hexane-soluble monomer, will be utilized to synthesize TFC and TFN membranes using commercial UF membranes as porous support. The properties of TFN membranes can be adjusted by selecting appropriate nanoparticles, which are incorporated in the membranes' selective layer. In this study, we selected halloysite nanotubes (HNTs) modified by the first generation of poly(amidoamine) (PAMAM) dendrimers as the nanoparticles. These nanoparticles were used previously in our lab to prepare TFN membranes for RO application [25]. The difference between TFN RO and TFN NF membranes is the water-soluble monomer in the IP synthesis. Our study used piperazine (PIP), a standard monomer, to prepare TFC NF membranes. Therefore, the specific objectives of this thesis are:

1) Synthesis of TFC membranes by in-situ interfacial polymerization of piperazine (PIP) with 1,3,5-benzenetricarbonyl trichloride (TMC).
2) Synthesis of TFN membranes by dispersing halloysite nanotubes (HNTs) modified by the first generation of poly(amidoamine) (PAMAM) dendrimers in TMC solution before interfacial polymerization with PIP.
3) A complete physicochemical characterization of the synthesized TFC and TFN membranes and their NF performance with low-molecular-weight divalent salts and heavy metals. Selection of the best-performing membrane for the FO tests.
4) Determination of the FO performance of the selected NF membranes with pure water and an aqueous heavy metals solution as a feed.
5) Comparison of NF and FO membrane performance and assessing suitability of using the same membrane in the FO-NF hybrid process to remove heavy metals.

1.4. Thesis Structure

This thesis consists of four chapters. The first chapter (current) presents a general introduction to the project, outlines the relevant theoretical background, and explains this research's general and specific objectives. The 2nd and 3rd chapters are written in the article format. Chapter 2 focuses on the fabrication and characterization of TFN membranes for NF application and finding the suitable draw solute for the FO process. Chapter 2 covers the specific objectives 1-3. Chapter 3 focuses on removing heavy metals from a feed using the FO process, which utilizes the membrane developed in Chapter 2. Chapter 3 covers the 4th specific objective. The results from Chapters 2 and 3 allow assessing the suitability of removing the heavy metals in a hybrid FO-NF process. Chapter 4 provides general conclusions of this research and outlines recommendations for future work. The appendix also presents a recently published article in the Journal of Membrane Science, which used the same type of nanoparticles as those in this study for a low-pressure RO application. The candidate is one of the co-authors of this publication to which he contributed by testing the membranes as part of his MEng Project.

1.5. References

[1] World Health Organization, UNICEF, Progreso en agua potable, saneamiento e higiene, 2017. https://doi.org/10.1371/journal.pone.0164800.

[2] C.J. Vörösmarty, P.B. McIntyre, M.O. Gessner, D. Dudgeon, A. Prusevich, P. Green, S. Glidden, S.E. Bunn, C.A. Sullivan, C.R. Liermann, P.M. Davies, Global threats to human water security and river biodiversity, Nature. 467 (2010) 555–561. https://doi.org/10.1038/nature09440.

[3] N. Abdullah, N. Yusof, W.J. Lau, J. Jaafar, A.F. Ismail, Recent trends of heavy metal removal from water/wastewater by membrane technologies, J. Ind. Eng. Chem. 76 (2019) 17–38. https://doi.org/10.1016/j.jiec.2019.03.029.

[4] Overview of Membrane Science and Technology, Membr. Technol. Appl. (2012) 1–14. https://doi.org/https://doi.org/10.1002/9781118359686.ch1.

[5] T.A. Kurniawan, G.Y.S. Chan, W.H. Lo, S. Babel, Physico-chemical treatment techniques for wastewater laden with heavy metals, Chem. Eng. J. 118 (2006) 83–98. https://doi.org/10.1016/j.cej.2006.01.015.

[6] S.E. Bailey, T.J. Olin, R. Mark Bricka, D. Dean Adrian, and 2 USAE Waterways Experiment Station, 3909 Halls Ferry Rd, 33 (1999).

[7] C. Blöcher, J. Dorda, V. Mavrov, H. Chmiel, N.K. Lazaridis, K.A. Matis, Hybrid flotation - Membrane filtration process for the removal of heavy metal ions from wastewater, Water Res. 37 (2003) 4018–4026. https://doi.org/10.1016/S0043-1354(03)00314-2.

[8] P. Dutournie, P. Fievet, L. Limousy, P. Bourseau, Concentration polarization phenomenon during the nanofiltration of multi-ionic solutions : Influence of the filtrated solution and operating conditions, 7 (2013). https://doi.org/10.1016/j.watres.2013.01.044.

[9] T.S. Chung, L. Luo, C.F. Wan, Y. Cui, G. Amy, What is next for forward osmosis (FO) and pressure retarded osmosis (PRO), Sep. Purif. Technol. 156 (2015) 856–860. https://doi.org/10.1016/j.seppur.2015.10.063.

[10] A. A.Mohammed, A.F. Al-Alawy, T.K. Hussein, Removal of Lead , Copper and Nickel Ions From Wastewater By Forward Osmosis Process, (2015) 893–908.

[11] L.Y. Ng, A.W. Mohammad, C.P. Leo, N. Hilal, Polymeric membranes incorporated with metal/metal oxide nanoparticles: A comprehensive review, Desalination. 308 (2013) 15–33. https://doi.org/10.1016/j.desal.2010.11.033.

[12] Z. Yang, H. Peng, W. Wang, T. Liu, Crystallization behavior of poly(ε-caprolactone)/layered double hydroxide nanocomposites, J. Appl. Polym. Sci. 116 (2010) 2658–2667. https://doi.org/10.1002/app.

[13] A.K. Ghosh, E.M.V. Hoek, Impacts of support membrane structure and chemistry on polyamide-polysulfone interfacial composite membranes, J. Memb. Sci. 336 (2009) 140–148. https://doi.org/10.1016/j.memsci.2009.03.024.

[14] M.M. Pendergast, E.M.V. Hoek, A review of water treatment membrane nanotechnologies, Energy Environ. Sci. 4 (2011) 1946–1971. https://doi.org/10.1039/c0ee00541j.

[15] S. Tul Muntha, A. Kausar, M. Siddiq, Advances in Polymeric Nanofiltration Membrane: A Review, Polym. - Plast. Technol. Eng. 56 (2017) 841–856. https://doi.org/10.1080/03602559.2016.1233562.

[16] S. Darvishmanesh, T. Robberecht, P. Luis, J. Degrève, B. Van Der Bruggen, Performance of nanofiltration membranes for solvent purification in the oil industry, JAOCS, J. Am. Oil Chem. Soc. 88 (2011) 1255–1261. https://doi.org/10.1007/s11746-011-1779-y.

[17] F. Fu, Q. Wang, Removal of heavy metal ions from wastewaters: A review, J. Environ. Manage. 92 (2011) 407–418. https://doi.org/10.1016/j.jenvman.2010.11.011.

[18] Y.C. Chiang, Y.Z. Hsub, R.C. Ruaan, C.J. Chuang, K.L. Tung, Nanofiltration membranes synthesized from hyperbranched polyethyleneimine, J. Memb. Sci. 326 (2009) 19–26. https://doi.org/10.1016/j.memsci.2008.09.021.

[19] A. Bhinder, Effect of Internal and External Concentration Polarizations on the Performance of Forward Osmosis Process, in: S. Shabani (Ed.), IntechOpen, Rijeka, 2018: p. Ch. 4. https://doi.org/10.5772/intechopen.71343.

[20] H.A. Qdais, H. Moussa, Removal of heavy metals from wastewater by membrane processes: A comparative study, Desalination. 164 (2004) 105–110. https://doi.org/10.1016/S0011-9164(04)00169-9.

[21] R. Levenstein, D. Hasson, R. Semiat, Utilization of the Donnan effect for improving electrolyte separation with nanofiltration membranes, J. Memb. Sci. 116 (1996) 77–92. https://doi.org/10.1016/0376-7388(96)00029-4.

[22] A.W. Mohammad, Y.H. Teow, W.L. Ang, Y.T. Chung, D.L. Oatley-Radcliffe, N. Hilal, Nanofiltration membranes review: Recent advances and future prospects, Desalination. 356 (2015) 226–254. https://doi.org/10.1016/j.desal.2014.10.043.

[23] Y. Babaee, S.M. Mousavi, S. Danesh, A. Baratian, Influence of transmembrane pressure and feed concentration on the retention of arsenic, chromium and cadmium from water by nanofiltration, J. Environ. Sci. & Eng. 52 (2010) 1–6. http://europepmc.org/abstract/MED/21114097.

[24] Y. Zhou, S. Yu, C. Gao, X. Feng, Surface modification of thin film composite polyamide membranes by electrostatic self deposition of polycations for improved fouling resistance, Sep. Purif. Technol. 66 (2009) 287–294. https://doi.org/10.1016/j.seppur.2008.12.021.

[25] F. Asempour, S. Akbari, D. Bai, D. Emadzadeh, T. Matsuura, B. Kruczek, Improvement of stability and performance of functionalized halloysite nano tubes-based thin film nanocomposite membranes, J. Memb. Sci. 563 (2018) 470–480. https://doi.org/10.1016/j.memsci.2018.05.070.

Chapter 2. Incorporation of functionalized halloysite nanotubes (HNTs) into thin-film nanocomposite (TFN) nanofiltration membranes for water softening

[a]Amirsajad Atashgar, [a]Daryoush Emadzadeh, [b]Somaye Akbari, [a]Boguslaw Kruczek

[a] Department of Chemical and Biological Engineering, University of Ottawa, 161 Louis Pasteur St, ON, Canada, K1N 6N5

[b] Textile Engineering Department, Amirkabir University of Technology, 424 Hafez Ave, Tehran, Iran

Abstract

Incorporating nanoparticles (NPs) into the selective layer of thin-film composite (TFC) membranes is a common approach to improve the performance of the resulting thin-film nanocomposite (TFN) membranes. In this study, we used halloysite nanotubes (HNTs) modified by the first generation of poly(amidoamine) (PAMAM) dendrimers (G1) as the NPs. The TFN and reference TFC membranes were fabricated by in-situ interfacial polymerization of piperazine (PIP) and 1,3,5-benzenetricarbonyl trichloride (TMC). When synthesizing TFN membranes, the NPs were dispersed in the TMC solution before the polymerization with PIP. The modified HNTs were characterized by ATR-FTIR, TEM, SEM, zeta potential, and thermogravimetric TGA analyses. Fabricated membranes were also characterized by SEM, ATR-FTIR, Zeta potential, and contact angle measurements. Membranes' selectivity and pure water flux were evaluated in cross-flow nanofiltration (NF) system using 3000 ppm aqueous solutions of $MgCl_2$, Na_2SO_4 and NaCl, respectively, as feed at 10 bar and ambient temperature. All membranes showed high rejections of Na_2SO_4 (around 97-98%) and low NaCl rejections (less than 40%), with the corresponding water fluxes greater than 100 L m^{-2} hr^{-1}. The rejection of $MgCl_2$ (ranging from 82 to 90%) was less than Na_2SO_4. However, our values are much greater than those reported in the literature for other TFN membranes. The remarkable rejections of $MgCl_2$ are attributed to positively charged HNTs-G1 nanoparticles incorporated in the selective polyamide (PA) layer of TFN membranes. Considering the combination of the water flux and $MgCl_2$ rejection, the TFN membrane with 0.05% of nanoparticle loading appears to have the best NF performance.

2.1. Introduction

Membrane separation is widely used for water desalination, solvent purification, and wastewater treatment in different industries such as petrochemical, food, etc. Pressure-driven processes such as microfiltration (MF), ultrafiltration (UF), nanofiltration (NF), and reverse osmosis (RO) are commonly used technologies [1–6]. The RO membranes, which can reject monovalent salts, are the most selective among membranes for pressure-driven processes. Still, they require high operating pressures and hence are energy-intensive. Although not suitable for the rejection of monovalent salts, NF membranes can effectively separate multivalent salts and heavy metals from aqueous solutions and require lower operating pressures. At the same time, the NF membranes are more permeable than the RO counterparts. Therefore, NF, which is also referred to as low-pressure RO, has become an exciting field of research in membrane separation technology used for water desalination, solvent purification, and wastewater treatment [7–9].

The pore size of the NF membranes is between UF membranes and RO membranes. Generally, the NF membranes have a charged surface; therefore, in addition to the size exclusion, they can reject solutes, such as different inorganic salts and organic molecules, based on an electrostatic repulsion [10,11]. The NF membranes can be categorized into two groups: integrally-skinned asymmetric and thin-film composite (TFC) structures. The first group is mostly formed by a phase inversion process, while a standard method to prepare TFC NF membranes is interfacial polymerization (IP)[12]. The TFC membranes, consisting of an ultra-thin selective polyamide (PA) layer and porous polymeric support, are widely used as NF membranes and dominate the market. To optimize TFC membrane performance, the porous support structure and the selective PA layer can be independently modified [13,14]. The performance of TFC membranes can be improved by incorporating nanoparticles (NPs) such as halloysite nanotubes (HNTs), titanium oxide (TiO_2), titanium nanotubes (TNTs), carbon nanotubes (CNTs) into the support or the selective layer of the membrane. The resulting membranes represent a new category of membranes referred to as thin-film nanocomposite (TFN) membranes [15–20].

HNTs with a molecular formula of $Al_2Si_2O_5(OH)_4 \cdot nH_2O$ have natural multi-layer aluminosilicates. They are an excellent nanofiller candidate for polymeric membranes for water treatment applications due to their low production cost, unique structure, and minimal

environmental risk [21]. HNTs exterior surface is composed of siloxane groups with some hydroxyl groups, which enable their functionalization [20,22]. In some studies, HNTs were used to synthesize TFN forward osmosis (FO) and NF membranes, which improved membranes' antifouling properties and performance [23,24]. For example, Ghanbari et al. used HNTs for water desalination by TFN FO membranes[18]. They reported that by incorporating 0.05% (W/V) of HNTs into the selective layer, the water flux increased 50%. Ormanci-Acar et al. fabricated TFN NF membranes by incorporating different amounts of HNTs in the membrane's selective layer [23]. They evaluated the rejection of their TFN NF membranes with $MgSO_4$ and observed that the resultant TFN membrane showed an increase in water flux without a noticeable salt rejection loss.

Despite great potential, there are also some significant problems with TFN membranes; for example, nanoparticles (NPs) tend to aggregate, resulting in uneven distribution of NPs in the selective layer, leading to defects in the membrane structure[20]. Another critical challenge for TFN membranes is that NPs could have a toxic effect on the environment and living organisms if they leach out of the membrane. One of the methods to overcome all of the above-stated problems is the surface modification of NPs. By functionalizing the NPs, they can be better dispersed in the selective layer resulting in more stable and more selective TFN membranes[18].

Poly(amidoamine) (PAMAM) dendrimers have a hyperbranched hydrophilic structure consisting of many amine groups. PAMAM dendrimers have high hydrophilicity. Grafting them directly or through NPs into a membrane could increase its hydrophilicity and enhance the antifouling properties[25]. Asempour et al. fabricated RO TFN membranes by incorporating modified HNTs with the first generation of poly(amidoamine) (PAMAM) dendrimers into the selective layer. They reported that the resulting membranes were more stable compared to the TFN membranes with unmodified HNTs. Also, they had a higher water flux without sacrificing their rejection in brackish water desalination compared to other TFN and reference TFC membranes[20].

In this study, we hypothesize that the approach used by Asempour et al. to improve the performance and stability of TFN RO membranes is also applicable for TFN NF membranes. Consequently, we synthesized TFC and TFN membranes by in-situ interfacial polymerization (IP) of piperazine (PIP) and 1,3,5-benzenetricarbonyl trichloride (TMC) on commercial ultrafiltration (UF) membrane (PS35). We dispersed different loadings of modified HNTs with PAMAM

dendrimers into TMC solution before the IP when preparing TFN membranes. The modified NPs and NF membranes were thoroughly characterized using different methods, including membrane performance tests.

2.2. Experimental

2.2.1. Material

The Sloecta Inc. company donated polysulfone ultrafiltration membrane (PS35) with a molecular weight cut-off of 20,000 Da. Piperazine (PIP), 1,3,5-benzenetricarbonyl trichloride (TMC), n-hexane, aminopropyltriethoxysilane (APTES), ethanol, diethyl ether, dimethylformamide (DMF), ethylenediamine (EDA), magnesium chloride ($MgCl_2$), sodium sulphate (Na_2SO_4), and sodium chloride (NaCl) were all laboratory grades and purchased from Sigma-Aldrich. Delta-Dolsk, Poland, provided HNTs. Deionized water was used to prepare PIP solution, and distilled water was used to wash the membranes and prepare aqueous feed solutions.

2.2.2. Functionalization of HNTs

The detailed synthesis procedure of dendrimers and functionalization of HNT are fully described elsewhere [26]. Briefly, acid treatment was the first step in functionalization to remove all contaminants. In this step, a mixture of HNTs and aqueous HCl solution (35%) were magnetically stirred for 24 hours and then washed with distilled water. For the HNTs' amine functionalization (HNT-NH_2), the dry acid-treated HNTs were refluxed with APTES solution in toluene (4/15 (v/v)) for 12 hours at 60°C. For synthesizing the first generation of the PAMAM dendrimers on HNTs (HNTs-G1), 32.15 g of the HNTs-NH_2 was reacted (Micheal reaction) with methyl acrylate (15 mL) in ethanol solution at 60^{o}C for 24 hours. The final solution was put into a centrifuge to separate the HNTs. Before drying the HNTs at 60°C, the HNTs were washed and centrifuged with diethyl ether, ethanol, and methanol to remove impurities. In the next step, ethylene diamine was added to the mixture of HNT in ethanol and stirred at 60°C for 24 hours. After the separation of the HNT by centrifugation, the resulting NPs, HNT-G1, were washed with distilled water and dried. Figure 2-1 shows the chemical structure of the functionalized HNTs.

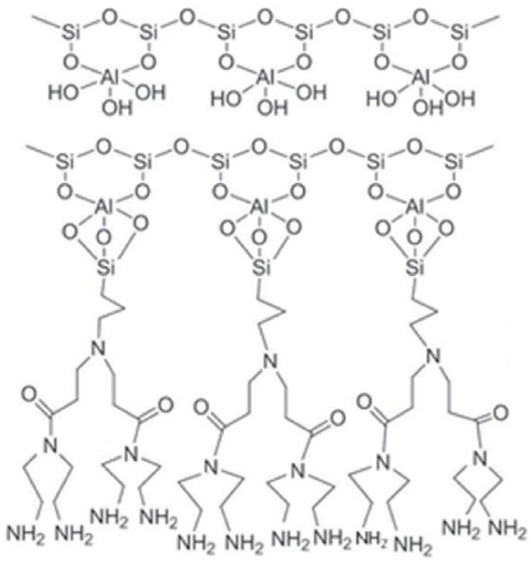

Figure 2-1. Schematic structure of the HNTs-G1[20]

2.2.3. Synthesis of the TFC and TFN membranes

The PS35 UF membrane was used as a substrate for the thin PA layer formation, synthesized by in-situ interfacial polymerization of monomers PIP and TMC. Fabrication of the TFC membrane started with pouring a 2% (W/V) solution of PIP in deionized water on the substrate. After 5 minutes, the excess solution was drained off using a Teflon roller (any visible droplets were removed from the surface). This was followed by pouring 0.05% (W/V) solution of TMC in n-hexane on the support for 1 minute; after that, the excess solution was drained off, and the membrane was rinsed thoroughly with n-hexane. Afterward, the membranes were placed in the oven for 10 minutes at 95 ºC (Figure 2-2). In the end, the TFC membranes were rinsed with distilled water and stored in deionized water. The only difference in synthesizing TFC and HNT-based TFN membrane is in their TMC solution. Different amounts of NPs were dispersed in the TMC solution in n-hexane solution (Table 2-1). To minimize the NPs agglomeration, the resulting suspension was sonicated for 1 hour before the IP. TFN membranes were named according to the concentration of HNTs-G1 in the solution of TMC in n-hexane.

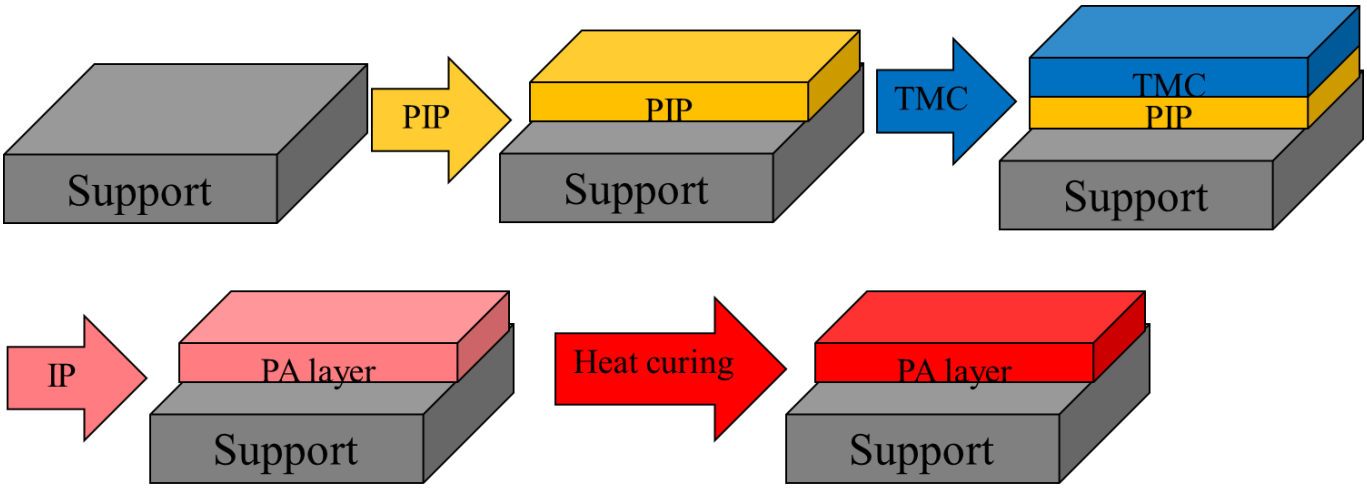

Figure 2-2. Schematic representation of fabrication of TFC membrane

Table 2-1. Monomer concentration and HNTs-G1 loading for the fabrication of TFC and TFN membranes.

Membrane	**PIP in H_2O (w/v) %**	**TMC in n-hexane (w/v) %**	**HNTs-G1 in TMC/n-hexane (w/v) %**
TFC	2	0.05	0
TFN (0.025%)	2	0.05	0.025
TFN (0.05%)	2	0.05	0.05
TFN (0.1%)	2	0.05	0.1

2.2.4. Nanofiltration performance

To evaluate the solute rejection and water flux of the membranes, they were tested in a cross-flow system with three parallel membrane cells. Each cell has an effective area for permeation of 17.54 cm^2. The system, which is shown schematically in Figure 2-3, is described elsewhere [27]. The feed solution's temperature and pressure were 25 ± 2 ºC and 10-20 ± 0.1 bar, respectively. The feed flow rate was controlled at 2.4 ± 0.2 L/min. Permeate flux (J) [$L.m^{-2}.hr^{-1}$] was calculated by Eq.(1), using the volume of collected permeate (V) [L], per area of the membrane (A) [m^2], and time (t) [hr]. The membrane selectivity was evaluated using 3000 ppm single-solute aqueous solutions, including $MgCl_2$, Na_2SO_4, and NaCl. Also, Table 2-2 lists the critical parameters of different salt ions. The pH of the salt solutions was in the range of 6-7. The salt rejection (R) was

calculated by Eq. (2), in which C_p and C_f are the salt concentration of permeate and feed, respectively. The concentration of feed and permeate solution was measured by an Oakton CON 6+ conductivity meter.

$$J = \frac{V}{A \times t} \tag{1}$$

$$R = \frac{C_f - C_P}{C_f} \times 100\% \tag{2}$$

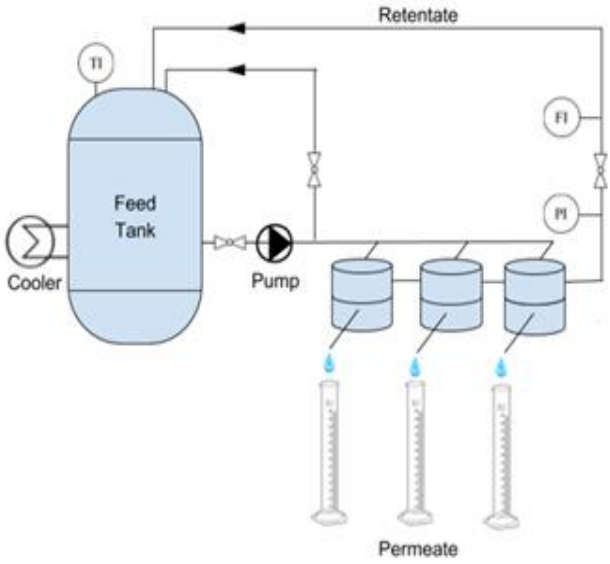

Figure 2-3. Cross-flow NF membrane testing system, PI, FI and, TI stands for pressure, flow and temperature indicator, respectively[27]

Table 2-2.Hydrated radius of different salts[28]

Ion	**Hydrated radius (Å)**
Cl^-	3.32
SO_4^{2-}	3.79
Na^+	3.58
Mg^{2+}	4.28

2.2.5. Membranes and nanoparticles characterization

To determine the percentage of functionalization of HNTs, a Q5000 thermal gravimetric analyzer (TGA) (TA Instruments Ltd, USA) was used. Under the nitrogen atmosphere, the heating rate was 10 °C/min from 30 °C to 800 °C. The top surface of the membrane's morphology was evaluated by using scanning electron microscopy (SEM). All of the samples were coated by gold sputtering. Attenuated Total Reflection-Fourier Transform Infrared (ATR-FTIR) spectra of the membranes (TFC and TFN membranes) and NPs were obtained using a Nicolet 6700 FTIR with a diamond crystal (Thermo Fisher) equipment. OMNIC ™ software was utilized to analyze the spectra. To investigate the TFC and TFN membranes' hydrophilicity, VCA Optima goniometer (AST products, Inc., Billerica, MA) was used. The morphology of the nanoparticle was characterized using a TEM(Philips CM30). Also, the zeta potential of the surface of membranes was conducted by a zeta analyzer (Zetasizer PSS0012-22, Malvern Instruments).

2.3. Result and discussion

2.3.1. Characterization of the nanoparticles

The characterization of NPs is similar to the last work [20]. Figure 2-4 shows the TEM image of the acid-washed HNTs. It is known that HNTs are heterogeneous in size [29]. HNTs have a tubular structure with the inner diameter and outer diameters of 28 nm and 170 nm, respectively. Figure 2-5 presents the SEM images of acid-washed HNTs and HNTs-G1. The arrows in Figure 2-5 show the diameter and the length of the HNTs. It appears that the modification of the HNTs does not change the morphology and the structure of HNTs.

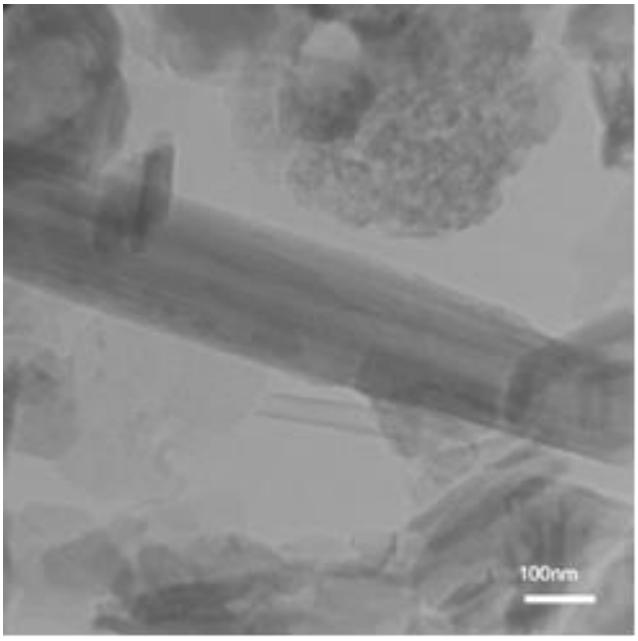

Figure 2-4. TEM image of acid-washed HNTs[20]

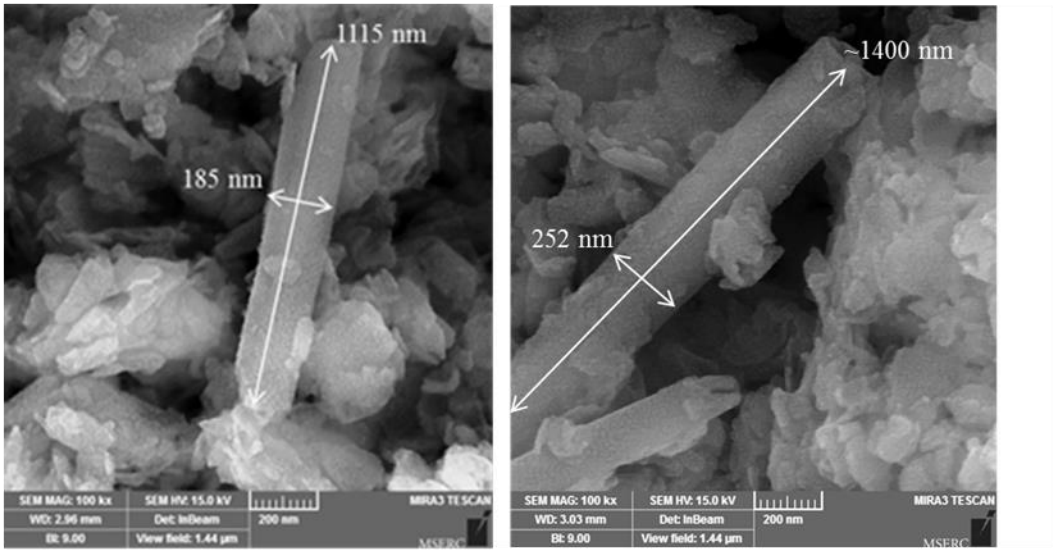

Figure 2-5. SEM images of a) HNTs b) HNTs-G1[20]

The effects of the modification on the surface charge of the NPs were investigated by using zeta potential. The summary of zeta potential analysis is presented in Table 2-3. Due to the existence of the hydroxyl groups, the surface of the unmodified HNTs is negatively charged. After functionalization with the first generation of PAMAM dendrimers, the zeta potential of HNTs-G1

increases to +2.2 mV. The changes in zeta potential after modification of HNTs indicate amino-functionalized groups' presence on the surface of HNTs in the first generation of PAMAM dendrimers.

The summary of TGA analyses is also presented in Table 2-3. The percentage of weight loss at 800ºC of HNTs-G1 (22.94%) is greater than that of HNTs (17.65%). Subtracting the percentage of weight loss of HNTs from the percentage of weight loss of HNTs-G1, which is 5.29 %, is a measure of the organic weight increment resulting from functionalization of HNTs with the first generation of PAMAM dendrimers.

Table 2-3. TGA and Zeta potential results of modified HNTs

NPs	**Weight loss at 800°C (%)**	**Zeta potential (mV)**
HNTs	17.65	- 34.5
HNTs-G1	22.94	+ 2.2

An appropriate way to evaluate the chemical reaction that occurs when modifying the HNTs is the ATR-FTIR analysis. Figure 2-6 shows the ATR-FTIR spectra of HNTs and HNTs-G1. The peaks of HNTs, which appear at 3621 and 3695 cm^{-1}, are the stretching vibration of the inner surface of Al-OH groups[20]. The peaks at 1630 and 910 cm^{-1} are ascribed to the OH bending vibrations associated with the interlayer molecules of HNTs of water and Al-OH, respectively. The peak related to the stretching bond of Si-O appears at 1030 cm^{-1}. In the spectrum of the HNTs-G1, two new peaks appear at 1646 and 1562 cm^{-1}. These peaks result from the N–H bond's stretching vibrations and bending vibrations of the C–N bond, respectively. Therefore, Fig. 6 confirms the expected chemical reaction associated with the functionalization of HNTs with the first generation of PAMAM dendrimers.

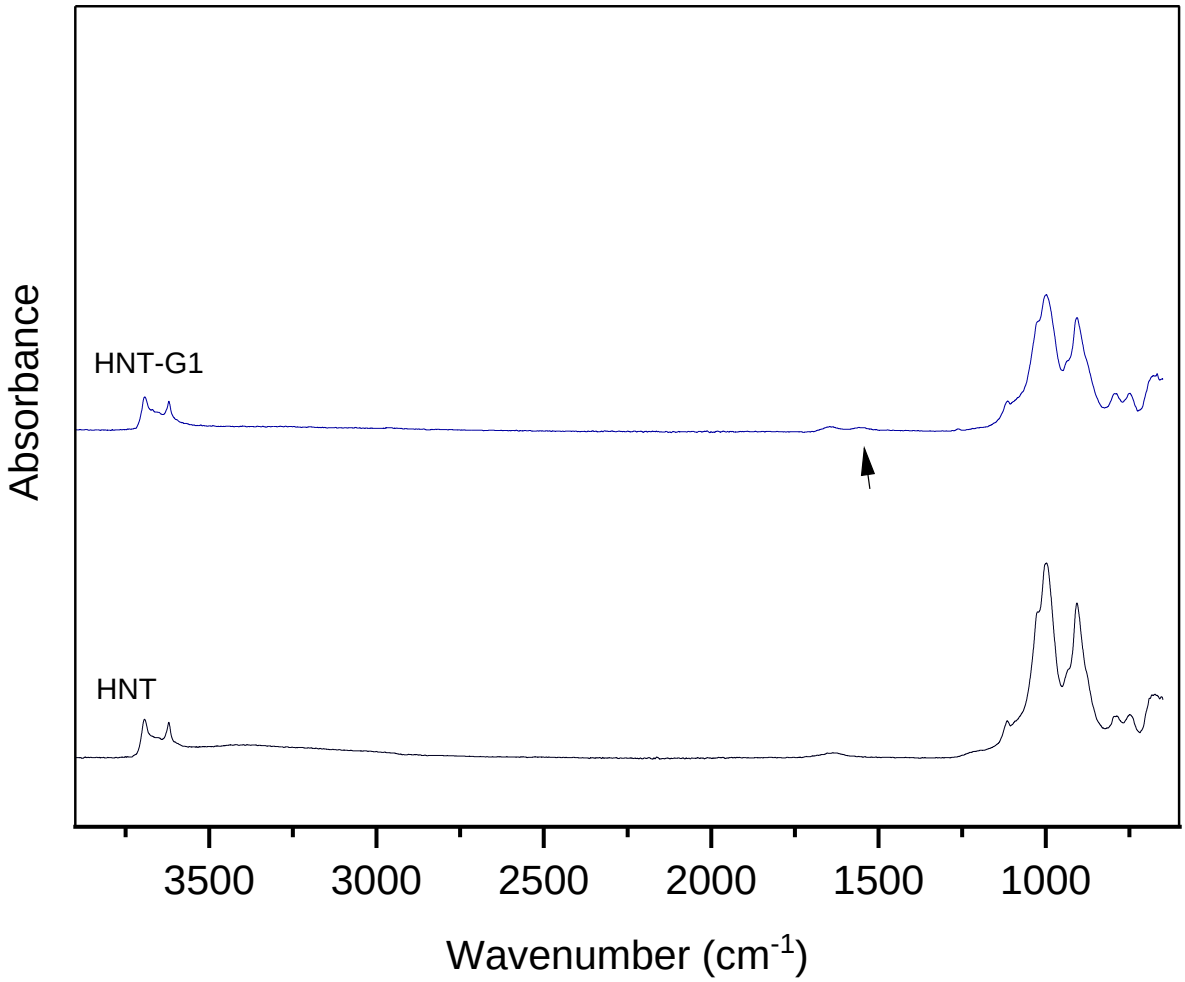

Figure 2-6. ATR-FTIR spectra of HNTs and HNTs-G1. The arrow shows the presence of a new peak according to amid group

From the results presented in this section, it is evident that the functionalization of HNTs with the first generation of PAMAM dendrimers was successful.

2.3.2. Characterization of the Membranes

The results of the contact angle measurement are illustrated in Figure 2-7. The reported values and their corresponding error bars represent the average and standard deviation from at least 10 droplets of DI water, each with a volume of 2 µL for a given type of membrane. Despite some overlapping of the error bars, it is evident that the incorporation of HNTs-G1 has decreased the water contact angle, indicating an increase in surface hydrophilicity of the resulting membranes. Among the TFN membranes, the lowest and highest water contact angles are for the TFN(0.05%)

and the TFN(0.025%), respectively. The increase of contact angle for 0.1 % could be related to the agglomeration of HNTs-G1. Agglomeration of NPs could result in more exposure of silane groups leading to a decrease of hydrophilicity of agglomerated HNTs.

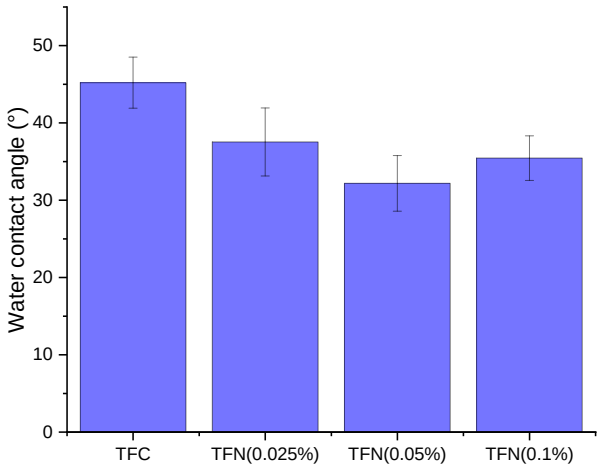

Figure 2-7. Top surface water contact angle of TFC and TFN membranes.

Figure 2-8 shows the SEM images of the top surface TFC and TFN membranes. The surface of the TFC membrane appears to have a uniform nodular structure. Incorporating HNTs-G1 leads to horizontal cylindrical particles' appearance on the top surface, which could be the NPs. There are also some irregular particles on the surface of the TNF-G1 membranes (Figs 2.8 B and D), which could be agglomerates of HNTs penetrating the top surface. Interestingly, these distinctive features are most evident on the TFN-G1 membrane with the lowest percentage of NPs. While TFN membranes' surface remains to have a nodular structure in the background, the size of nodules is smaller than that on the TFC membrane's surface. Moreover, as the percentage of HNTs-G1 increases, the membrane surface becomes less uniform. The nodular structure is typical for membranes that are synthesized by interfacial polymerization [30,31].

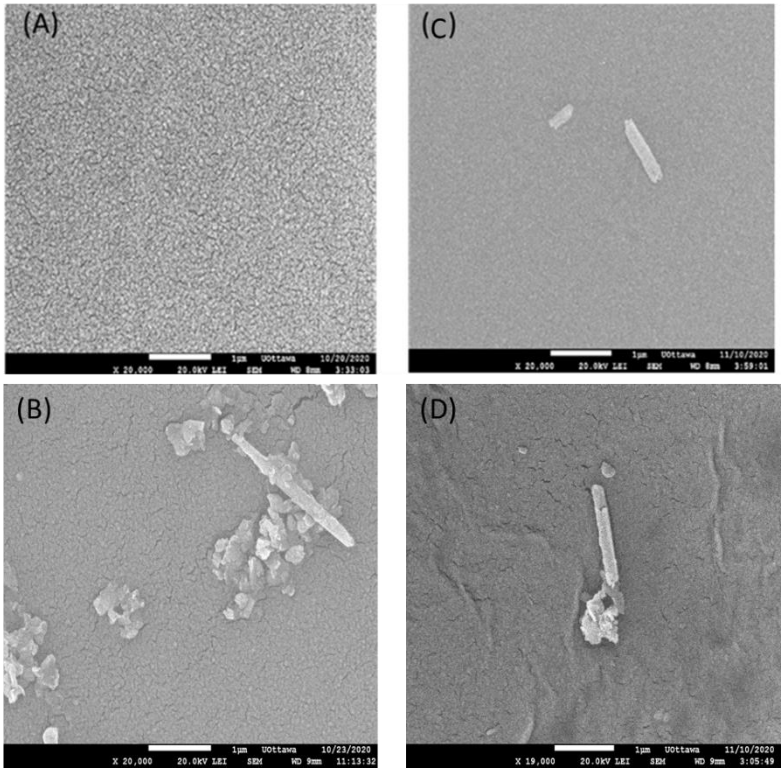

Figure 2-8. SEM images of the top surface of (A) TFC (B) TFN(0.025%) (C) TFN(0.05%) (D) TFN(0.1%) membranes.

Figure 2-9 presents the FTIR spectra for the PS35, TFC, and TFN membranes. To normalize the membranes' FTIR spectra, each spectrum's peak was divided by the intensity of the internal reference, i.e. the peak at 1584 cm^{-1}, which is attributed to the polysulfone. Table 2-4 presents the normalized intensities of all peaks in the ranges corresponding to amide I (1618–1720 cm^{-1}), aromatic amide (1600–1620 cm^{-1}), and various peaks in the 3120–3706 cm^{-1} range corresponding to the PS35 support. Interestingly, the amide peaks are also present in the PS35 support. This is probably due to the manufacturer's modification of the polysulfone to enhance the substrate's water flux [20]. Moreover, the intensity of amide peaks on PS35 support is lower than in TFC and TFN membranes. Therefore, based on the results in Table 2-4, it can be concluded that the PA layer was formed in all TFC and TFN membranes.

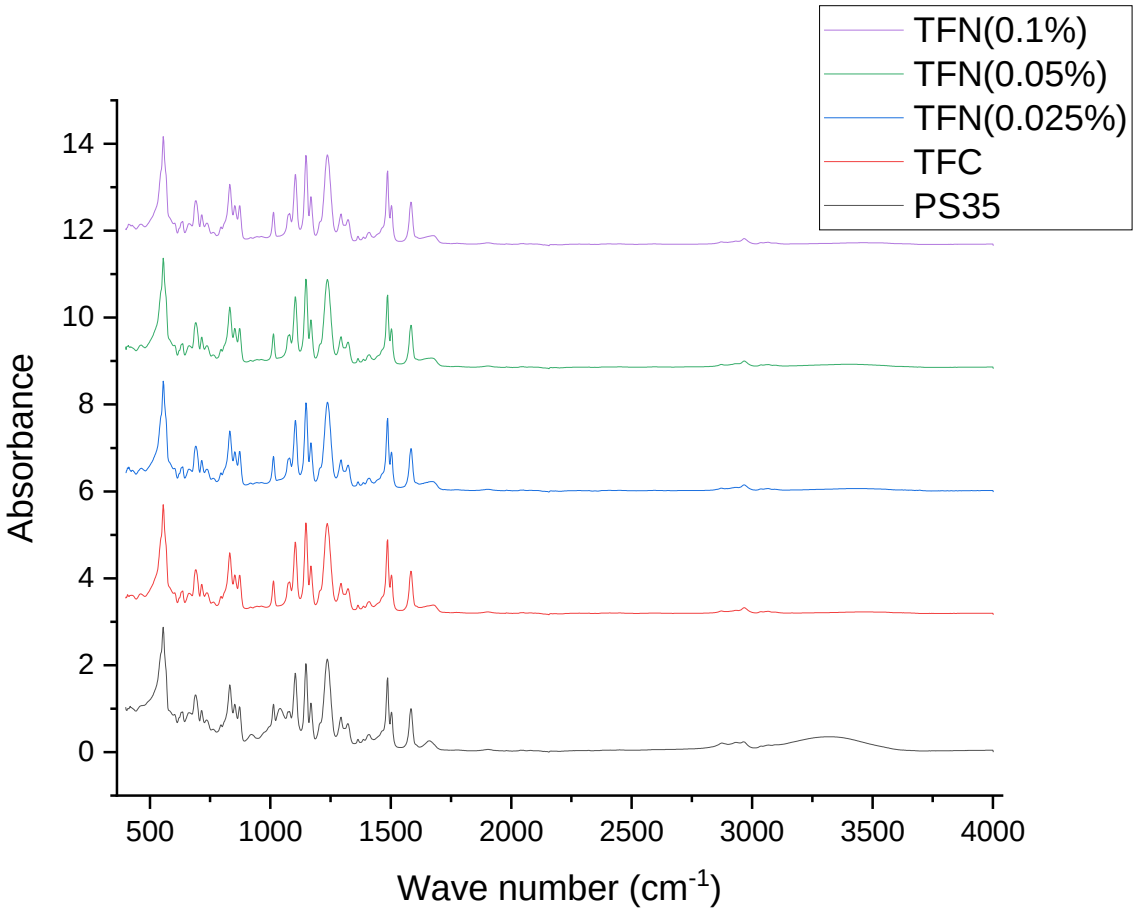

Figure 2-9. FTIR spectra of the PS35 (support), TFC, and TFN membranes.

Table 2-4. Total peak area under 1618–1720 cm^{-1}(amideI), 1600–1620 cm^{-1}(aromatic amide), and various peaks in the 3120–3706 cm^{-1} range for the PS35 (support), TFC and TFN membranes.

Membrane	**Primary amide (1618-1720 cm^{-1})**	**Aromatic amide (1600-1618 cm^{-1})**	**3120-3706 cm^{-1}**
PS35	15.6	2.6	123.2
TFC	16.7	3.2	29.1
TFN (0.025%)	18.4	3.5	36.5
TFN (0.05%)	18.8	3.7	44.3
TFN (0.1%)	17.3	3.3	30.6

The surface charge of the TFC and TFN membranes was evaluated by measuring their surface zeta potential under different pH levels. In turn, the zeta potential of the selective layer influences solute rejection of NF membranes. Figure 2-10 summarizes the zeta potential results. In general, the zeta potential of all membranes decreases with an increase in the pH. In other words, the surface charge in a basic environment is greater than that in an acidic one. At acidic pH, TFN membranes' zeta potential is less negative than that of the TFC membrane. There is no clear trend at neutral pH. However, at the basic pH, the surface charge of TFN membranes is greater than that of the TFC membrane. This phenomenon can be attributed to the amine groups via incorporating HNTs functionalized with the first generation of PAPAM dendrimers. The zeta potential results are in an acceptable agreement with the enhanced membrane hydrophilicity (Figure 2-7) [32]. The residual COCl functional groups in TMC monomer are turned into carboxylic acid groups (COOH) by hydrolyzation in the aqueous solution, which leads to negatively charged membranes [33].

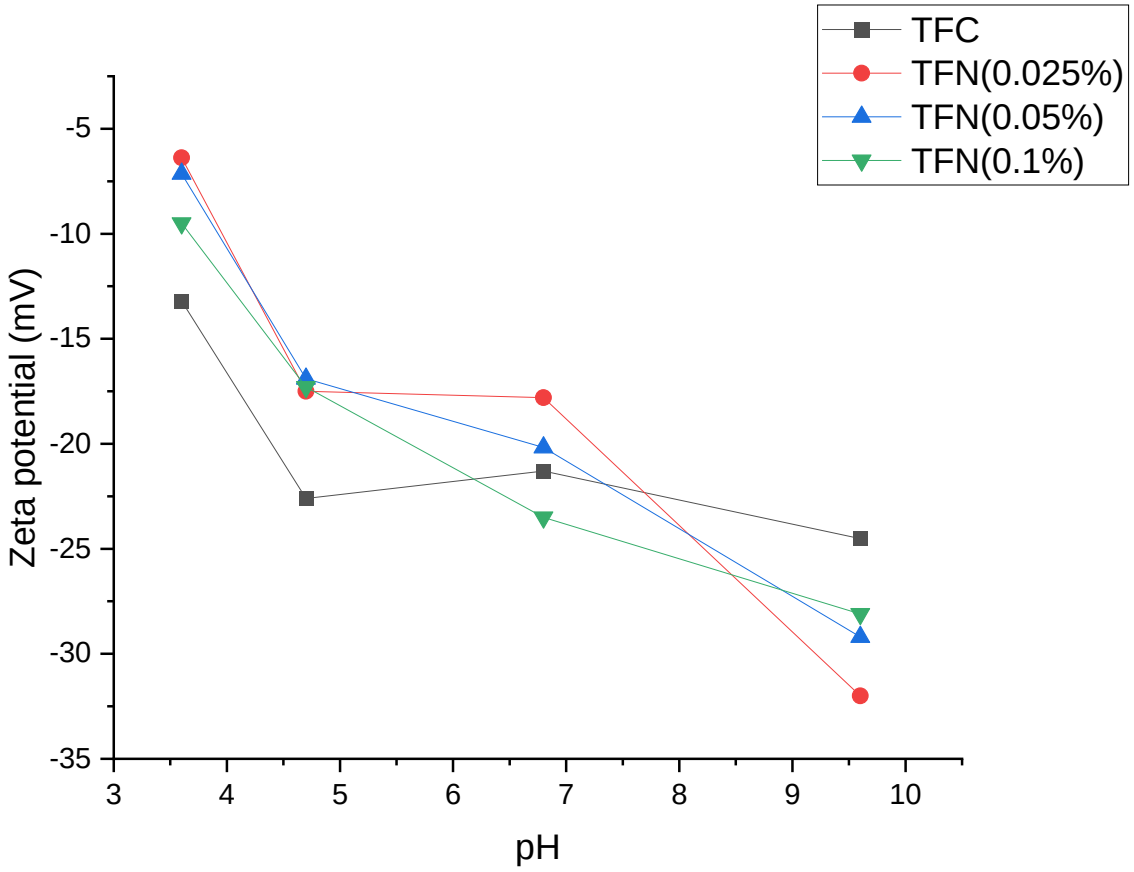

Figure 2-10. Surface zeta potential of TFC and TFN membranes.

2.3.3. Membranes separation performance

The TFC and TFN NF membranes' separation performance was examined with 3000 ppm feed solution of different salts at 10 bar and 25°C. Figure 2-11 shows the pure water flux of the TFC and TFN membranes. The reported values and the corresponding error bars represent the average and standard deviation from at least 4 coupons for a given type of membrane. The water flux of the pristine TFC membrane of 115 $L.m^{-2}.hr^{-1,}$ is higher than the TFN membranes. The lowest water flux of 96 $L.m^{-2}.hr^{-1}$ is observed for the TFN membrane with the lowest loading of NPs (0.025%). According to the contact angle measurements (Figure 2-7), TFN membranes are more hydrophilic than the reference TFC membrane. Therefore, the expected trend of increased water flux with increased surface hydrophilicity of the membrane is not observed. On the other hand, considering only TFN membranes, the water flux correlates very well with these membranes' water contact angle. It is important to note that considering the error bars' magnitude, the differences between different membranes' water fluxes are insignificant.

Figure 2-12 shows the TFC and TFN membranes' rejection of inorganic salts ($MgCl_2$, Na_2SO_4, NaCl). As expected, the rejection of NaCl by all membranes is very low (around or below 40%). NF membranes are not suitable for the separation of monovalent salts. The general trend for rejection is Na_2SO_4 > $MgCl_2$ > NaCl. Although NaCl and Na_2SO_4 have the same monovalent cation (Na^+), the hydration radius of SO_4^{2-} is higher than Cl^- [33,34]. However, the difference in the hydration radii, i.e. size exclusion, is not the main reason for the difference in the rejections of NaCl and Na_2SO_2. As seen in Figure 2-10, all membranes fabricated in this study were negatively charged, which is generally the case for NF membranes. The negatively charged NF membranes have a higher rejection toward divalent SO_4^{2-} anions than monovalent Cl^- anions due to stronger electrostatic repulsion. Electroneutrality of the feed solution then requires corresponding rejections of the Na^+ cations. Therefore, the Donnan effect is the main reason for a huge difference in the rejections of NaCl and Na_2SO_2. The size exclusion also contributes to the rejection of dissolved salts in the NF process. For example, $MgCl_2$ and NaCl have the same anion (Cl^-), but the divalent Mg^{2+} has a larger hydration radius than the Na^+; therefore, the $MgCl_2$ rejection is higher than NaCl because of size exclusion [28,33,34].

The dominance of the Donnan effect over the size exclusion in NF filtration explains a higher rejection of Na_2SO_4 compared to $MgCl_2$. As seen in Table 2-2, among all ions, Mg^{2+} has the highest hydration radius. Yet, since the membranes are negatively charged, the rejection of the salts must be primarily determined by the rejection of anions. In contrast, the rejection of the corresponding cations must follow accordingly to maintain the feed solution's electroneutrality.

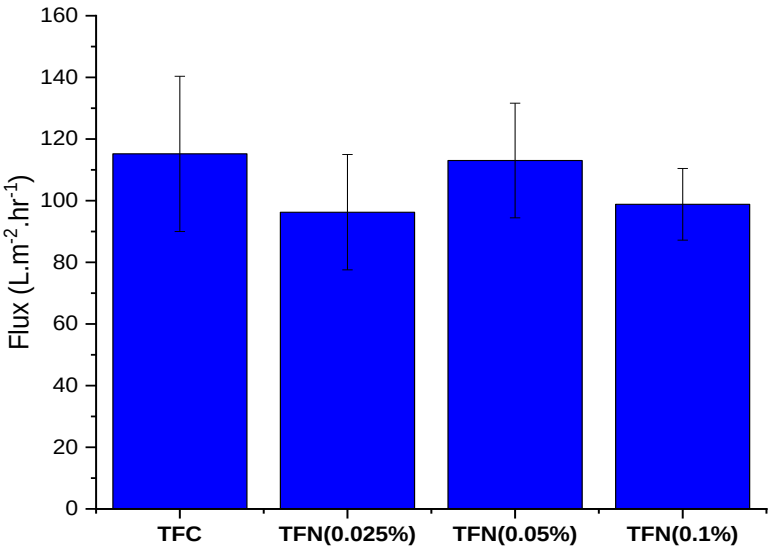

Figure 2-11. Pure water flux performance of the TFC and TFN membranes at 20 bar and 25°C.

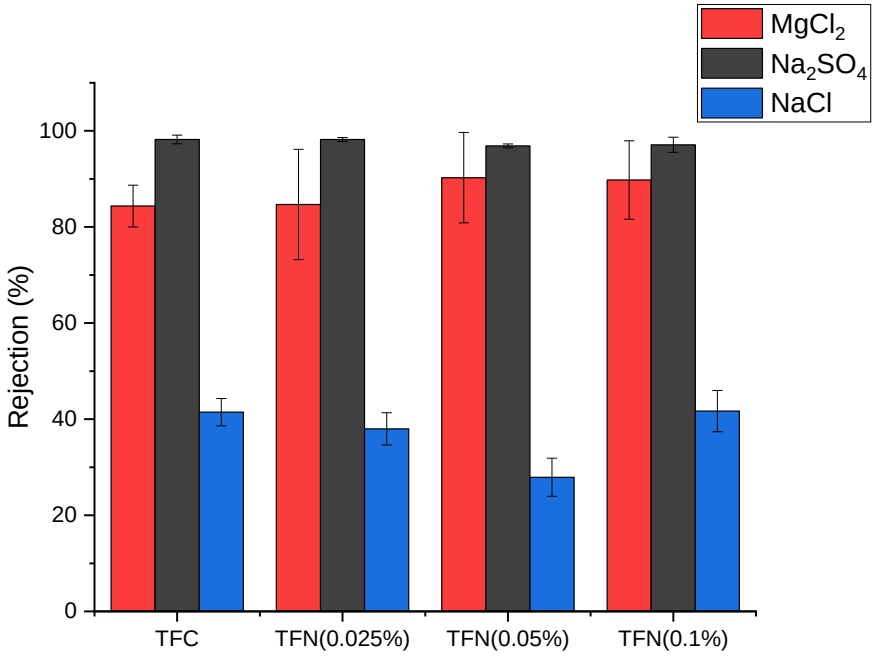

Figure 2-12. Rejection performance of different salts for the TFC and TFN with 3000 ppm feed aqueous solution 10 bar and 25 °C.

Table 2-5 compares the performance of our TFN membranes based HNTs-G1 with TFN membranes based on other nanomaterials. Since NF tests can be carried out at different feed pressures, the productivity of the membranes in Table 2-5 is compared based on water permeance rather than the water flux. The water permeance is a pressure gradient-normalized water flux. It can be noticed that many membranes reported in Table 2-5 are more productive than our TFN membranes, and some also exhibit a comparable or even higher rejection of Na_2SO_4. However, compared to other membranes listed in Table 2-5, our TFN membranes exhibit very high rejection towards $MgCl_2$. Only poly(doamine) MWCNT-based TFN membranes reported by Zhao et al. [49] exhibit similar rejection as our membranes. These authors claim that a high rejection of $MgCl_2$ by poly(doamine) MWCNT-based TFN membranes is due to a positive surface charge of the membrane. Consequently, the Donnan effect arises from the repulsion of divalent Mg^{2+} cations rather than monovalent Cl^- anions. As shown in Figure 2-10, our TFC and TFM membranes are negatively charged. However, since HNTs-G1 are positively charged (Table 2-3), they slightly decrease the negative charge of the resulting TFN membranes (Figure 2-10). Also, in the vicinity of positively charged HNTs-G1, the rejection should be governed by the repulsion of positively charged Mg^{2+} cations. In other words, as the HNTs-G1 loading increases, the rejection of $MgCl_2$ should increase. This trend is indeed present in Figure 2-12 despite the size of the error bars.

Considering high rejections of Na_2SO_4 and $MgCl_2$, the TFC and TFN membranes fabricated in this study are suitable for water softening, requiring removing multivalent salts. However, due to their unique high rejection of $MgCl_2$, a commonly used draw solute, our membranes could also be used in forward osmosis (FO) separations using $MgCl_2$ as a draw solution. High rejection of $MgCl_2$ in NF separation promises a low reverse flux of $MgCl_2$ in FO applications. Although the rejection of Na_2SO_4 by our membranes was higher than $MgCl_2$, the former has a higher molecular weight than the latter. Therefore, an aqueous solution of $MgCl_2$ of a given weight percentage concentration will create a higher osmotic pressure than an aqueous solution of Na_2SO_4 of the same concentration.

Chapter 3 will examine the forward osmosis performance of our TFC and TFN membranes in the presence and absence of heavy metals in the feed solution to evaluate their potential for heavy metal removal from wastewater.

Table 2-5. Performance comparison between TFN (HNTs-G1) membrane and other reported TFN membranes

Nanomaterial	**$MgCl_2$ rejection (%)**	**Na_2SO_4 rejection (%)**	**Water permeance ($L.m^{-2}.hr^{-1}.bar^{-1}$)**	**Salt concentration ($g.L^{-1}$)**	**Ref**
HNTs-G1 *	90.25	96.88	5.65	3	This work
ATP	20	92	23	1	[35]
GO	-	96.56	15.63	1	[36]
TiO_2 @ GO	6.2	98.8	5.60	1	[37]
GO-COCl *	-	97.1	3.76	1	[38]
ZNGs	41.1	97.8	10.63	1	[39]
COFs (SNW-1)	-	83.5	19.25	1	[40]
SGO	-	96.45	2.37	2.5	[41]
PDA-Si *	68	97	13.33	1	[42]
NH2-SWCNT	51.63	96.34	17.8	2	[43]
Aluminosilicate SWCNT	-	97	<1.2	2	[44]
PMMA- MWNT *	-	99	7	2	[45]
Poly(doamine) MWCNT	91.5	45.2	15.32	1	[46]
* NPs added into the organic phase, all of the other NPs were added into the aqueous phase.					

The TFC rejection for $MgCl_2$, Na_2SO_4, NaCl is 84.35 %, 98.20 %, and 41.45 %, respectively. For the rejection of the $MgCl_2$, it seems that NPs had a positive effect. The rejection trend is in order of TFN(0.05%) > TFN(0.1%) > TFN(0.025%) > TFC. The highest $MgCl_2$ rejection is for TFN(0.05%), with an average of 90.25 %. The rise of the rejection for $MgCl_2$ and decreasing its difference with Na_2SO_4 can be attributed to the decrease of the negative charge from TFC to TFN

membranes[47], as can be seen in Figure 2-10. As Figure 2-10 illustrates, TFN membranes have a less negatively charged surface compared to TFC membranes in the pH range of the experiments (pH 6-7). Therefore, based on the Donnan effect, it can be concluded that the rejection of Mg^{2+} by TFN membranes increased, and to maintain the electroneutrality, the rejection of Cl^- also increased.

For the Na_2SO_4, the rejection slightly decreases by increasing the NPs loading. Although the TFN membranes' average rejection is slightly smaller than the TFC membrane, it is still greater than 95 %. The average rejection trend for the Na_2SO_4 is in order of TFC > TFN(0.025%) > TFN(0.1%) > TFN(0.05%). The NaCl rejection is poor in comparison to $MgCl_2$ and Na_2SO_4. It is due to the molecule size of NaCl, which is smaller than the pores of the membrane; therefore, they can easily pass through the membrane.

2.4. Conclusions

Halloysite nanotubes (HNTs) modified by the first generation of poly(amidoamine) (PAMAM) dendrimers were used as nanoparticles (NPs) in the fabrication of thin-film nanocomposite (TFN) membranes. The TFN and reference TFC membranes were synthesized by in-situ interfacial polymerization of piperazine (PIP) and 1,3,5-benzenetricarbonyl trichloride (TMC). When synthesizing TFN membranes, the NPs were dispersed in the TMC solution before the polymerization with PIP. The modified HNTs were characterized by ATR-FTIR, TEM, SEM, zeta potential, and thermogravimetric TGA analyses. Fabricated membranes were also characterized by SEM, ATR-FTIR, zeta potential, and contact angle measurements. The membranes were also evaluated in cross-flow nanofiltration (NF) tests using 3000 ppm aqueous solutions of $MgCl_2$, Na_2SO_4 and NaCl, respectively, as feed at 10 bar and ambient temperature.

All membranes showed high rejections of Na_2SO_4 (around 97-98%) and low NaCl rejections (less than 40%), with the corresponding water fluxes greater than 100 L m^{-2} hr^{-1}. The rejection of $MgCl_2$ (ranging from 82 to 90%) was less than Na_2SO_4. However, our values are much greater than those reported in the literature for other TFN membranes. Since for the same weight percentage in aqueous solution, the osmotic pressure $MgCl_2$ is much greater than Na_2SO_4; the former is more desirable as a draw solute than the latter. The remarkable rejections of $MgCl_2$ are attributed to a

less negative surface charge of TFN membranes. Because HNT-G1 nanoparticles are positively charged, their incorporation into the selective layer helps to reject $MgCl_2$ to the level that is acceptable for its application as a draw solute. By considering the combination of the water flux and $MgCl_2$ rejection, the TFN membrane with 0.05% of nanoparticle loading appears to have the best NF performance.

2.5. Acknowledgment

The authors gratefully acknowledge the financial support provided by the Natural Science and Engineering Research Council (NSERC) Canada, Discovery Grant (DG), grant number: 04443.

2.6. References

[1] C. Conidi, A. Cassano, F. Caiazzo, E. Drioli, Separation and purification of phenolic compounds from pomegranate juice by ultrafiltration and nanofiltration membranes, J. Food Eng. 195 (2017) 1–13. https://doi.org/10.1016/j.jfoodeng.2016.09.017.

[2] C.M. Galanakis, G. Fountoulis, V. Gekas, Nanofiltration of brackish groundwater by using a polypiperazine membrane, Desalination. 286 (2012) 277–284. https://doi.org/10.1016/j.desal.2011.11.035.

[3] A. Bes-Piá, J.A. Mendoza-Roca, L. Roig-Alcover, A. Iborra-Clar, M.I. Iborra-Clar, M.I. Alcaina-Miranda, Comparison between nanofiltration and ozonation of biologically treated textile wastewater for its reuse in the industry, Desalination. 157 (2003) 81–86. https://doi.org/10.1016/S0011-9164(03)00386-2.

[4] J. Chandrapala, M.C. Duke, S.R. Gray, M. Weeks, M. Palmer, T. Vasiljevic, Nanofiltration and nanodiafiltration of acid whey as a function of pH and temperature, Sep. Purif. Technol. 160 (2016) 18–27. https://doi.org/10.1016/j.seppur.2015.12.046.

[5] W. Zhang, G. He, P. Gao, G. Chen, Development and characterization of composite nanofiltration membranes and their application in concentration of antibiotics, Sep. Purif. Technol. 30 (2003) 27–35. https://doi.org/10.1016/S1383-5866(02)00095-3.

[6] C. Tang, V. Chen, Nanofiltration of textile wastewater for water reuse, Desalination. 143 (2002) 11–20. https://doi.org/10.1016/S0011-9164(02)00216-3.

[7] S. Mondal, S.R. Wickramasinghe, Produced water treatment by nanofiltration and reverse osmosis membranes, J. Memb. Sci. 322 (2008) 162–170. https://doi.org/10.1016/j.memsci.2008.05.039.

[8] L.C. Juang, D.H. Tseng, H.Y. Lin, Membrane processes for water reuse from the effluent of industrial park wastewater treatment plant: a study on flux and fouling of membrane, Desalination. 202 (2007) 302–309. https://doi.org/10.1016/j.desal.2005.12.068.

[9] I. Koyuncu, D. Topacik, E. Yuksel, Reuse of reactive dyehouse wastewater by

nanofiltration: Process water quality and economical implications, Sep. Purif. Technol. 36 (2004) 77–85. https://doi.org/10.1016/S1383-5866(03)00154-0.

[10] B. Van der Bruggen, M. Mänttäri, M. Nyström, Drawbacks of applying nanofiltration and how to avoid them: A review, Sep. Purif. Technol. 63 (2008) 251–263. https://doi.org/10.1016/j.seppur.2008.05.010.

[11] L.F. Liu, X. Huang, X. Zhang, K. Li, Y.L. Ji, C.Y. Yu, C.J. Gao, Modification of polyamide TFC nanofiltration membrane for improving separation and antifouling properties, RSC Adv. 8 (2018) 15102–15110. https://doi.org/10.1039/c8ra01374h.

[12] B. Rajaeian, A. Rahimpour, M.O. Tade, S. Liu, Fabrication and characterization of polyamide thin film nanocomposite (TFN) nanofiltration membrane impregnated with TiO2 nanoparticles, Desalination. 313 (2013) 176–188. https://doi.org/10.1016/j.desal.2012.12.012.

[13] R.L. McGinnis, M. Elimelech, Global challenges in energy and water supply: The promise of engineered osmosis, Environ. Sci. Technol. 42 (2008) 8625–8629. https://doi.org/10.1021/es800812m.

[14] C. Kong, T. Shintani, T. Tsuru, “Pre-seeding”-assisted synthesis of a high performance polyamide-zeolite nanocomposite membrane for water purification, New J. Chem. 34 (2010) 2101–2104. https://doi.org/10.1039/c0nj00581a.

[15] D. Emadzadeh, W.J. Lau, M. Rahbari-Sisakht, A. Daneshfar, M. Ghanbari, A. Mayahi, T. Matsuura, A.F. Ismail, A novel thin film nanocomposite reverse osmosis membrane with superior anti-organic fouling affinity for water desalination, Desalination. 368 (2015) 106–113. https://doi.org/10.1016/j.desal.2014.11.019.

[16] M.S.A.S. Shah, M. Nag, T. Kalagara, S. Singh, S. V. Manorama, Silver on PEG-PU-TiO2 polymer nanocomposite films: An excellent system for antibacterial applications, Chem. Mater. 20 (2008) 2455–2460. https://doi.org/10.1021/cm7033867.

[17] K.C. Wong, P.S. Goh, B.C. Ng, A.F. Ismail, Thin film nanocomposite embedded with polymethyl methacrylate modified multi-walled carbon nanotubes for CO2 removal, RSC

Adv. 5 (2015) 31683–31690. https://doi.org/10.1039/c5ra00039d.

[18] M. Ghanbari, D. Emadzadeh, W.J. Lau, S.O. Lai, T. Matsuura, A.F. Ismail, Synthesis and characterization of novel thin film nanocomposite (TFN) membranes embedded with halloysite nanotubes (HNTs) for water desalination, Desalination. 358 (2015) 33–41. https://doi.org/10.1016/j.desal.2014.11.035.

[19] D. Emadzadeh, W.J. Lau, T. Matsuura, M. Rahbari-Sisakht, A.F. Ismail, A novel thin film composite forward osmosis membrane prepared from PSf-TiO2 nanocomposite substrate for water desalination, Chem. Eng. J. 237 (2014) 70–80. https://doi.org/10.1016/j.cej.2013.09.081.

[20] F. Asempour, S. Akbari, D. Bai, D. Emadzadeh, T. Matsuura, B. Kruczek, Improvement of stability and performance of functionalized halloysite nano tubes-based thin film nanocomposite membranes, J. Memb. Sci. 563 (2018) 470–480. https://doi.org/10.1016/j.memsci.2018.05.070.

[21] F. Asempour, S. Akbari, M.H. Kanani-Jazi, A. Atashgar, T. Matsuura, B. Kruczek, Chlorine-resistant TFN RO membranes containing modified poly(amidoamine) dendrimer-functionalized halloysite nanotubes, J. Memb. Sci. 623 (2021) 119039. https://doi.org/10.1016/j.memsci.2020.119039.

[22] A. Moslehyani, M. Mobaraki, A.F. Ismail, T. Matsuura, S.A. Hashemifard, M.H.D. Othman, A. Mayahi, M. Rezaei Dashtarzhandi, M. Soheilmoghaddam, E. Shamsaei, Effect of HNTs modification in nanocomposite membrane enhancement for bacterial removal by cross-flow ultrafiltration system, React. Funct. Polym. 95 (2015) 80–87. https://doi.org/10.1016/j.reactfunctpolym.2015.08.007.

[23] T. Ormanci-Acar, F. Celebi, B. Keskin, O. Mutlu-Salmanlı, M. Agtas, T. Turken, A. Tufani, D.Y. Imer, G.O. Ince, T.U. Demir, Y.Z. Menceloglu, S. Unal, I. Koyuncu, Fabrication and characterization of temperature and pH resistant thin film nanocomposite membranes embedded with halloysite nanotubes for dye rejection, Desalination. 429 (2018) 20–32. https://doi.org/10.1016/j.desal.2017.12.005.

[24] M. Ghanbari, D. Emadzadeh, W.J. Lau, T. Matsuura, M. Davoody, A.F. Ismail, Super hydrophilic TiO2/HNT nanocomposites as a new approach for fabrication of high performance thin film nanocomposite membranes for FO application, Desalination. 371 (2015) 104–114. https://doi.org/10.1016/j.desal.2015.06.007.

[25] R. Esfand, D.A. Tomalia, A. Arbor, A. Arbor, Poly (amidoamine) (PAMAM) dendrimers : from biomimicry to drug delivery and biomedical applications, 6 (2001) 427–436.

[26] F. Shahamati Fard, S. Akbari, E. Pajootan, M. Arami, Enhanced acidic dye adsorption onto the dendrimer-based modified halloysite nanotubes, Desalin. Water Treat. 57 (2016) 26222–26239. https://doi.org/10.1080/19443994.2016.1160437.

[27] F. Asempour, D. Emadzadeh, T. Matsuura, B. Kruczek, Synthesis and characterization of novel Cellulose Nanocrystals-based Thin Film Nanocomposite membranes for reverse osmosis applications, Desalination. 439 (2018) 179–187. https://doi.org/10.1016/j.desal.2018.04.009.

[28] C. Wu, Q. Xie, Z. Hong, L. Shen, T. Yu, H. Guo, Y. Xiong, G. Zhang, Y. Lu, W. Shao, Thin-film nanocomposite nanofiltration membrane with enhanced desalination and antifouling performance via incorporating L-aspartic acid functionalized graphene quantum dots, Desalination. 498 (2021) 114811. https://doi.org/10.1016/j.desal.2020.114811.

[29] Y. Joo, Y. Jeon, S.U. Lee, J.H. Sim, J. Ryu, S. Lee, H. Lee, D. Sohn, Aggregation and stabilization of carboxylic acid functionalized halloysite nanotubes (HNT-COOH), J. Phys. Chem. C. 116 (2012) 18230–18235. https://doi.org/10.1021/jp3038945.

[30] L. Bai, Y. Liu, N. Bossa, A. Ding, N. Ren, G. Li, H. Liang, M.R. Wiesner, Incorporation of Cellulose Nanocrystals (CNCs) into the Polyamide Layer of Thin-Film Composite (TFC) Nanofiltration Membranes for Enhanced Separation Performance and Antifouling Properties, Environ. Sci. Technol. 52 (2018) 11178–11187. https://doi.org/10.1021/acs.est.8b04102.

[31] X.Q. Cheng, L. Shao, C.H. Lau, High flux polyethylene glycol based nanofiltration

membranes for water environmental remediation, J. Memb. Sci. 476 (2015) 95–104. https://doi.org/10.1016/j.memsci.2014.11.020.

[32] Z. Yang, X. Huang, J. Wang, C.Y. Tang, Novel polyethyleneimine/TMC-based nanofiltration membrane prepared on a polydopamine coated substrate, Front. Chem. Sci. Eng. 12 (2018) 273–282. https://doi.org/10.1007/s11705-017-1695-2.

[33] T. Ormanci-Acar, F. Celebi, B. Keskin, O. Mutlu-Salmanlı, M. Agtas, T. Turken, A. Tufani, D.Y. Imer, G.O. Ince, T.U. Demir, Y.Z. Menceloglu, S. Unal, I. Koyuncu, Fabrication and characterization of temperature and pH resistant thin film nanocomposite membranes embedded with halloysite nanotubes for dye rejection, Desalination. 429 (2018) 20–32. https://doi.org/10.1016/j.desal.2017.12.005.

[34] E.R. Nightingale, Phenomenological theory of ion solvation. Effective radii of hydrated ions, J. Phys. Chem. 63 (1959) 1381–1387. https://doi.org/10.1021/j150579a011.

[35] M. Wu, T. Ma, Y. Su, H. Wu, X. You, Z. Jiang, R. Kasher, Fabrication of composite nanofiltration membrane by incorporating attapulgite nanorods during interfacial polymerization for high water flux and antifouling property, J. Memb. Sci. 544 (2017) 79–87. https://doi.org/10.1016/j.memsci.2017.09.016.

[36] W. Zhao, H. Liu, N. Meng, M. Jian, H. Wang, X. Zhang, Graphene oxide incorporated thin film nanocomposite membrane at low concentration monomers, J. Memb. Sci. 565 (2018) 380–389. https://doi.org/10.1016/j.memsci.2018.08.047.

[37] J. Wang, Y. Wang, J. Zhu, Y. Zhang, J. Liu, B. Van der Bruggen, Construction of TiO2@graphene oxide incorporated antifouling nanofiltration membrane with elevated filtration performance, J. Memb. Sci. 533 (2017) 279–288. https://doi.org/10.1016/j.memsci.2017.03.040.

[38] P. Wen, Y. Chen, X. Hu, B. Cheng, D. Liu, Y. Zhang, S. Nair, Polyamide thin film composite nanofiltration membrane modified with acyl chlorided graphene oxide, J. Memb. Sci. 535 (2017) 208–220. https://doi.org/10.1016/j.memsci.2017.04.043.

[39] Y.L. Ji, Q.F. An, X.D. Weng, W.S. Hung, K.R. Lee, C.J. Gao, Microstructure and

performance of zwitterionic polymeric nanoparticle/polyamide thin-film nanocomposite membranes for salts/organics separation, J. Memb. Sci. 548 (2018) 559–571. https://doi.org/10.1016/j.memsci.2017.11.057.

[40] C. Wang, Z. Li, J. Chen, Z. Li, Y. Yin, L. Cao, Y. Zhong, H. Wu, Covalent organic framework modified polyamide nanofiltration membrane with enhanced performance for desalination, J. Memb. Sci. 523 (2017) 273–281. https://doi.org/10.1016/j.memsci.2016.09.055.

[41] Y. Kang, M. Obaid, J. Jang, I.S. Kim, Sulfonated graphene oxide incorporated thin film nanocomposite nanofiltration membrane to enhance permeation and antifouling properties, Desalination. 470 (2019) 114125. https://doi.org/10.1016/j.desal.2019.114125.

[42] M. Belle, M. Yap, C.A. Trilles, M. Reyes, D. Guzman, Separation and Puri fi cation Technology Improved performance of thin- fi lm nanocomposite nano fi ltration membranes as induced by embedded polydopamine-coated silica nanoparticles, Sep. Purif. Technol. 224 (2019) 113–120. https://doi.org/10.1016/j.seppur.2019.05.018.

[43] Q. Kong, H. Xu, C. Liu, G. Yang, M. Ding, W. Yang, T. Lin, W. Chen, S. Gray, Z. Xie, Fabrication of high performance TFN membrane containing NH2-SWCNTs: Via interfacial regulation, RSC Adv. 10 (2020) 25186–25199. https://doi.org/10.1039/d0ra02947e.

[44] G.N.B. Baroña, M. Choi, B. Jung, High permeate flux of PVA/PSf thin film composite nanofiltration membrane with aluminosilicate single-walled nanotubes, J. Colloid Interface Sci. 386 (2012) 189–197. https://doi.org/10.1016/j.jcis.2012.07.049.

[45] J.N. Shen, C.C. Yu, H.M. Ruan, C.J. Gao, B. Van der Bruggen, Preparation and characterization of thin-film nanocomposite membranes embedded with poly(methyl methacrylate) hydrophobic modified multiwalled carbon nanotubes by interfacial polymerization, J. Memb. Sci. 442 (2013) 18–26. https://doi.org/10.1016/j.memsci.2013.04.018.

[46] F.Y. Zhao, Y.L. Ji, X.D. Weng, Y.F. Mi, C.C. Ye, Q.F. An, C.J. Gao, High-Flux Positively Charged Nanocomposite Nanofiltration Membranes Filled with Poly(dopamine) Modified

Multiwall Carbon Nanotubes, ACS Appl. Mater. Interfaces. 8 (2016) 6693–6700. https://doi.org/10.1021/acsami.6b00394.

[47] J.S. Trivedi, D. V. Bhalani, G.R. Bhadu, S.K. Jewrajka, Multifunctional amines enable the formation of polyamide nanofilm composite ultrafiltration and nanofiltration membranes with modulated charge and performance, J. Mater. Chem. A. 6 (2018) 20242–20253. https://doi.org/10.1039/c8ta07841f.

Chapter 3. Evaluation of heavy metal removal in forward osmosis process using functionalized HNTs-based TFN NF membranes

Amirsajad Atashgar, Daryoush Emadzadeh, Boguslaw Kruczek

[a]Department of Chemical and Biological Engineering, University of Ottawa, 161 Louis Pasteur St, ON, Canada, K1N 6N5

Abstract

Novel TFN membranes, which exhibit good nanofiltration performance with $MgCl_2$ and Na_2SO_4 solutions, were tested for the removal of heavy metals (Cu and Pb) from synthetic wastewater in dynamic forward osmosis experiments. The TFN membranes were fabricated on top of a commercial PS35 ultrafiltration membrane by in-situ interfacial polymerization of piperazine (PIP) and 1,3,5-benzenetricarbonyl trichloride (TMC) containing different amounts of dispersed functionalized halloysite nanotubes (HNTs) nanoparticles. The HNTs nanoparticles were functionalized with the first generation of poly(amidoamine) (PAMAM) dendrimers. The TFN and the reference TFC membranes showed excellent rejections of Cu and Pb, ranging from 95% to 98%. The TFN membranes showed higher rejection to Cu than Pb, while the opposite was observed for the reference TFC membranes. The presence of heavy metal in the feed solution enhanced the FO performance of all membranes. In particular, the reverse flux of draw solute ($MgCl_2$) decreased at least 2.5 times compared to the experiments with pure water as a feed. Simultaneously, the water flux also increased. The improved FO performance of the membranes in the presence of heavy metals is attributed to their adsorption by the membranes. The adsorption of heavy metals was confirmed and quantified by the mass balance. All membranes showed a greater affinity towards Pb than Cu.

3.1. Introduction

Due to the fast development of the industries, many wastewaters containing heavy metals are discharged into the environment. Metals with an atomic mass between 63.5 and 200.6 and a specific gravity of more than five are classified as heavy metals[1]. Examples of heavy metals include zinc (Zn), copper (Cu), nickel (Ni) and lead (Pb). Heavy metals at low concentrations are vital for living organisms, including humans. However, at higher concentrations, they become toxic and harmful. For example, zinc is a crucial element for human health and is vital for living tissue's physiological functions. On the other hand, too much zinc can cause severe health problems, including skin irritation, vomiting, and nausea. Copper is essential for animal metabolism. However, copper's excessive ingestion can create toxicological problems such as cramps, vomiting, and even death. Nickel is known as a human carcinogen. Also, excessive nickel concentrations can bring about severe kidney and lung problems. Finally, lead can also cause severe kidney problems and damage the liver and central nervous system [1,2]. Since heavy metals are not biodegradable, they must be removed from wastewaters [1].

There are different methods to remove heavy metals from wastewater, such as chemical precipitation, adsorption, ion exchange, coagulation-flocculation, and membrane separation. The latter is environmentally friendly, offers high separation efficiency and energy savings [2]. Different membrane separation processes, including microfiltration (MF), ultrafiltration (UF), nanofiltration (NF), and reverse osmosis (RO) have been considered for heavy metal removal. However, NF and RO are the most feasible for heavy metal removal from wastewater. The NF mechanism for separation relies on size exclusion and the Donnan potential. In addition to these two, RO also relies on the solution-diffusion mechanism. Both the NF and RO are pressure-driven membranes; therefore, they both require external pressure. The higher the pressure, the higher the energy consumption, which increases the process's operating cost. Also, membranes used in pressure-driven processes are prone to fouling, which greatly reduces the membrane's life in NF and RO processes [1–3].

The NF and RO membranes can be used in forward osmosis (FO) separations, which do not require external pressure. In the absence of external pressure, fouling tendency is significantly reduced. However, the FO separation is not a stand-alone process; it must be combined with another

process. An example of a hybrid process involving FO osmosis for heavy metal removal is shown in Figure 3-1. In the FO process, heavy metals are rejected. At the same time, pure water permeates from the feed to the draw solution. Water permeation occurs because of an osmotic pressure gradient created by a solute in the draw solution. Therefore, the permeating water in the FO process is not the final product as it dilutes the draw solution. The purpose of the second stage, an NF process, is to regenerate the draw solution while producing pure water. The advantage of a hybrid process is nanofiltration of "clean" draw solution rather than direct nanofiltration of "dirty" wastewaters; this minimizes membrane fouling. The membranes for the FO and NF steps in Fig. 1 could be the same. If the NF-stage membrane effectively rejects the draw solute, it will also prevent a reverse draw solute transport in the FO-stage. Therefore, the membranes for the first stage in Fig. 1 are often referred to as "NF-like FO" membranes [4]. The hybrid process in Fig. 1 can also be used for water desalination. However, since monovalent salts (e.g. NaCl) are to be rejected in the FO stage, the process would require an RO membrane or "RO-like FO" membrane [5–8]. Heavy metals occur as multivalent salts; it is thus sufficient to use NF-like FO membranes for heavy metal removal from wastewater. Moreover, NF-like FO membranes could achieve higher water flux than RO-like FO membranes due to a looser selective layer [4,6,8].

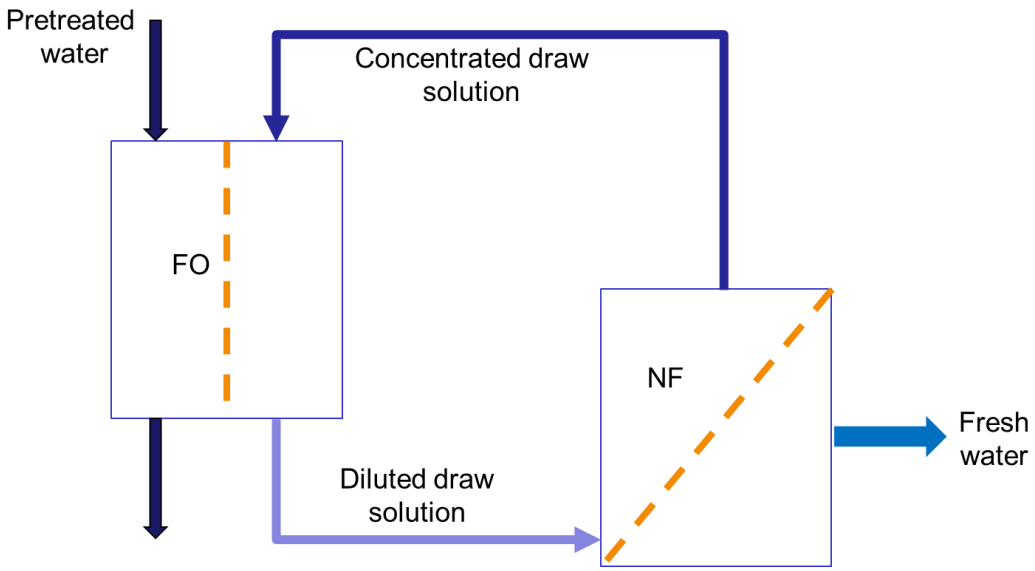

Figure 3-1. A hybrid two-stage FO-NF process for heavy metal removal from wastewater.

There is an increasing number of examples of NF-like FO applications. Abdullah et al. used commercial NF membranes in PRO and FO processes for treating aerobically treated palm oil mill effluent (AT-POME) [9]. They reported that the colour (i.e., impurity) of AT-POME could be removed entirely using magnesium chloride ($MgCl_2$) as a draw solution. Abdullah et al. also used four commercial NF membranes in the FO and PRO processes for copper ion removal from wastewater [4]. They reported near-complete removal of copper removal regardless of the membrane type and membrane orientation associated with low reverse draw-solute flux [4]. Setiawan et al. tested different types of in-house-made NF hollow fibre membranes in the FO process with pure water as a feed and 0.5 mol. L^{-1} $MgCl_2$ as a draw solution [10]. They reported a water flux as high as 9.74 $L.m^{-2}.h^{-1}$. Su et al. developed cellulose acetate-based NF membranes and studied the effect of draw solution concentration and membrane orientation (PRO vs FO) on the water flux [11]. Using 0.5 – 2.0 $mol.L^{-1}$ of $MgCl_2$ as a draw solution, they reported a higher water flux in the PRO mode (2.7 – 7.3 $L.m^{-2}.h^{-1}$) than in the FO mode (1.8 -5.0 $L.m^{-2}.h^{-1}$).

In the previous chapter, we reported on the synthesis and characterization of novel thin-film nanocomposite (TFN) membranes with different loadings of functionalized halloysite nanotubes (HNTs). The HNTs were functionalized by the first generation of poly(amidoamine) (PAMAM) dendrimers. The TFN and the reference thin-film composite (TFC) membranes were fabricated by in-situ interfacial polymerization (IP) of piperazine (PIP) and 1,3,5-benzenetricarbonyl trichloride (TMC). The membranes exhibited a high water flux (greater than 100 $L.m^{-2}.h^{-1}$) and high rejection of Na_2SO_4 (>95%) and $MgCl_2$ (>85%). Although the rejection of $MgCl_2$ was lower than Na_2SO_4, it was still higher than the values for many NF membranes in the literature. Moreover, some TFN membranes had $MgCl_2$ rejection higher than 90%.

Given a good performance NF of TFC and TFN membranes reported in Chapter 2 (2^{nd} stage in Figure 3-1), we considered them as NF-like FO membranes to remove heavy metals from wastewater (1^{st} stage in Figure 3-1). We, therefore, report the FO performance of TFC and TFN membranes in the experiments with pure water and synthetic wastewater as a feed, respectively. The wastewater was mimic by the respective 200 ppm solutions of copper and lead salts in deionized water. All experiments were performed in a novel experimental system, which allows continuous monitoring of the progress of dynamic FO tests. In addition, we also used some TFC

and TFN membranes to perform comparative NF tests with synthetic wastewater containing copper salt.

3.2. Experimental

3.2.1. Materials

The Sloecta Company Inc. donated polysulfone ultrafiltration membrane (PS35) with a molecular weight cut-off of 20,000 Da. Piperazine (PIP), 1,3,5-benzenetricarbonyl trichloride (TMC), n-hexane, aminopropyltriethoxysilane (APTES), ethanol, diethyl ether, dimethylformamide (DMF), ethylenediamine (EDA), Copper (II) sulphate pentahydrate ($CuSO_4.5H_2O$), and lead (II) nitrate ($Pb(NO_3)_2$) were all laboratory grades and purchased from Sigma-Aldrich. Also, magnesium chloride ($MgCl_2$) was purchased from Sigma-Aldrich and used as a draw solution. Deionized water was used to make PIP solution, and distilled water was used to wash the membranes and prepare and draw solutions.

3.2.2. Functionalization of HNTs

The detailed synthesis procedure of dendrimers and functionalization of HNT are fully described elsewhere [12]. Briefly, the first step was acid treatment to remove the contaminant. HNTs were magnetically stirred with a 35% HCl solution for 24 hours and then washed with distilled water. For the functionalization of HNTs with the amine (HNT-NH_2), the dry acid-treated HNTs were refluxed with a solution of APTES and toluene (4/15 (v/v)) for 12 hours at 60 °C. To synthesize the first generation of the PAMAM dendrimers on HNTs (HNTs-G1), 15 mL of methyl acrylate was reacted with 32.15 g HNTs-NH_2 in ethanol for 24 h at 60°C. The resulting NPs were separated by centrifugation, washed with diethyl ether, ethanol, and methanol, and recovered by centrifuging. After air-drying at 60°C, ethylene diamine was added to the mixture of HNT in ethanol and stirred at 60 °C for 24 hours. In the end, to recover the NPs, which is HNTs-G1, the reaction mixture was centrifuged, then washed with distilled water and air-dried. Figure 3-2 shows the repeating units of functionalized HNTs.

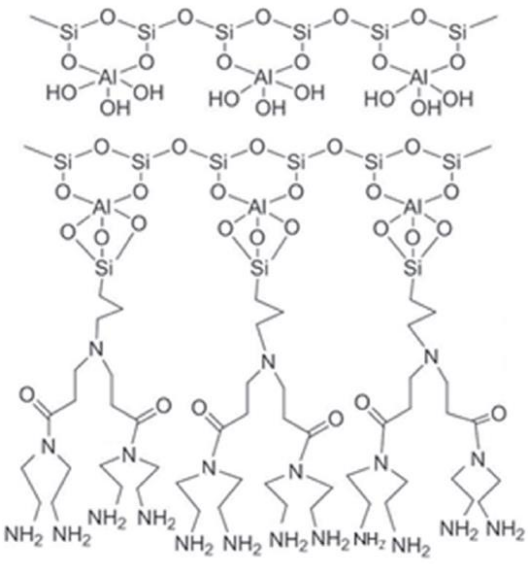

Figure 3-2. Schematic representation of the structure of HNTs-G1.

3.2.3. TFC and TFN membranes fabrication

The PS35 UF membrane was used as a substrate for the thin polyamide (PA) layer, synthesized by in-situ interfacial polymerization (IP) of two monomers PIP and TMC. To fabricate TFC membranes, a 2% (W/V) solution of PIP in deionized water was poured on the substrate. After 5 minutes, any visible droplets were drained off from the substrate by using a Teflon roller. After that, a 0.05% (W/V) solution of TMC in n-hexane was poured on the substrate for 1 minute. Then, the excess solution was drained off, and the membrane was washed with n-hexane. This was followed by placing the membrane in the oven at 95 ºC for 10 minutes.

Figure 3-3 shows the schematic diagram of making a TFC/TFN membrane. In the end, the membranes were washed thoroughly with distilled water and stored in deionized water. For the TFN membrane fabrication, different amounts of NPs were dispersed in the solution of TMC in n-

hexane, and the resulting suspension was used instead of the TMC solution. TFN membrane samples were named according to the HNTs-G1 loading in the organic solution (Table 3-1).

For each type of membrane, two membrane sheets were fabricated independently. From each sheet, four membrane coupons were extracted. Therefore, for each type, eight membranes were available for the performance tests.

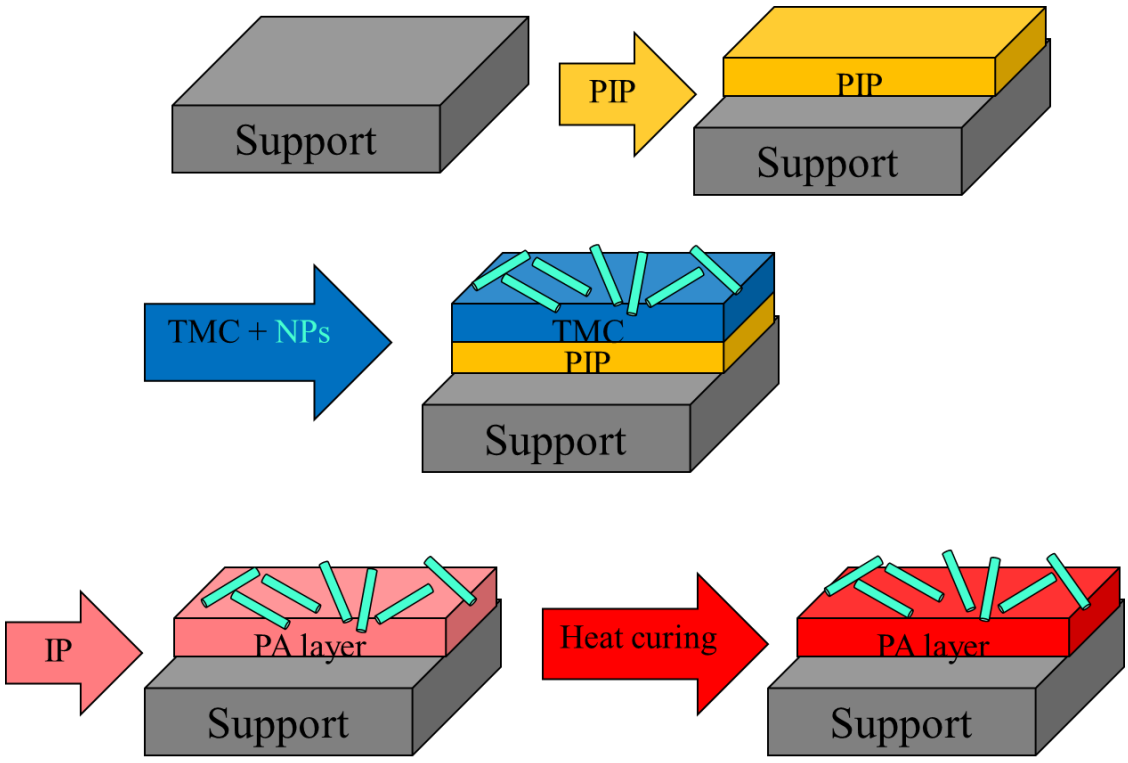

Figure 3-3. Schematic representation of fabrication of TFN membrane

Table 3-1. Monomer concentration and HNTs-G1 loading for the fabrication of TFC and TFN membranes.

Membrane	**PIP in H_2O (w/v) %**	**TMC in n-hexane (w/v) %**	**HNTs-G1 in TMC/n-hexane (w/v) %**
TFC	2	0.05	0
TFN (0.025%)	2	0.05	0.025
TFN (0.05%)	2	0.05	0.05
TFN (0.1%)	2	0.05	0.1

3.2.4. Forward osmosis tests and data analysis

A lab-scale FO setup, shown in Figure 3-4, was used to evaluate the membrane's performance. A detailed description of the system is presented elsewhere [13]. Briefly, the system's heart is the Teflon cross-flow membrane cell with a permeation area of 20.6 cm^2. For holding the feed and the draw solutions, two 1-L capacity plastic tanks are used. The tanks are placed on balances to precisely record the amount of water drawn from feed solution to draw solution. The balance for the feed tank has a resolution of 0.01 g, while the balance for the draw tank has a resolution of 0.1 g. The solutions were circulated independently using two centrifugal pumps. The feed solution passes through the lower part and the draw solution through the upper part of the cell. Two heat exchangers are connected to a refrigerated/heated bath circulator to maintain and control the temperature. Also, the temperature and the conductivity of the feed are monitored by the temperature/conductivity meter. All the membranes were tested in the FO-mode, i.e., the active layer facing feed solution (AL-FS). The temperature was maintained at 23 ± 2 °C.

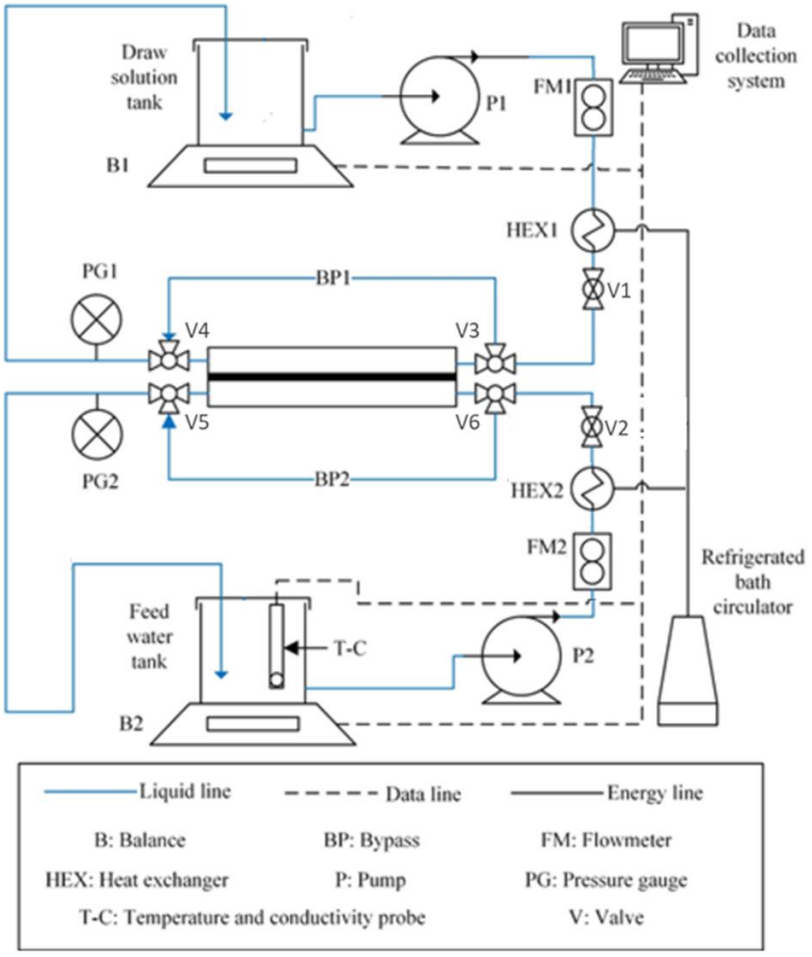

Figure 3-4. Schematic diagram of FO experimental system.[13]

As previously stated, for each type of membrane listed in Table 1, 8 coupons were prepared in two independent syntheses. Four membranes (two from each synthesis) were tested with DI water as a feed, two (one from each synthesis) with the feed containing Cu, and two (one from each synthesis) with the feed containing Pb. The draw solution in each experiment was the same, i.e., 1 mol.L^{-1} $MgCl_2$ in water.

The protocol for the FO experiment is described elsewhere [13]. Briefly, at first, the system was thoroughly cleaned by circulating DI water such that the conductivity dropped below 30 µs/cm. This required several batches of fresh DI water. After installing a membrane, fresh DI water was again circulated at both sides to remove any contaminants from the membrane. The system was then switched to a bypass mode, and DI water in the draw and feed solution tanks were replaced

by the draw solution (1 mol.L^{-1} $MgCl_2$ in water) and the feed solution (200 ppm of a heavy metal salt solution), respectively. The system was run in bypass mode at the flow rate of 2.4 L/min and the set temperature of 24 ^oC for several minutes until both the flow rate and the temperature stabilized at the set values. The experiment was initiated by switching the flows from the bypass to the membrane cell, which took not more than a couple of seconds. In other words, the experiment was initiated by a step-change in the concentration at both sides of the membranes. During the experiments, the mass of the feed and draw solution containers and the conductivity and temperature of the solution in the feed tank were recorded continuously using LabView data acquisition. The concentration of heavy metals was determined using an inductively coupled plasma emission spectrometer (ICP-MS). For each experiment with heavy metal, three samples were analyzed: 1) the initial feed solution (before initiation of the experiment), 2) the final feed solution, 3) the final draw solution.

For both heavy metals, the respective salts' concentration ($CuSO_4.5H_2O$ and $Pb(NO_3)_2$) in the feed solution was 200 ppm. Therefore, the corresponding theoretical concentrations of Cu^{2+} and Pb^{2+} were 50.9 ppm and 125.1 ppm, respectively (Table 3-2). However, the actual concentrations of heavy metals in the initial feed solution were lower than the values listed in Table 3-2. When the solution containing heavy metal replaced DI water in the feed tank, the system's tubing, pump and membrane cell contained DI water, which diluted the feed solution. The effect of dilution of feed and draw solution will be further discussed later. The pH of the feed solution with and without heavy metals was constant at 5.5 – 6 during the entire experiment.

Table 3-2. The calculated concentration of the heavy metals based on their molecular weight.

Heavy metal	**Calculated heavy metal concentrations in 200 ppm salt solution**
Cu (II)	50.9
Pb (II)	125.1

The water flux (J) and the reverse draw solute flux (J_s) were evaluated from the respective steady-state mass transfer rates of water (dm_w/dt) and the draw solute (dm_s/dt):

$$J = \frac{dm_w/dt}{\rho A} \tag{3}$$

$$J_s = \frac{dm_s/dt}{A} \tag{2}$$

where, ρ is the density of water, and A is the membrane area.

In the experiments with feed solution containing heavy metal, the solute and water permeate in the same direction. Therefore, the heavy metal rejection (R) is:

$$R = \left(1 - \frac{C_p}{C_f}\right) \times 100\% \tag{4}$$

where, C_p and C_f are steady-state concentrations of heavy metal in permeate and feed, respectively. It is essential to remember that during experiments, both feed and draw solutions were circulated at the respective sides of the membrane while the water permeated from the feed to the draw side. Therefore, in principle, no steady-state could be attained. However, since the volume of water permeated across the membrane was negligible compared to the volumes of feed and draw solutions, a pseudo-steady-state, which we will refer to as a steady-state, could be reached. The following section will show that the steady-state existed almost instantaneously after the experiment's initiation. Since the initial concentration of heavy metal in the draw solution was zero, the C_p was evaluated from:

$$C_p = \frac{C_{d,f} V_{d,f}}{\Delta V_d} \tag{5}$$

where: $C_{d,f}$, which is the concentration of heavy metal in the draw solution at the end of the experiment, and ΔV_d, which is the total volume of water permeated from the feed to the draw solution, were measured directly. The final volume of the draw solution at the end of the experiment ($V_{d,f}$) was estimated from:

$$V_{d,f} = V_{d,i} + V_{r,d} + \Delta V_d \tag{6}$$

where: $V_{d,i}$ is the initial volume of the draw solution, which in every experiment was 840 mL, and $V_{r,d}$ is the residual volume of water in the system, which represents the volume of water in the tubing, the membrane cell and the pump. According to Du et al.[13], who designed and constructed the system shown in Figure 3-4, $V_{r,d}$ is 161.5 mL on the draw side. The corresponding residual volume of water at the feed side ($V_{r,f}$) is 155.5 mL.

As previously mentioned, the concentration of heavy metal in the feed solution (C_f) required by Eq. (3) was measured before ($C_{f,i}$) and after the experiment ($C_{f,f}$). In principle, since ΔV_d was much less than the feed solution's initial volume ($V_{f,i}$), the $C_{f,i}$ and $C_{f,f}$ should be similar. However, we hypothesized that heavy metals could be rejected, size exclusion/Donnan potential and membrane adsorption. The mass of heavy metal adsorbed by the membrane (m_{ads}) was evaluated by performing a mass balance on the heavy metal:

$$m_{ads} = C_{f,i}(V_{f,i}) - C_d \Delta V_d - C_{f,f}(V_{f,i} + V_{r,f} - \Delta V_d) \quad (6)$$

3.2.5. Rejection of heavy metals in NF process

As previously described, the TFC and TFN membranes were synthesized using PIP as a water-soluble monomer in the IP. As such, they are nanofiltration (NF) membranes. Therefore, in addition to rejecting heavy metals in FO experiments, we also performed some comparative and NF tests to determine copper rejection from a 200 ppm copper (II) sulphate pentahydrate ($CuSO_4.5H_2O$) solution using TFC and TFN(0.05%) membranes. The experiments were performed in a continuous cross-flow filtration system shown in Figure 3-5. The system consists of 3 parallel cells, the effective permeation area in each cell is 17.35 cm^2. The experiments were carried out at 24 ± 2 °C and 10 ±1 bar. The rejection of heavy metal was evaluated using Eq. (3). Like the FO tests, the copper concentrations in the feed (C_f) and the permeate (C_p) were determined using ICP-MS. The feed and permeate samples for the ICP-MS analysis were taken once the system reached steady-state as determined by the constant permeate flow rate.

Of the four types of membranes (Table 3-1), TFC and TFN(0.05%) membranes were used in NF experiments. For each membrane, six coupons fabricated in two independent syntheses were tested.

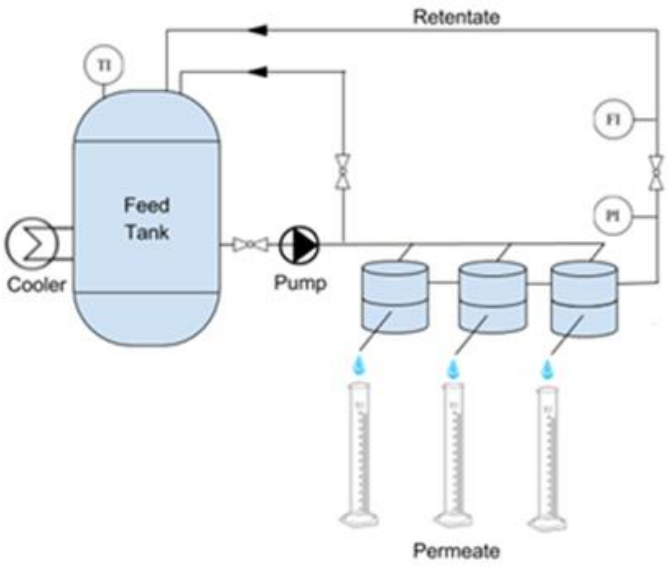

Figure 3-5. Cross-flow NF membrane testing system, PI, FI and, TI stands for pressure, flow and temperature indicator, respectively [14]

3.2.6. Characterization of membrane and nanoparticles

To confirm and find the functionalized HNTs percentage, a Q5000 thermal gravimetric analyzer (TGA) (TA Instruments Ltd, USA) was used. Under the nitrogen atmosphere, the heating rate was 10°C/min from 30°C to 800°C. The morphology of the membrane's top surface was evaluated by using scanning electron microscopy (SEM). All of the samples were coated by gold sputtering. Also, the morphology of the nanoparticle was characterized using transmission electron microscopy (TEM), Philips CM30. Attenuated Total Reflection-Fourier Transform Infrared (ATR-FTIR) spectra of the membranes and NPs were obtained using a Nicolet 6700 FTIR with a diamond crystal (Thermo Fisher) equipment. OMNIC ™ software was utilized to analyze the spectra. To investigate the TFC and TFN membranes' hydrophilicity, VCA Optima goniometer (AST products, Inc., Billerica, MA) was used. The zeta potential of the surface of membranes was also conducted by a zeta analyzer (Zetasizer PSS0012-22, Malvern Instruments).

3.3. Results and discussion

3.3.1. Nanoparticle characterization

Nanoparticles characterization was already discussed in Chapter 2. Briefly, the SEM images indicated that the first generation of the PAMAM dendrimers did not change the shape of HNTs. The TGA analysis showed a higher mass loss of HNTs-G1 than HNTs. The difference in mass loss could be attributed to the decomposition of the first generation of PAMAM dendrimers. The ATR-FTIR spectrum HNTs-G1 revealed two peaks (not present in the spectrum of HNTs) at 1646 and 1562 cm^{-1}. These peaks result from the N–H bond's stretching vibrations and bending vibrations of the C–N bond, which confirmed the successful modification of the HNTs. Furthermore, functionalization of HNTs with the first generation of PAMAM dendrimers leads to an increase of zeta potential from -34.5 mV to 2.2 mV.

3.3.2. Membrane Characterization

Similar to nanoparticles, physicochemical characterization (SEM, FTIR, water contact angle, and zeta potential) of TFC and TFN membranes was discussed in Chapter 2. Briefly, the SEM images revealed a nodular structure of the surface of TFC and TFN membranes, typical for polyamide-based NF membranes [15,16]. The nodular structure results from a fast and uniform crosslinking between the two monomers of TMC and PIP [17]. The FTIR analysis confirmed the successful formation of the polyamide layer in the TFC and TFN membranes. The water contact angle measurements revealed that the incorporation of nanoparticles increased the membranes' hydrophilicity of the resulting membranes. Finally, the zeta potential measurements showed a decrease in zeta potential with an increase in pH. The zeta potential of TFN membranes was more sensitive to the pH of the solution. TFN membranes' zeta potential was slightly higher than that of the TFC membrane at a pH of 5.5 – 6.0, which is the feed solution's pH during the actual performance experiments. There was no clear trend between the zeta potential and the loading of NPs in the TFN membranes.

3.3.3. FO performance

The FO performance of the membranes strongly depends on a draw solute. The latter should generate high osmotic pressure while the permeation of salt across the membrane is minimized. Chapter 2 studied the NF performance of TFC and TFN membranes, which are also used in FO tests considered in this Chapter. Of the three solutes studied in Chapter 2, NaCl could generate the highest osmotic pressure but is poorly rejected by our TFC and TFN membranes. Therefore, NaCl is not suitable as a draw solute in our tests. Of the remaining two solutes, our TFC and TFN membranes showed higher rejection of Na_2SO_4 than $MgCl_2$. Simultaneously, since $MgCl_2$ has a smaller molecular weight than Na_2SO_4, for the same weight percentage of the two solutes, according to the van't Hoff equation, $MgCl_2$ could generate a higher osmotic pressure Na_2SO_4 [9]. Although the rejection of Na_2SO_4 was greater than $MgCl_2$, it was still higher than 85% for TFC and 90% for TFN membranes. Therefore, we selected $MgCl_2$ as a draw solute and used 1 $mol.L^{-1}$ of $MgCl_2$ in DI water as a draw solution in all FO experiments.

Figure 3-6 shows the progress of the dynamic FO experiments with the TFC membrane using DI water as a feed (Fig 3-6. A) and a 200 ppm $CuSO_4.5H_2O$ (Fig3-6. B). The processing of the raw experimental data is described elsewhere [12]. It can be noticed that in both experiments, the steady-state is established immediately after the initiation of the experiment. A constant water mass increase at the draw-side and a constant mass decrease at the feed-side indicate the steady-state conditions. Since the water permeates from the feed side to the draw side, the observed slopes are the same but have the opposite sign. The most remarkable observation in Fig3-6. is that the water flux in the experiment with the feed containing Pb^{2+} is higher than in the experiment with DI water as a feed. In principle, heavy metal salt in the feed solution decreases the osmotic pressure difference across the membrane. As a result, one could expect the water flux in the experiment with pure water to be higher than with the experiment with a heavy metal salt solution in the feed.

Figure 3-7 presents the progress of the same dynamic FO experiments with the TFC membrane as Figure 3-6, focusing on the reverse salt flux of the draw solute ($MgCl_2$) as a function of time. Unlike the water flux, it takes several minutes for $MgCl_2$ transport to become constant, particularly in the experiment with DI water as a feed. The instantaneous mass of $MgCl_2$ in the feed solution is a product of the instantaneous volume and concentration of $MgCl_2$. The presence of heavy metal

in the feed solution suppresses the reverse of $MgCl_2$, which is very desirable. When analyzing the experiment results with the feed containing 200 ppm $CuSO_4.5H_2O$, we assumed that the membrane completely rejects the heavy metal salt. In other words, the changes in the feed solution's conductivity are solely determined by the transport of $MgCl_2$ from the draw to the feed solution. As previously mentioned, one of the concerns with using $MgCl_2$ as a draw solute was its incomplete rejection by our membranes in the NF experiments. However, it appears that the presence of heavy metal in the feed solution partially alleviates this problem.

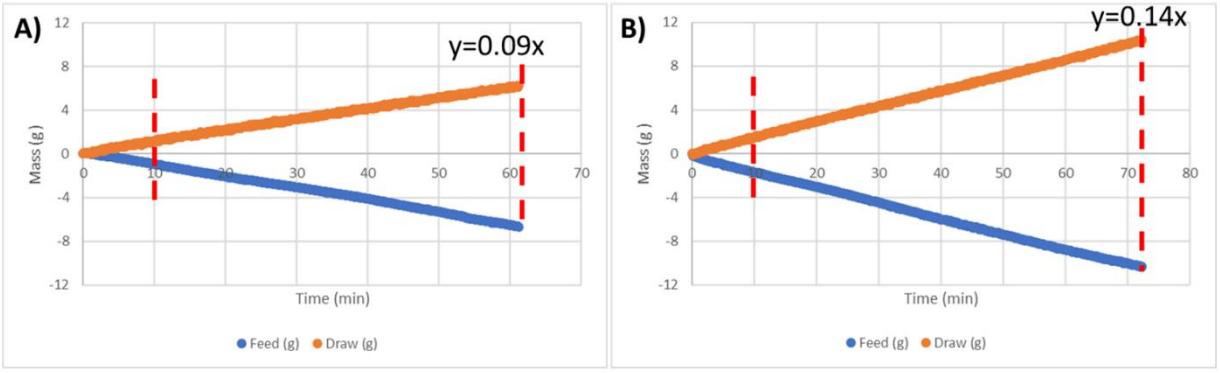

Figure 3-6. Progress of dynamic FO experiments using a TFC membrane in the AL-FS orientation; the mass of the feed and draw solutions as a function of time. Draw solution: 1 M $MgCl_2$. **A)** DI water as a feed; **B)** 200 ppm $CuSO_4.5H_2O$ solution as a feed.

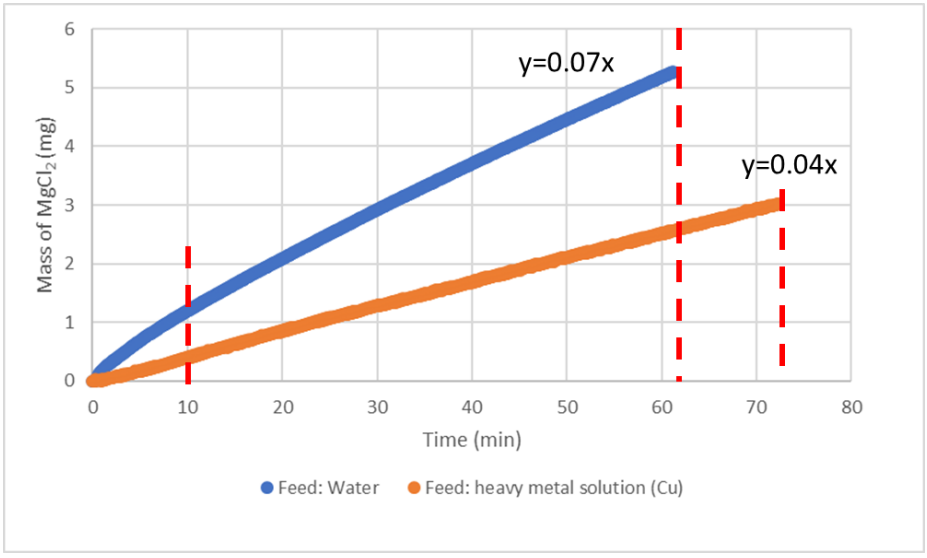

Figure 3-7. Progress of dynamic FO experiments using a TFC membrane in the AL-FS orientation; the mass of $MgCl_2$ as a function of time. Draw solution: 1 M $MgCl_2$. **Blueline:** DI water as a feed; **Orangeline:** 200 ppm $CuSO_4.5H_2O$ solution as a feed.

Table A1 in the appendix shows the results (steady-state water flux and reverse salt flux) of all 32 FO experiments. The results are then summarized in Figure 3-8 and Figure 3-9, which show the average water flux and the average reverse salt flux, respectively, for TFC and TFN membranes. Figure 3-8 confirms that heavy metal salt in the feed solution enhances the water flux. For TFC membranes, the water flux increases in the following: DI water < $Pb(NO_3)_2$ solution < $CuSO_4.5H_2O$ solution. For TFN membranes, the water flux for the $Pb(NO_3)_2$ solution is higher than for the $CuSO_4.5H_2O$ solution. The latter order coincides with the heavy metal concentration in the feed solution (Table 3-2). There is no clear trend between the water flux and the loading of HNT-G1. However, the positive effect of the heavy metal in the feed on the water flux is undeniable.

As determined by the zeta potential analysis, both TFC and TFN membranes are negatively charged. It is, therefore, possible that heavy metal cations are adsorbed on the surface of the membranes. In turn, these adsorbed cations would enhance the water flux across the membrane. It is important to note that the observed water fluxes of less than 4 $L.m^{-2}.hr^{-1}$ are relatively low for FO processes. Nonwoven support, a part of commercial PS35 membranes on which TFC and TFN membranes were synthesized, is responsible for internal concentration polarization (ICP). The latter significantly reduces the effective osmotic pressure gradient, the driving force for water transport in FO processes [4].

As shown in Figure 3-9, the effect of heavy metals in feed solution on the reverse $MgCl_2$ flux is even more significant than on the water flux. More importantly, the undesirable reverse salt flux is significantly reduced in the presence of heavy metals. For both TFC and TFN membranes, the reverse $MgCl_2$ flux decreases in the following order DI water > $CuSO_4.5H_2O$ solution > $Pb(NO_3)_2$ solution. There is no clear trend between the loading of HNTs-G1 and the reverse salt flux. However, the reverse $MgCl_2$ flux in the presence of $Pb(NO_3)_2$ solution can be as low as 1/6 of that with DI water as a feed. Similar to the increase in the water flux, a decrease in the reverse $MgCl_2$ flux in the presence of heavy metal salt in the feed solution can be explained by the adsorption of heavy metal cations on the membrane surface. The adsorbed Cu^{2+} or Pb^{2+} would facilitate the rejection of Mg^{2+} cations based on charge repulsion. To maintain the electroneutrality, Cl^- anions would remain at the draw side of the membrane.

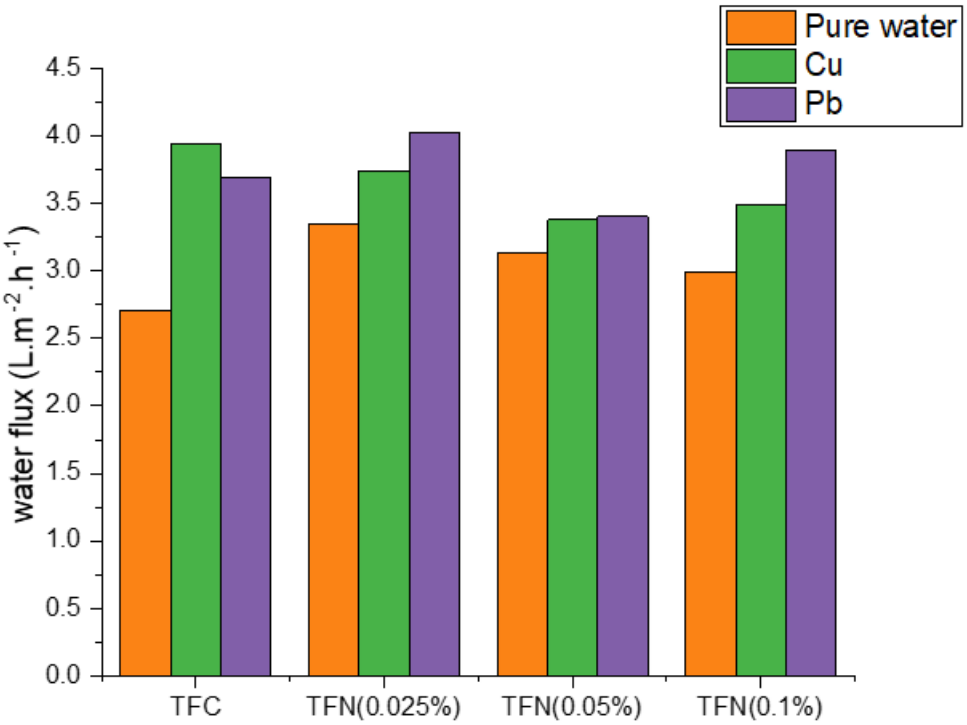

Figure 3-8. The average water flux of TFC and TFN membranes using the different feed. **Orange:** DI water; **green:** 200 ppm $CuSO_4.5H_2O$ solution; **purple:** 200 ppm $Pb(NO_3)_2$ solution. Draw solution in all experiments: 1 mol. L^{-1} $MgCl_2$.

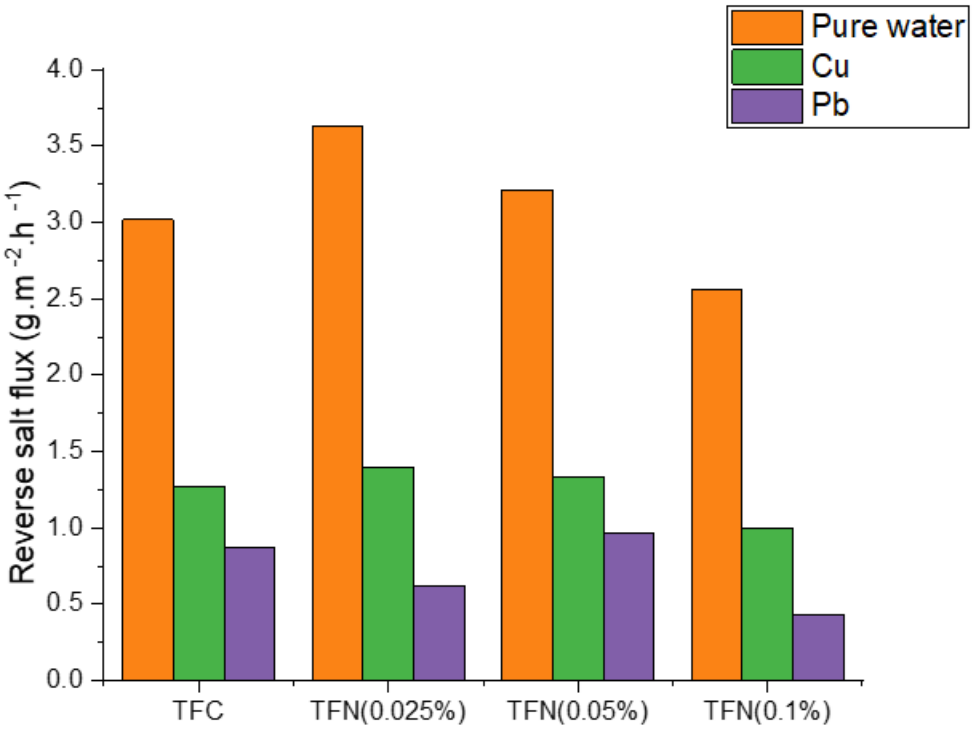

Figure 3-9. The average reverse flux of $MgCl_2$ TFC and TFN membranes using the different feeds. **Orange:** DI water; **green:** 200 ppm $CuSO_4.5H_2O$ solution; **purple:** 200 ppm $Pb(NO_3)_2$ solution. Draw solution in all experiments: 1 mol. L^{-1} $MgCl_2$.

3.3.4. Rejection of heavy metals in FO and NF processes

The presence of heavy metal cations in feed solution improves the FO performance of TFC and TFN membranes. However, the membrane's primary role in the FO process is to reject heavy metals while allowing water to permeate from the feed to the draw solution.

The rejection of heavy metals in the FO and NF processes was evaluated based on the concentration of heavy metal ions determined using ICP-MS. Table 3-3 presents the summary of concentrations in the initial feed solution (before initiation of the experiment), the final feed solution, and the final draw solution, along with the calculated rejection and absorption of the heavy metal in each FO experiment. Two experiments were performed using two independently fabricated membranes for a given type of membrane and heavy metal. It is important to note that the initial feed concentrations in Table 3-3 are lower than the calculated feed concentrations listed in Table 3-2. The difference arises from the dilution of the feed solution by the DI water present in the system [13]. Unless otherwise stated, the calculated rejections use the initial feed concentration, which should be similar to the final feed concentration. It is evident that $C_{f,i}$ was markedly higher than $C_{f,f}$. For a given final draw solution concentration, the rejection increases as the feed concentration increases. However, in all cases, the rejection calculated using $C_{f,i}$ was less than 1% greater than the rejection calculated using $c_{f,f}$. For example, in three FO experiments listed in Table 3-3, we did not record $C_{f,i}$, and the rejection was calculated using $C_{f,f}$. The corresponding rejections are similar to values calculated using $C_{f,i}$.

Since all experiments' rejections were greater than 90%, the difference between $C_{f,i}$ and $C_{f,f}$ suggests adsorption of heavy metals by the membranes. The adsorption was quantified by the mass balance on heavy metal using Eq. (6). For the three experiments in which we did not record $C_{f,i}$, the adsorption is not available. The membranes adsorbed both Pb^{2+} and Cu^{2+}, but the mass of adsorbed Pb^{2+} was 3 – 4 times the mass of adsorbed Cu^{2+}. The exact concentration of the heavy metal salt was used in all experiments, but because of the molecular weight difference between the respective salts, the initial concentration of Pb^{2+} in the feed was 2 – 2.5 times the initial

concentration of Cu^{2+}. Therefore, it appears that Pb^{2+} is more adsorbed by the TFC and TFN membranes than Cu^{2+}. In both cases, the membranes' adsorption can be attributed to amine groups' chelation reaction with heavy metal catios [18]. The results presented in Table 3-3 confirm the adsorption of heavy metals by the membrane, which is likely responsible for the improved FO performance of the membranes in the presence of heavy metals in the feed solution.

Table 3-3. Summary rejection and adsorption of heavy metals TFC and TFN membranes in FO experiments.

Membrane	**Heavy metal**	**Initial feed concentration (ppm)**	**Final feed concentration (ppm)**	**Final draw concentration (ppm)**	**Adsorption (mg)**	**Rejection (%)**
TFC	Pb^1	111.1	75.51	0.010	23.7	**97.4**
	Cu^1	N.A.	37.73	0.006	N.A.	**96.9***
	Pb^2	N.A.	92.53	0.020	N.A.	**97.7***
	Cu^2	40.22	34.39	0.020	4.17	**95.1**
TFN(0.025%)	Pb^1	104.3	89.76	0.040	10.8	**97.3**
	Cu^1	41.47	35.26	0.006	4.33	**98.1**
	Pb^2	102.9	78.64	0.040	16.5	**94.8**
	Cu^2	42.04	34.17	0.006	5.44	**98.4**
TFN(0.05%)	Pb^1	101.8	76.51	0.040	17.1	**94.4**
	Cu^1	41.02	34.37	0.006	4.60	**97.9**
	Pb^2	99.27	77.60	0.030	14.7	**95.0**
	Cu^2	42.78	34.47	0.006	5.72	**98.2**
TFN(0.1%)	Pb^1	101.3	79.75	0.040	14.9	**96.1**
	Cu^1	N.A.	35.43	0.010	N.A.	**97.0***
	Pb^2	102.1	80.02	0.040	15.2	**95.7**
	Cu^2	39.04	34.42	0.006	3.23	**97.3**

[1] Comes from sheet 1
[2] Comes from sheet 2
* The rejection based on the final feed solution concetration

Figure 3-10 presents the average rejections of Cu^{2+} and Pb^{2+} by TFC and TFN membranes in FO tests. It is important to emphasize that the rejection of heavy metals is enhanced by their adsorption on the membrane surface. The average rejection of Pb^{2+} by TFC membranes is higher than Cu^{2+}. On the other hand, for TFN membranes, the situation is the opposite; the average rejection of Cu^{2+} by TFN membranes is higher than Pb^{2+}. As a result, the rejection of Pb^{2+} by TFC membranes is

higher than by TFN membranes. On the other hand, the rejection of Cu^{2+} by TFN membranes is higher than by TFC membranes. The average rejections range from 95%, Pb^{2+} by TFN(0.05%), to 98%, Cu^{2+} by TFN(0,025%). However, there is no apparent trend between the loading of HNTs-G1 and heavy metal rejection by the membranes.

In addition to the rejection of heavy metals in FO experiments, we also tested 6 TFC and 6 TFN(0.05%) membranes in NF experiments with a 200 ppm $CuSO_4.5H_2O$ feed solution at 10 bar. The average rejection of Cu^{2+} by the TFC membranes was 96.25%, comparable to the corresponding value in the FO tests. On the other hand, the average rejection of Cu^{2+} by the TFN(0.05) membranes was only 92.89%, considerably lower than 98% by the same membranes in the FO tets. A lower rejection of heavy metals in NF compared to FO could be expected. In both processes, the transport of heavy metals is driven by the concentration gradient across the membrane. Besides, heavy metals might also be dragged along the permeating water in the NF process, driven by the hydraulic pressure gradient across the membrane.

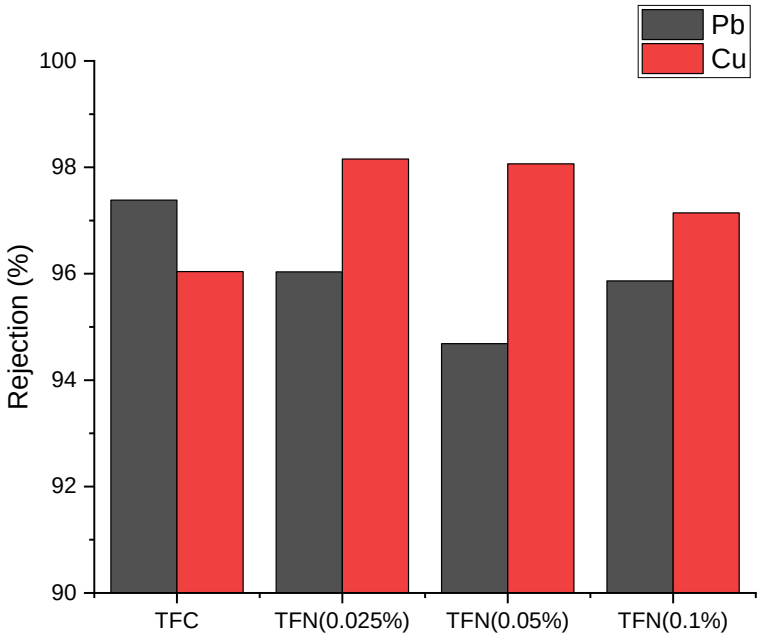

Figure 3-10. The average rejections of Cu^{2+} and Pb^{2+} by TFC and TFN membranes in FO tests.

3.4. Conclusions and Recommendations

The TFN membranes were fabricated on top of a commercial PS35 ultrafiltration membrane by in-situ interfacial polymerization of piperazine (PIP) and 1,3,5-benzenetricarbonyl trichloride (TMC) containing different amounts of dispersed functionalized halloysite nanotubes (HNTs) nanoparticles. The HNTs nanoparticles were functionalized with the first generation of poly(amidoamine) (PAMAM) dendrimers. Since the TFN and the reference TFC membranes exhibited good nanofiltration performance with $MgCl_2$ and Na_2SO_4 solutions, they were considered for the removal of heavy metals (Cu and Pb) from synthetic wastewater in dynamic forward osmosis experiments.

The membranes showed excellent rejections of Cu and Pb, ranging from 95% to 98%. The TFN membranes showed higher rejection to Cu than Pb, while the opposite was observed for the reference TFC membranes. In comparison, the rejection of Cu by TFN membranes in nanofiltration tests was 93%, thus lower than in the FO process. The presence of heavy metal in the feed solution enhanced the FO performance of all membranes. In particular, the reverse flux of draw solute ($MgCl_2$) decreased by at least 2.5 times compared to the experiments with pure water as a feed. Simultaneously, the water flux also increased. The improved FO performance of the membranes in the presence of heavy metals is attributed to their adsorption by the membranes. The adsorption of heavy metals was confirmed and quantified by the mass balance. All membranes showed a greater affinity towards Pb than Cu.

Although the mass balance proved the adsorption of heavy metals by membranes, it is recommended to perform an ICP-MS analysis of the membranes tested with feed solutions containing Cu and Pb cations, respectively. These tests would provide direct proof of heavy metal adsorption by the membranes. Also, if the membranes adsorb heavy metal cations, these membranes' zeta potential may be affected. Therefore, a systematic zeta potential investigation of membranes exposed to heavy metals and those that were tested with pure water is also recommended. In addition to providing another confirmation of heavy metal adsorption, this investigation could further elucidate the observed improvement of the membranes' FO performance exposed to feed solutions containing heavy metal.

3.5. Acknowledgment

The authors gratefully acknowledge the financial support provided by the Natural Science and Engineering Research Council (NSERC) Canada, Discovery Grant (DG), Grant number: 04443.

3.6. Appendix

Table A3-4. Summary of FO performance of TFC and TFN membranes in the experiments with pure water and 200 ppm solutions of $Pb(NO_3)_2$ and $CuSO_4.5H_2O$ as a feed. In all experiments, the draw was 1 $mol.L^{-1}$ $MgCl_2$ solution.

Membrane	Feed solution	Water flux ($L.m^{-2}.hr^{-1}$)	Reverse salt flux ($gr.m^{-2}.hr^{-1}$)
TFC *(1)	**Water**	1.8	3.72
	Water	2.15	3.29
	Cu	3.7	1.22
	Pb	3.4	1.04
TFC*(2)	**Water**	3.8	2.32
	Water	3.1	2.74
	Cu	4.1	1.33
	Pb	3.9	0.7
TFN(0.025)*(1)	**Water**	3.2	5.35
	Water	3.1	4.38
	Cu	3.5	2.04
	Pb	4.4	0.79
TFN(0.025)*(2)	**Water**	3.3	2.26
	Water	3.8	2.53
	Cu	3.9	0.76
	Pb	3.5	0.46
TFN(0.05)*(1)	**Water**	3.4	3.69
	Water	3.2	3.35
	Cu	3.06	1.69
	Pb	3.59	0.97
TFN(0.05)*(2)	**Water**	3.14	2.45
	Water	2.8	3.36
	Cu	3.7	0.98
	Pb	3.22	0.96
TFN(0.1)*(1)	**Water**	2.8	2.25
	Water	3.47	2.05
	Cu	4.1	0.99
	Pb	3.3	0.29
TFN(0.1)*(2)	**Water**	2.7	3.25
	Water	3.02	2.71
	Cu	2.89	1.003
	Pb	4.1	0.58

3.7. References

[1] F. Fu, Q. Wang, Removal of heavy metal ions from wastewaters: A review, J. Environ. Manage. 92 (2011) 407–418. https://doi.org/10.1016/j.jenvman.2010.11.011.

[2] N. Abdullah, N. Yusof, W.J. Lau, J. Jaafar, A.F. Ismail, Recent trends of heavy metal removal from water/wastewater by membrane technologies, J. Ind. Eng. Chem. 76 (2019) 17–38. https://doi.org/10.1016/j.jiec.2019.03.029.

[3] M. Peydayesh, T. Mohammadi, S.K. Nikouzad, A positively charged composite loose nanofiltration membrane for water purification from heavy metals, J. Memb. Sci. 611 (2020) 118205. https://doi.org/10.1016/j.memsci.2020.118205.

[4] W.N.A.S. Abdullah, S. Tiandee, W. Lau, F. Aziz, A.F. Ismail, Potential use of nanofiltration like-forward osmosis membranes for copper ion removal, Chinese J. Chem. Eng. 28 (2020) 420–428. https://doi.org/10.1016/j.cjche.2019.05.016.

[5] M. Ghanbari, D. Emadzadeh, W.J. Lau, H. Riazi, D. Almasi, A.F. Ismail, Minimizing structural parameter of thin film composite forward osmosis membranes using polysulfone/halloysite nanotubes as membrane substrates, Desalination. 377 (2016) 152–162. https://doi.org/10.1016/j.desal.2015.09.019.

[6] D. Emadzadeh, W.J. Lau, M. Rahbari-Sisakht, H. Ilbeygi, D. Rana, T. Matsuura, A.F. Ismail, Synthesis, modification and optimization of titanate nanotubes-polyamide thin film nanocomposite (TFN) membrane for forward osmosis (FO) application, Chem. Eng. J. 281 (2015) 243–251. https://doi.org/10.1016/j.cej.2015.06.035.

[7] D. Emadzadeh, W.J. Lau, M. Rahbari-Sisakht, A. Daneshfar, M. Ghanbari, A. Mayahi, T. Matsuura, A.F. Ismail, A novel thin film nanocomposite reverse osmosis membrane with superior anti-organic fouling affinity for water desalination, Desalination. 368 (2015) 106–113. https://doi.org/10.1016/j.desal.2014.11.019.

[8] D. Emadzadeh, M. Ghanbari, W.J. Lau, M. Rahbari-Sisakht, T. Matsuura, A.F. Ismail, B. Kruczek, Solvothermal synthesis of nanoporous TiO2: The impact on thin-film composite membranes for engineered osmosis application, Nanotechnology. 27 (2016). https://doi.org/10.1088/0957-4484/27/34/345702.

[9] W.N.A.S. Abdullah, W.J. Lau, F. Aziz, D. Emadzadeh, A.F. Ismail, Performance of Nanofiltration-Like Forward-Osmosis Membranes for Aerobically Treated Palm Oil Mill Effluent, Chem. Eng. Technol. 41 (2018) 303–312. https://doi.org/10.1002/ceat.201700339.

[10] L. Setiawan, R. Wang, K. Li, A.G. Fane, Fabrication of novel poly(amide-imide) forward osmosis hollow fiber membranes with a positively charged nanofiltration-like selective layer, J. Memb. Sci. 369 (2011) 196–205. https://doi.org/10.1016/j.memsci.2010.11.067.

[11] J. Su, Q. Yang, J.F. Teo, T. Chung, Cellulose acetate nanofiltration hollow fiber membranes for forward osmosis processes, J. Memb. Sci. 355 (2010) 36–44.

https://doi.org/10.1016/j.memsci.2010.03.003.

[12] F. Shahamati Fard, S. Akbari, E. Pajootan, M. Arami, Enhanced acidic dye adsorption onto the dendrimer-based modified halloysite nanotubes, Desalin. Water Treat. 57 (2016) 26222–26239. https://doi.org/10.1080/19443994.2016.1160437.

[13] D. Bai, F. Asempour, B. Kruczek, Can the time-lag method be used for the characterization of liquid permeation membranes?, Chem. Eng. Res. Des. 162 (2020) 228–237. https://doi.org/10.1016/j.cherd.2020.08.012.

[14] F. Asempour, D. Emadzadeh, T. Matsuura, B. Kruczek, Synthesis and characterization of novel Cellulose Nanocrystals-based Thin Film Nanocomposite membranes for reverse osmosis applications, Desalination. 439 (2018) 179–187. https://doi.org/10.1016/j.desal.2018.04.009.

[15] L. Bai, Y. Liu, N. Bossa, A. Ding, N. Ren, G. Li, H. Liang, M.R. Wiesner, Incorporation of Cellulose Nanocrystals (CNCs) into the Polyamide Layer of Thin-Film Composite (TFC) Nanofiltration Membranes for Enhanced Separation Performance and Antifouling Properties, Environ. Sci. Technol. 52 (2018) 11178–11187. https://doi.org/10.1021/acs.est.8b04102.

[16] X.Q. Cheng, L. Shao, C.H. Lau, High flux polyethylene glycol based nanofiltration membranes for water environmental remediation, J. Memb. Sci. 476 (2015) 95–104. https://doi.org/10.1016/j.memsci.2014.11.020.

[17] Y. ling Liu, Y. ying Zhao, X. mao Wang, X. hua Wen, X. Huang, Y.F. Xie, Effect of varying piperazine concentration and post-modification on prepared nanofiltration membranes in selectively rejecting organic micropollutants and salts, J. Memb. Sci. 582 (2019) 274–283. https://doi.org/10.1016/j.memsci.2019.04.018.

[18] M. Qiu, C. He, Efficient removal of heavy metal ions by forward osmosis membrane with a polydopamine modified zeolitic imidazolate framework incorporated selective layer, J. Hazard. Mater. 367 (2019) 339–347. https://doi.org/10.1016/j.jhazmat.2018.12.096.

Chapter 4. General Discussion, Conclusion, and Recommendations

This research's main objective was to develop a membrane to remove heavy metals from wastewater in a hybrid FO-NF process. Processing the wastewater in an FO process, which does not require applied hydraulic pressure, minimizes membrane fouling, one of the significant challenges of membrane-based wastewater treatment. The FO membrane must reject heavy metals and draw solutes. Consequently, we developed the FO membrane by considering its NF performance. Simultaneously, in the proposed hybrid FO-NF process, pure water is produced in the NF step, concentrating the draw solution for the FO process. Therefore, the membrane's NF performance has a dual role; as a tool to design the membrane's selective layer and as a critical element of the proposed FO-NF process.

We selected thin-film nanocomposite (TFN) membranes utilizing halloysite nanotubes (HNTs) modified by the first generation of poly(amidoamine) (PAMAM) dendrimers as nanoparticles for the proposed hybrid FO-NF process. The TFN membranes were fabricated via in situ interfacial polymerizations of PIP and TMC monomers on top of the PS35 ultrafiltration membrane. The nanoparticles were dispersed in the hexane solution of TMC before the interfacial polymerization. The selection of nanoparticles for this project resulted from their successful application in another project, in which we synthesized TFN RO membranes with improved chlorine resistance. The recently published article summarizing the other project is presented in Appendix.

In the first part of the thesis (Chapter 2.), we studied the effect of nanoparticle loading on the NF performance of the reference TFC and TFN membranes. We considered $MgCl_2$, Na_2SO_4, and NaCl as solutes in the performance experiments. All membranes showed high rejections of Na_2SO_4 (around 97-98%) and low NaCl rejections (less than 40%), with the corresponding water fluxes greater than 100 L m^{-2} hr^{-1}. The rejection of $MgCl_2$ (ranging from 82 to 90%) was less than Na_2SO_4. However, our values are much greater than those reported in the literature for other TFN membranes. Since for the same weight percentage in aqueous solution, the osmotic pressure $MgCl_2$ is much greater than Na_2SO_4; the former is more desirable as a draw solute than the latter. The remarkable rejections of $MgCl_2$ are attributed to a less negative surface charge of TFN membranes. Also, since HNT-G1 nanoparticles are positively charged, their incorporation into the selective

layer helped to reject $MgCl_2$ to the level that is acceptable for its application as a draw solute. By considering the combination of the water flux and $MgCl_2$ rejection, the TFN membrane with 0.05% of nanoparticles loading appears to have the best NF performance.

In the second part of the thesis (Chapter 3.), we tested TFC and TFN membranes in FO experiments using $MgCl_2$ as a draw solute and three different feed solutions. We first used pure water as a feed to determine the water flux and the reverse salt flux. Compared to the reference TFC membrane, TFN membranes had higher water flux and lower reverse salt flux, i.e., showed a better FO performance compared to the reference TFC membrane. As the nanoparticle loading increases, the water flux and the reverse salt flux decrease. Two other sets of FO experiments were with Cu^{2+} and Pb^{2+} in the feed solution, respectively. The membranes showed excellent rejections of Cu and Pb, ranging from 95% to 98%. The TFN membranes showed higher rejection to Cu than Pb, while the opposite was observed for the reference TFC membranes. In comparison, the rejection of Cu by TFN membranes in nanofiltration tests was 93%, thus lower than in the FO process. The presence of heavy metal in the feed solution enhanced the FO performance of all membranes. In particular, the reverse flux of draw solute ($MgCl_2$) decreased by at least 2.5 times compared to the experiments with pure water as a feed. Simultaneously, the water flux also increased. The improved FO performance of the membranes in the presence of heavy metals is attributed to their adsorption by the membranes. The adsorption of heavy metals was confirmed and quantified by the mass balance. All membranes showed a greater affinity towards Pb than Cu.

We have therefore validated the primary assumption of this research. The selective layer of TFC and TFN membranes can be optimized by considering the membranes' NF performance. More importantly, our results indicate that the FO treatment of wastewater containing heavy metals is advantageous to the NF treatment because of reduced membrane fouling and a higher rejection of heavy metals by the same membrane. Therefore, this thesis justifies using the hybrid FO-NF process for the recovery of heavy metals from wastewaters.

In this research, we used the same membrane for both the FO and NF steps. The membranes were synthesized on a commercial UF (PS35) membrane. The UF membrane consists of a nonwoven polyester layer, which is integral to the actual polysulfone membrane. The nonwoven layer provides mechanical support in pressure-driven membrane processes. It does not affect membrane

productivity in NF and RO applications. However, the nonwoven layer generates internal concentration polarization (ICP), significantly reducing the water flux in FO applications. Therefore, in the next phase of this research, it will be necessary to develop a support layer (asymmetric PS membrane) with a similar structure as the PS35 membrane without the nonwoven layer.

This research demonstrated the concept of a hybrid FO-NF system by studying the NF and FO performance in separate membrane experiments. To further demonstrate this concept, it is recommended to design and build a lab-scale system (Fig. 1 in Chapter 1) for the continuous processing of synthetic wastewater containing heavy metals while circulating the draw solution between the FO and the NF processes.

Appendix

Journal of Membrane Science 623 (2021) 119039

Contents lists available at ScienceDirect

Journal of Membrane Science

journal homepage: http://www.elsevier.com/locate/memsci

Chlorine-resistant TFN RO membranes containing modified poly (amidoamine) dendrimer-functionalized halloysite nanotubes

Farhad Asempour [a,b], Somaye Akbari [c,**], Mohammad Hassan Kanani-Jazi [c], Amirsajad Atashgar [a], Takeshi Matsuura [a,d], Boguslaw Kruczek [a,*]

[a] Department of Chemical and Biological Engineering, University of Ottawa, 161 Louis Pasteur, ON, K1N 6N5, Canada
[b] Department of Chemical Engineering, McGill University, 3610 University St, Montréal, QC, H3A 0C5, Canada
[c] Textile Engineering Department, Amirkabir University (Polytechnic Tehran), 424 Hafez Ave, Tehran, Iran
[d] Advanced Membrane Technology Research Center (AMTEC), Universiti Teknologi Malaysia, 81310, Skudai, Johor, Malaysia

ARTICLE INFO

Keywords:
Reverse osmosis
Membrane
Chlorine
Thin film nanocomposite
PAMAM dendrimers

ABSTRACT

Incorporation of additional amines into polyamide-based reverse osmosis (RO) membranes has been suggested as a strategy to increase the chlorine resistance of such membranes. In this work, we investigate the effects of the poly(amidoamine) PAMAM dendrimers of different generations on the separation performance and chlorine resistance of thin-film nanocomposite (TFN) membranes. Three generations of PAMAM dendrimers were grafted on halloysite nanotubes (HNTs) and incorporated into the reverse osmosis (RO) membranes synthesized by interfacial polymerization of m-phenylenediamine (MPD) and trimesoyl chloride (TMC). ATR-FTIR, SEM, XPS, TGA, and surface contact angle analyses were used to characterize the physicochemical properties of the nanoparticles and membranes. Membranes' separation performance was tested in a cross-flow RO system with synthetic brackish water. Compared to thin-film composite (TFC) membranes, TFN membranes showed a two-fold increase in water flux with a slight decrease in NaCl rejection. In addition, passive chlorination tests showed that the overall effects of chlorination on membrane performance varied based on the generation of the PAMAM dendrimers. After 12,000 ppm.h chlorine exposure, a decrease in salt rejection with an increase in the water flux of the control TFC membrane was observed. In contrast, membranes with the second and third generations of PAMAM dendrimers (TFN-HNT-G2 & G3) displayed enhanced membrane stability with no statistically significant alteration in their salt rejection after chlorination. TFN-HNT-G2 had the optimum overall desalination performance after chlorination with ~85.6% water flux improvement while maintaining its average salt rejection of 96.6%. The enhanced chlorination resistance of these membranes was attributed to the scavenger role of the extra amine and amide groups from the PAMAM functionalized HNTs.

1. Introduction

Climate change, increasing global water demand, and the contamination of water resources have forced us to search for new freshwater resources [1]. Desalination and water reuse are our limited options to generate new water supplies beyond the available hydrological cycle. Reverse osmosis (RO) is widely used in desalination, water purification, and wastewater treatment [2,3]. Polyamide (PA) based thin film composite (TFC) membranes are currently the predominant RO and nanofiltration (NF) membranes in the industry [4,5]. These multilayered membranes are typically made of a 200 nm-thick and highly crosslinked polyamide layer on top of a porous polysulfone backing and a non-woven polyester web. The PA layer provides selectivity and has a complex microstructure consisting of 3D crumples and voids, while the other layers provide mechanical support [4,6]. Although TFC membranes are known for their high selectivity and water flux, some of their performance challenges are yet to be overcome. One approach to enhance the performance of RO membranes is the incorporation of nanoparticles (NPs) within the PA layer of the resulting thin film nanocomposite (TFN) membranes [7]. TFN membranes have attracted a lot of attention in the past decade with significant permeability improvements [8–13]. However, their use at the industrial scale is still

* Corresponding author.
** Corresponding author.
E-mail addresses: farhad.asempour@mail.mcgill.ca (F. Asempour), akbari_s@aut.ac.ir (S. Akbari), bkruczek@uottawa.ca (B. Kruczek).

https://doi.org/10.1016/j.memsci.2020.119039
Received 24 September 2020; Received in revised form 2 December 2020; Accepted 29 December 2020
Available online 6 January 2021

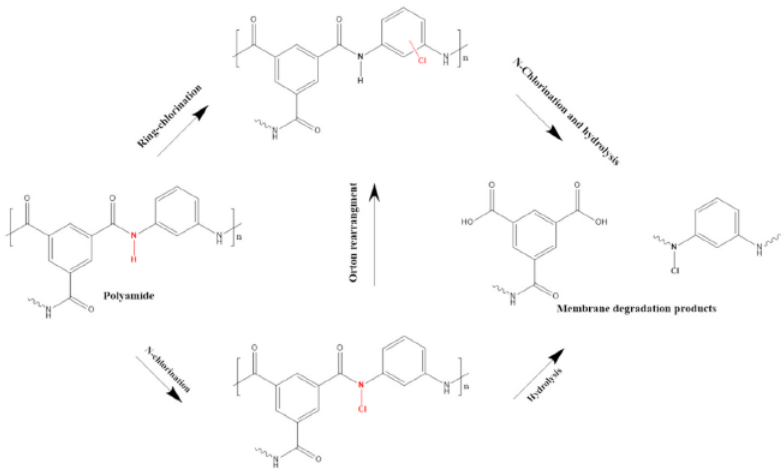

Fig. 1. N-chlorination, ring chlorination, and hydrolysis mechanisms for chlorine attack on PA TFC membranes [5,15].

limited. Concerns about the chemical stability of TFN membranes are of the main limiting factors [9]. For TFN membranes to become more cost-effective and industrially available, they need to possess an enhanced separation performance and have better resistance to chlorine [9,14]. Herein, we are addressing the intolerance to disinfectant and oxidizing agents of the TFC and TFN membranes.

Chlorine exposure reduces the performance of PA-based RO membranes and significantly shortens their lifetime [15,16]. To prevent membrane degradation, water must be dechlorinated before entering the RO modules. The chlorination-dechlorination-rechlorination procedures decrease the efficiency of the RO plants and increase the overall operational costs [17]. A study on 99 industrial or pilot-scale seawater RO membranes autopsies found that membrane oxidation added up to 18% of membrane failure causes [17,18]. A membrane with an enhanced chlorine resistance can effectively eliminate the challenges associated with biofouling by the addition of chlorine in the feed or during the backwash [9]. It is estimated that chlorine resistant membranes could save up to 30% of the total plant costs [17]. Therefore, many studies have been devoted to understand the mechanisms of chlorine attack of the membrane and to develop mitigation strategies [15,17,19–21]. Fig. 1 illustrates the suggested mechanisms of the chlorine attack on PA membranes [15,21]. It is commonly believed that PA degradation mainly involves the secondary amide bonds (–CO–NH–) [8,14,15]. Partially positive $Cl^{\delta+}$, attacks the lone electron pair of the amidic N. Substitution of Cl with H in the amide group, known as N-chlorination, disrupts intermolecular hydrogen bonds of the polymer chain and results in the polymer's free-volume to increase. This may be followed by the hydrolysis and cleavage of the C–N bond. Also, Cl can form chlorinated aromatic rings by directly attacking them or through intramolecular Orton rearrangements. N-chlorination followed by Orton rearrangement is the dominant chlorine uptake mechanism in an acidic environment, while the N-chlorination step is the rate-limiting [15,22]. Ring chlorination causes amide bond scissions, and irreversibly breaks the PA chains [5,15,23,24]. However, ring chlorination is highly unlikely to happen in alkaline conditions [15,22]. Another suggested competing mechanism for the chlorine attack is the chlorine promoted hydrolysis. In this route, chlorine attacks the amidic N and polarizes the amidic C. This facilitates the hydrolysis of the C–N bond [5,21,25–27]. It is safe to suggest that in alkaline conditions, the dominant chlorination mechanisms are N-chlorination. The exact chemical reactions during the chlorine attack heavily depend on the membrane materials, feed water, pH, and chemical composition. It is important to note that the chlorination of PA membranes is still not fully understood, and many conflicting results are reported in the literature [15,17,19].

Various strategies have been suggested to improve the chlorine tolerance of TFC RO membranes, such as the membrane's surface coating, graft polymerization, use of other monomers and tertiary amide groups, and the incorporation of NPs into the membranes [10,20,28,29]. Each of these methods faces certain practical limitations [15,17]. For example, often surface modification by coating and grafting results in the addition of extra resistance to mass transfer and reduction of the permeability [30–32]. Besides, in some cases, grafting reduces salt rejection because it affects the surface charge and lowers the Donnan repulsion effect [30]. The primary objective of incorporating NPs is to improve the membrane's performance. The nature of the NPs, (i.e. size, structure, surface functionality) and loading are of great importance [8–10]. NPs' surface functionality contributes to their uniform dispersion in the PA layer as well as to the formation of chemical bonds with the matrix of the PA [8]. NPs can also have an active role in the interfacial polymerization of PA [8,33]. They affect the degree of the polymer's crosslinking, free volume, crystallinity, and thus overall membrane performance, including chlorine tolerance [8,14,34]. Due to PA's inherent chemical structure, some researchers attempted to graft amino groups on the incorporated NPs [13,34,35]. Park et al. and Kim et al. reported that hyper-branched aromatic PA-grafted silica NPs improved the separation performance and chlorine tolerance of the TFN membranes [36,37]. They argued that the addition of free amino groups increased hydrogen bonds between the polymer chains leading to the enhancement of the chlorine resistance. Although the use of amino-functionalized NPs in TFN membranes has been reported, no systematic study on the effect of the number of amino and amide groups on chlorine-resistance of the resulting membranes is available.

In this work, we examined the effects of incorporating amino groups in TFN membranes by functionalizing halloysite nanotubes (HNTs). HNTs are naturally occurring, tubular, and multilayer aluminosilicates. They have a length ranging from 500 nm to ~1 μm, with the outer and inner diameters of ~60 nm and ~20 nm, respectively. HNTs are abundant, inexpensive, and environmentally friendly [38–40]. Clay particles are proven to be effective nanofillers as they can tailor the hydrophilicity and surface charge of the TFN membranes [40–42]. For example, Ghanbari et al. and Asempour et al. investigated the introduction of HNTs to TFN membranes. HNTs with grafted carboxylic acid and amino groups in the PA layer significantly enhanced the TFN membranes' permeance with slight/no reduction of the selectivity. More importantly, amino groups from the HNTs formed covalent bonds with the monomers and the PA layer [34]. Therefore, we may hypothesize that

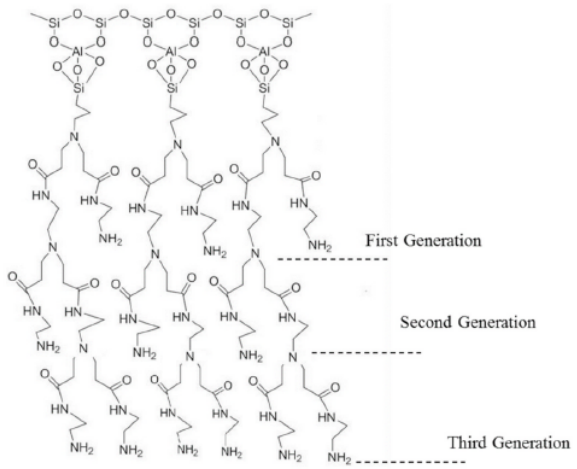

Fig. 2. Schematic representation of HNTs with 1st to 3rd generation of PAMAM functionalization.

the additional amino groups and amide bonds can act as sacrificial agents to mitigate or change a chlorine attack route. This work's novelty is the systematic investigation of the effects of the number of amino groups on the chlorine resistance of TFN membranes. We functionalized HNTs with three different generations of amine-terminated poly(amidoamine) (PAMAM) dendrimers. PAMAM dendrimers are highly branched and symmetrical polymers with a 3-dimensional nanoscopic structure. They are made of iterative constructs of amidoamines terminated by the primary amine groups [43]. Thus, these dendrimers offer an abundant number of primary amine and secondary amide groups in a controlled fashion and can be more reactive to chlorine than the ones from the PA layer [30,44,45].

2. Experimental

2.1. Materials

M-phenylenediamine (MPD) and 1,3,5-benzenetricarbonyl trichloride (TMC), aminopropyltriethoxysilane (APTES), ethanol, diethyl ether, dimethylformamide (DMF), ethylenediamine (EDA), n-hexane, sodium chloride, sodium hypochlorite solution (available chlorine 10–15%), methyl acrylate, ethylenediamine, and 35% hydrochloric acid (HCl) were purchased from Sigma-Aldrich in their respective laboratory reagent grades. HNTs were provided by Delta-Dolsk, Poland. PS35 membrane was purchased from Nanostone Water, Waltham, MA, USA. PS35 is a polysulfone ultrafiltration membrane with a molecular weight cut-off of 20 kDa. Deionized water was used to make the MPD solution, and distilled water was used to rinse and store the membranes as well as to make a chlorine solution, and the synthetic brackish feed water.

2.2. Functionalization of HNTs

Synthesis methods and procedures for the functionalization of HNTs are described in detail elsewhere [34,44]. Briefly, surface modification of HNTs started with an acid treatment, in which HNTs were magnetically stirred with a 35% HCl solution for 24 h and then washed with distilled water and air-dried. The dry acid-treated HNTs were refluxed with a 4/15 (v/v) solution of APTES and toluene for 12 h at 60 °C, which led to the silanization with the APTES and produced HNTs-NH_2. In turn, the amine groups of HNTs-NH_2 acted as a core for growing the dendritic structures in a divergent synthesis route. To synthesize the 1st generation PAMAM dendrimers on HNTs (HNT-G1), 15 mL of methyl acrylate was reacted with 32.15 g of HNTs-NH_2 in ethanol for 24 h at 60 °C. The resulting NPs, acrylated HNTs, were separated from the reaction mixture by centrifugation, washed with diethyl ether, ethanol, and methanol, and recovered by centrifuging. After air-drying at 60 °C, the acrylated HNTs were reacted with a solution of ethylenediamine (5 mL) and ethanol (50 mL) at 60 °C under continuous stirring for 24 h. The reaction mixture was centrifuged to recover the NPs, HNT-G1, which were then washed with distilled water and air-dried. To synthesize the 2nd and 3rd generations of PAMAM dendrimers on HNTs (HNT-G2 and HNT-G3, respectively), we followed the same protocol, i.e. Michael's addition of methyl acrylate followed by amidation of the ester groups with ethylene diamine using HNT-G1 and HNT-G2, respectively. Fig. 2 presents the structure of repeating cycles of PAMAM dendrimers, which constitute a generation, by showing the progress from the HNG-G1 to HNT-G3. As illustrated in this figure, the number of terminal amine groups increases exponentially from one generation to another.

To study possible chemical reactions with TMC, functionalized HNTs were immersed in a 0.05 w/v % TMC in n-hexane solution, and the suspension was sonicated for 2 h. The latter was to minimize possible agglomeration of NPs. The suspension of NPs in the TMC solution was primarily used for the synthesis of TFN membranes, which will be described in the next section. Also, the NPs, which are referred to as HNT-x-TMC (x indicates the type of functionalization), were recovered from the suspension in TMC solution for further analysis, as well as for subsequent chlorination.

2.3. Membrane fabrication and chlorination procedure

RO membranes were fabricated by in-situ interfacial polymerization of MPD and TMC on top of the PS35 ultrafiltration membrane, which was used as a substrate. First, a 2 (w/v)% solution of MPD in deionized water was poured on the substrate. After 5 min, the excess solution was drained-off and further blotted using a Teflon roller to ensure no visible droplets on the substrate surface. Then, a 0.05 (w/v)% solution of TMC in n-hexane was poured on the substrate; after 1 min of contact, the excess solution was drained off, and the membrane was rinsed with pure n-hexane. This was followed by curing the membrane in a preheated oven at 95 °C for 10 min. Finally, the TFC membrane was thoroughly rinsed with distilled water. Such a prepared membrane was stored in distilled water until the membrane was subjected to chlorination procedure or a performance test. The method of in-situ interfacial polymerization for TFN membranes was similar to that of the TFC membrane, except the second step was carried out using a 0.05 (w/v)% suspension of HNT-x-TMC in the solution of TMC in n-hexane, instead of just the solution of TMC.

Passive chlorination of TFC and TFN membranes and HNT-x-TMC NPs involved immersion in a 500 ppm solution of NaOCl at room temperature and pH of 9 for 24 h in the absence of open-air and light in a sealed container. It is commonly reported that chlorination is less aggressive in basic environments [9,19,40]. The slower rate of chlorination allows more accurate monitoring of the effects of incorporating NPs on the chlorine tolerance of the membranes. Chlorinated membranes and NPs were thoroughly rinsed and stored in distilled water until their analysis or performance tests. The TFN membranes are coded as TFN-HNT-x, where x is either G1, G2, or G3, indicating PAMAM dendrimers' generation. The "x" is left out for acid-washed HNTs with no dendrimers; chlorinated membranes and chlorinated NPs are denoted by adding "-Cl" at the end, for example, TFC-Cl and HNT-G1-TMC-Cl.

2.4. Membrane performance test

All membranes were tested in a cross-flow system with three parallel membrane cells. The effective permeation area in each cell was 17.54 cm^2. The details of the system, its materials, and the design of the cells are provided elsewhere [33]. Synthetic brackish water with 3000 ppm of sodium chloride was used as the feed solution. The pressure and

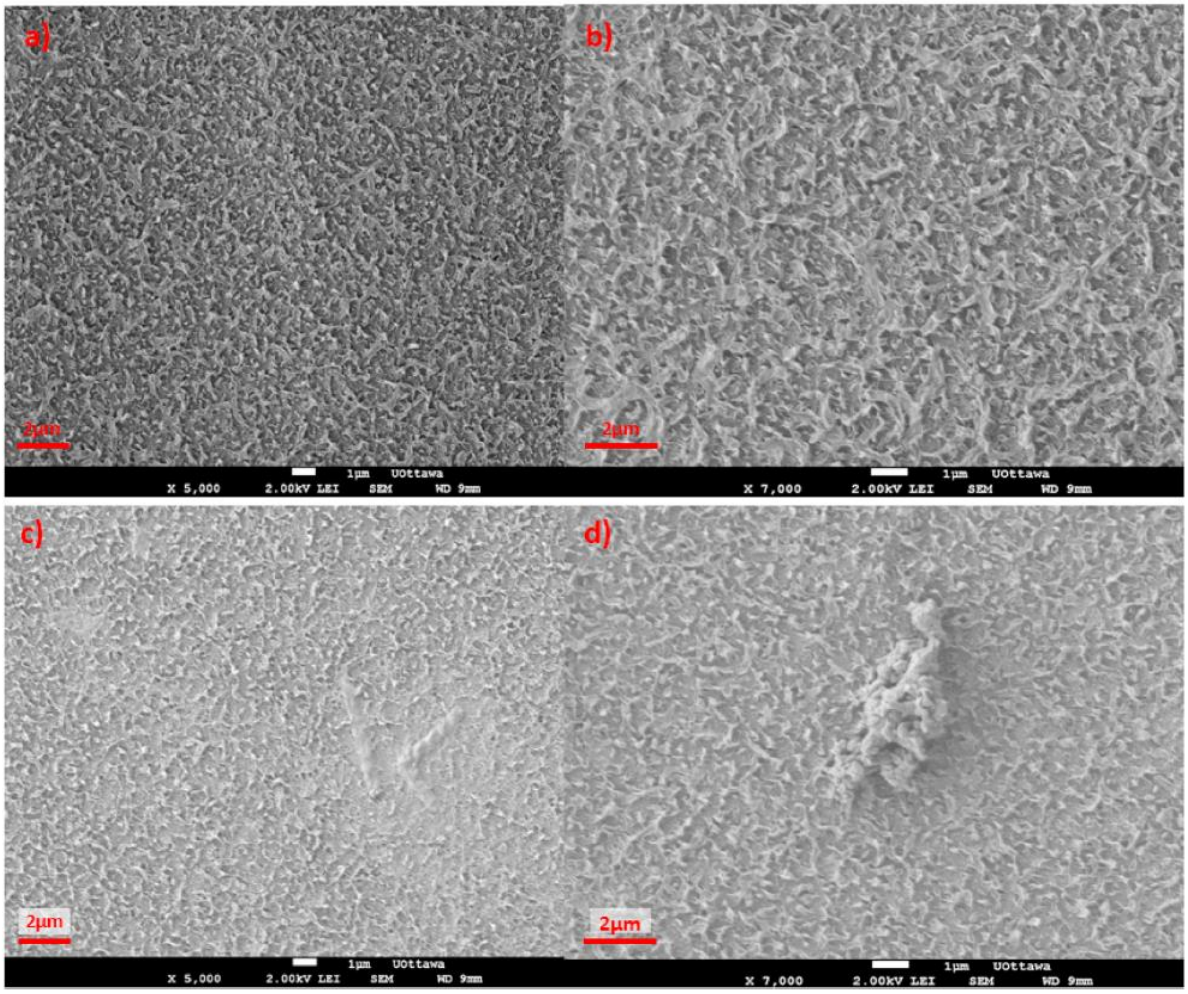

Fig. 3. SEM images of top surface of a) TFC, b) TFC-Cl, c) TFN-HNT-G2 d) TFN-HNT-G2-Cl membranes.

temperature of the feed solution were 20 ± 0.1 bar(g) and 25 ± 2 °C, respectively. The concentration of permeate solution was measured using an Oakton CON 6+ conductivity meter. The feed flow rate was controlled at 2.4 ± 0.2 L/min. Permeate flux, J_w [L/(m^2 h)], was calculated by Eq. (1) using the volume of the permeate, V_p [L], collected in time, t [h], per surface area of the membrane, A_p [m^2]. Salt rejection, R, was calculated using Eq. (2), in which C_f and C_p are the salt concentrations in feed and permeate, respectively.

$$J_w = \frac{V_p}{A_p.t} \tag{1}$$

$$R = 1 - \left(\frac{C_p}{C_f}\right) \tag{2}$$

2.5. Membranes and nanoparticles characterizations

A Q5000 thermal gravimetric analyzer (TGA) (TA Instruments Ltd, USA) was used to confirm and find the percentage of the HNTs functionalization. The heating rate was 10 °C/min, from 30 °C to 800 °C, under the nitrogen. X-ray photoelectron spectroscopy (XPS) (Kratos Analytical model Axis Ultra DLD spectrometer) equipment with monochromated aluminum-K α X rays at the power of 140 W was used to obtain the wide scan spectra of the NPs. Morphology of the membranes' top surface was characterized by scanning electron microscopy (SEM) using a JEOL JEM-2100F instrument. Samples were coated to a thickness of 5 nm using gold sputtering. Attenuated Total Reflection-Fourier Transform Infrared (ATR-FTIR) spectra of the membranes and NPs before and after chlorination were obtained using a Nicolet 6700 FTIR (Thermo Fisher) equipment. ATR- FTIR scans were recorded in the range of 650 to 4000 cm^{-1} with a resolution of 4 cm^{-1}. OMNIC ™ and FTIR Essential® software were utilized to analyze the spectra. The hydrophilicity of the TFC and TFN membranes before and after chlorination was investigated using a VCA Optima goniometer (AST products, Inc., Billerica, MA). At least 12 droplets of deionized water (~1 µL each droplet) at room temperature were examined on top of each membrane to report the average contact angle.

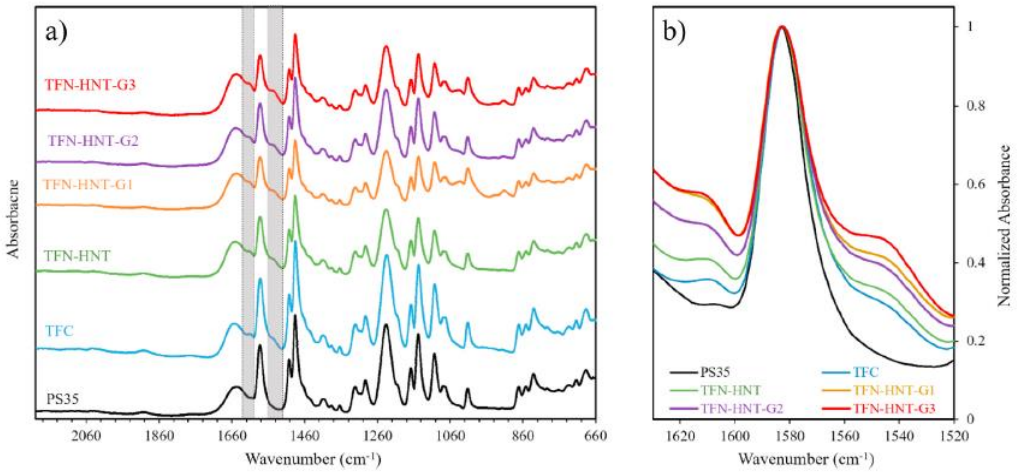

Fig. 4. ATR-FTIR spectra of a) the ultrafiltration PS35 substrate, TFC, and TFN membranes; grey bands show 1541 and 1609 cm^{-1} peaks. b) Comparing intensities of 1541 and 1609 cm^{-1} peaks normalized by 1580 cm^{-1}.

3. Results and discussion

3.1. Physicochemical characterization of nanoparticles and membranes

TGA and XPS, given in Figs. S1 and S2, respectively, confirm the successful modification of the HNTs with the dendrimers. The percentage of NPs' functionalization intensified with the generation of PAMAM dendrimers. Fig. 3 shows the SEM images of the top surface of (a) TFC, (b) TFC-Cl, (c) TFN-HNT-G2, and (d) TFN-HNT-G2-Cl membranes. SEM images of TFN-HNT-G1 and G3 membranes (not shown) were similar to the TFN-HNT-G2 samples. In both chlorinated and non-chlorinated membranes, the typical ridge and valley structure of the PA RO membranes was observed, which indicates the successful formation of the active layer. Figures also confirm the successful incorporation of the HNTs in the TFN membranes. A "lump-like" structure in Fig. 3. d is attributed to the formation of HNTs aggregate. These aggregates were also observed in other HNT-based membranes. It is possible that the aggregates generated some defects and contributed to the decrease of membrane selectivity, as later discussed in section 3.2. Comparing Fig. 3a with c and b with d, it appears that the TFN membrane had less "leaf-like" structures. These structures have been attributed to the reaction of diffused MPD with TMC; thus, their decrease could indicate interactions of the PAMAM with TMC. This is in line with the findings of Li et al., who reported the same trend in the morphology of TFN membranes [46]. For both TFC and TFN-HNT-G2 membranes, no significant change was observed in the ridge and valley after chlorination at 12,000

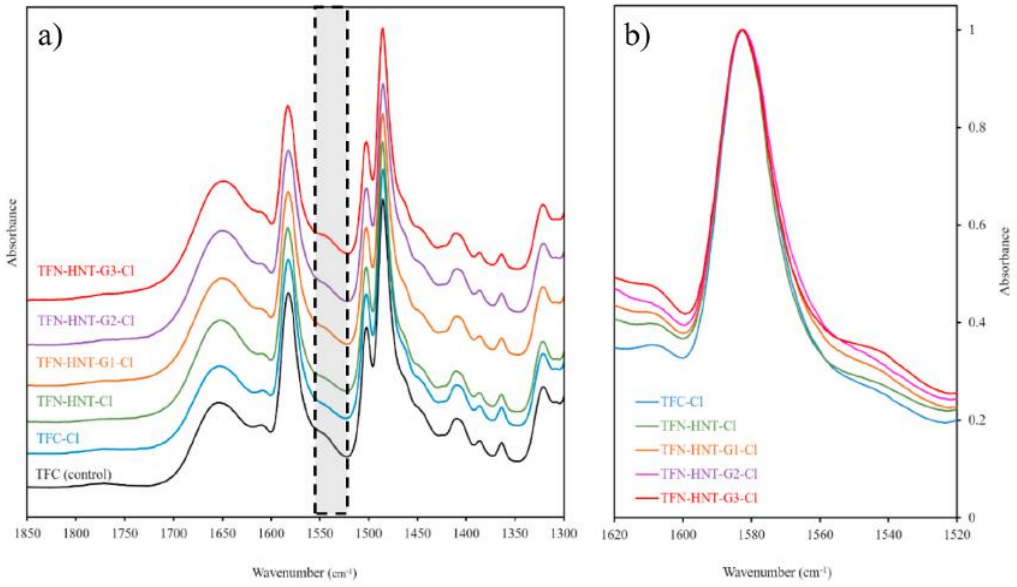

Fig. 5. a) ATR-FTIR spectra of TFC membrane and 12,000 ppm.h chlorine exposed TFC and TFN membranes. b) Comparison of 1541 cm^{-1} peak normalized intensities.

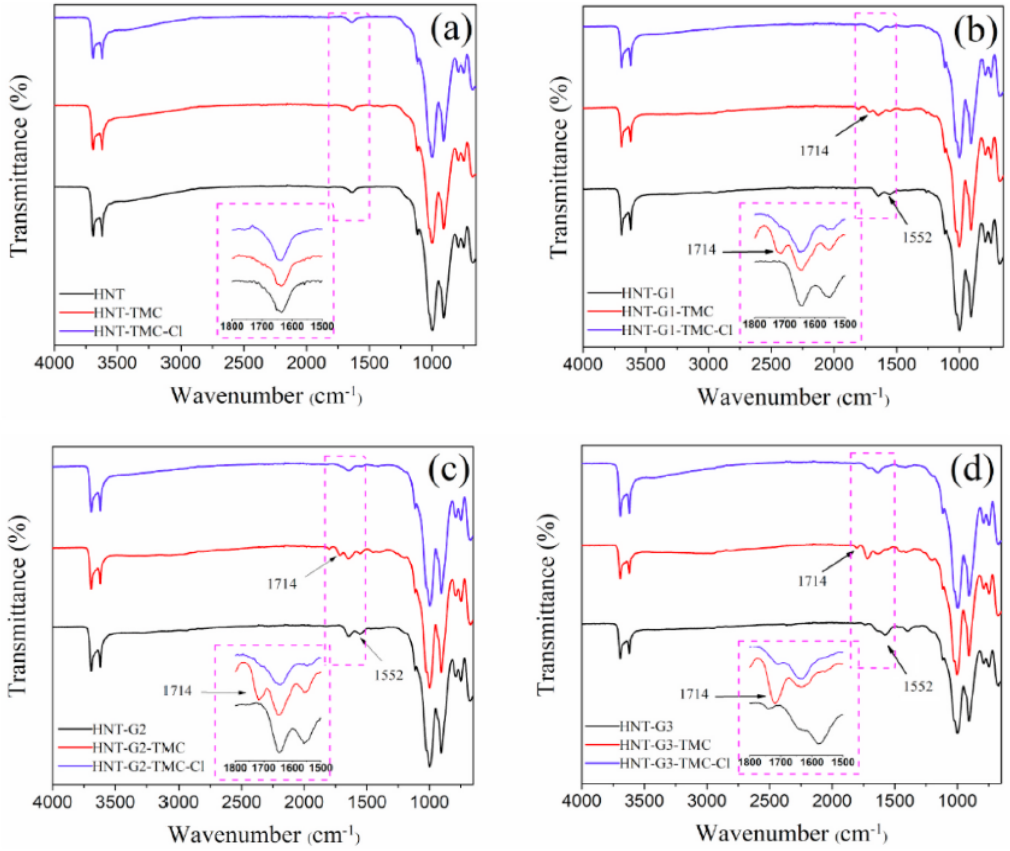

Fig. 6. ATR-FTIR spectra of a) HNT, b) HNT-G1, c) HNT-G2, and d) HNT-G3 contacted with TMC and their subsequent chlorination. PAMAM dendrimer functionalization resulted in the appearance of new peaks when the NPs were treated with TMC (red lines). Also, chlorination of such NPs lowered the corresponding peak intensities (black lines), showing the ability of HNT-G1, G2, and G3 to act as scavengers. (For interpretation of the references to colour in this figure legend, the reader is referred to the Web version of this article.)

ppm.h in a basic environment. As the pH increases, OCl^- rapidly becomes the main chlorine species in the solution [17,47]. OCl^- has lower relative reactivity with PA. This allowed for having better control over the membranes' chlorination extent. As confirmed later in the performance section, by not completely disintegrating the PA layer, i.e., generating defects, we could see the effects of the NPs on the membranes' chlorine tolerance within the reverse osmosis performance region.

Fig. 4 presents the ATR-FTIR spectra of the PS35 substrate and the TFC, TFN-HNT, TFN-HNT-G1, TFN-HNT-G2, and TFN-HNT-G3 membranes. In both TFC and TFN membranes, the characteristic peaks of PA appear at 1541, 1609, and 1663 cm^{-1}. The peak at 1541 cm^{-1} is related to amide II, which is arising mostly from N–H in-plane bending motion [25]. The peak at 1609 cm^{-1} corresponds to C═C ring stretching, or aromatic amide N–H deformation vibrations [28]. The peak at 1663 cm^{-1} is attributed to amide I, corresponding to C═O stretching, C–N stretching, and C–C–N deformation vibrations [48–50]. The presence of these peaks confirms the successful formation of the PA layer in the TFC and all TFN membranes. Furthermore, Fig. 4. b illustrates the internally normalized spectra of all membranes by the intensity of the peak at 1580 cm^{-1}, which corresponds to polysulfone. Comparing the intensities of at 1541 and 1609 cm^{-1} peaks, a systematic increase from TFC to TFN-HNT-G3 was observed, indicating the existence of more amide linkages due to the incorporation of PAMAM dendrimers or their reactions with TMC/PA. This is consistent with the results of our previous investigation on hydrophilic and amide functionalized HNTs-based TFN membranes [7,34,40].

Fig. 5 illustrates the ATR-FTIR spectra of chlorinated TFC and TFN membranes. The spectrum of the pristine TFC membrane, previously shown in Fig. 4, is also included as a reference in Fig. 5. a. It can be noticed that the PA characteristic peak at 1541 cm^{-1} of amide II is broader and has a lower intensity in the TFC-Cl membrane compared to the TFC membrane. This is due to the replacement of hydrogen with chlorine in the N–H bond, i.e., N-chlorination. The peak intensity at 1541 cm^{-1} keeps increasing in the order TFC-Cl < TFN-HNT-Cl < TFN-HNT-G1-Cl < TFN-HNT-G2-Cl < TFN-HNT-G3-Cl, Fig. 5. b. This indicates the degree of amide cleavage becomes less pronounced when we have more amide linkages because of PAMAM dendrimers' incorporation. The active amide functional groups on the HNTs from PAMAM dendrimers are accessible to chlorine, and they protect PA amide groups from the chlorine attack.

To confirm the hypothesis that amide groups of PAMAM dendrimers protect the amide groups from the PA layer, we also investigated possible reactions of PAMAM dendrimer-functionalized HNTs with TMC and chlorine using ATR-FTIR. Fig. 6 presents the effect of contacting NPs, (a) HNT, (b) HNT-G1, (c) HNT-G2, and (d) HNT-G3, with TMC solution in n-hexane followed by their subsequent chlorination. Considering Fig. 6. a, it is evident that the spectra of HNT, HNT-TMC,

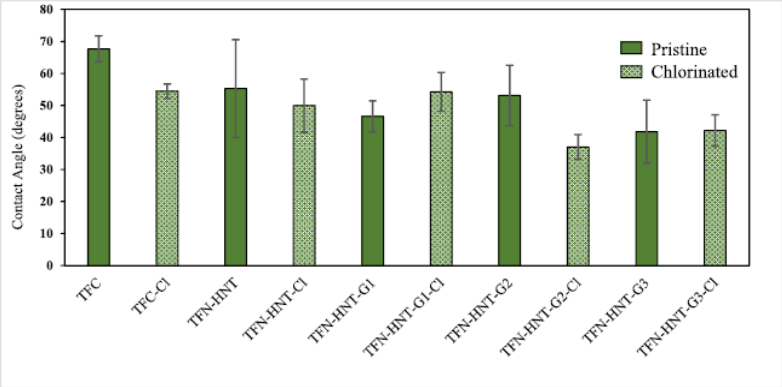

Fig. 7. Effect of chlorination (12,000 ppm.h) at pH of 9 on the surface contact angle of TFC and TFN membranes.

and HNT-TMC-Cl are the same because acid-treated HNTs had no amine groups, and consequently, they did not react with TMC and chlorine. On the other hand, after contacting with TMC, the spectra of dendrimer-functionalized HNTs (Fig. 6. b–d exhibit a new peak at 1714 cm^{-1}. The intensity of this peak increases from HNT-G1-TMC to HNT-G3-TMC. This peak is attributed to the formation of amide groups resulting from the reaction between the amine groups of the dendrimers and TMC. In other words, TMC can react with functionalized HNTs before the interfacial polymerization process. Chlorination of TMC-reacted NPs led to a significant decrease in the intensity of the 1714 cm^{-1} peak while the intensity of the peak at 1552 cm^{-1} increased. This can be attributed to the hydrolysis of the newly formed amide groups resulting from the reaction with chlorine. Therefore, incorporating the PAMAM functionalized HNTs into the TFN membranes should provide them with amide and primary amine groups that would act as the sacrificial agent. Especially, primary amine groups protect the amide group in the PA layer more effectively. Hence, PAMAM functionalized HNTs improve the chlorine resistance of the membrane [15,36,51].

Fig. 7 shows the contact angle of the pristine and chlorinated TFC and TFN membranes. The contact angle of the TFC membrane was 67.7 ± 4.1°, which is a typical value of PA-based membranes [33,52]. Incorporation of HNTs lowered the contact angle of TFN-HNT to 55.3 ± 15.3°. That is, the TFN-HNT membrane has a more hydrophilic surface than the TFC membrane. The functionalization of HNTs with PAMAM dendrimers further reduced the contact angle. The lowest contact angle of 48.1 ± 9.8° was observed for the TFN-HNT-G3 membrane. This trend is in line with the previous studies on TFN membranes. It is commonly reported that the incorporation of hydrophilic NPs within the PA layer increases the hydrophilicity of the membrane's active layer [53,54].

Chlorination affected the membranes' contact angle in different ways based on their type. Chlorination of the TFC and TFN-HNT membranes reduced their contact angle to 54.4 ± 2.3° and 50.0 ± 8.3°, respectively. Do et al. attributed a decrease of contact angle in a basic environment to the chlorine-promoted hydrolysis of PA [55]. However, this trend changed as the dendrimers' generation increased. Chlorination reduced the average contact angle of the TFN-HNT-G2 membrane from 53.1 ± 9.5° to 37.0 ± 3.9°, whereas practically no change was observed after chlorination of TFN-HNT-G3. It should be noted that relatively large error bars were observed, which can be the result of variations in the membranes' surface roughness. However, the variations in the average contact angle can indicate the dependence of chlorination mechanisms on the generation of the PAMAM dendrimers. On the one hand, an increase of hydrophilicity after chlorination can be attributed to the formation of hydroxyl and carboxylic acid groups resulting from hydrolysis of the C–N bond [55]. On the other hand, it has also been suggested that the incorporation of chlorine into the PA layer via N-chlorination and/or ring chlorination makes the membrane more hydrophobic [17,55]. Various competing reactions happen simultaneously during membrane chlorination [56]. Therefore, the best way to examine the effects of chlorine exposure on the membranes is to investigate their RO performance before and after chlorine exposure.

3.2. Membrane separation performance

Fig. 8 shows the separation performance of the reference TFC and TFN membranes before and after chlorination. The values for each membrane in Fig. 8 represent the average and standard deviation from at least 6 membranes of a given type. It is evident from Fig. 8. a that the water flux of all TFN membranes was at least doubled compared to the reference TFC membrane (0.8 ± 0.09 L/(m^2 h bar)). The enhanced water flux due to the incorporation of hydrophilic nanofillers has been commonly reported in the literature [48,57]. The highest water flux of 2.12 ± 0.2 L/(m^2 h bar) was observed for TFN-HNT-G1. The water fluxes of TFN-HNT-G2 and TFN-HNT-G3 were similar and slightly lower than 2 L/(m^2 h bar). The increased water flux can be attributed to the increased surface hydrophilicity, tubular nature of the HNTs, providing water flow paths. Considering the salt rejection of the pristine membranes (Fig. 8. b), the highest value of 98.6 ± 0.4% was observed for the reference TFC membrane. The average value of salt rejection progressively decreased from the TFN-HNT membrane to the TFN-HNT-G3 membrane. Although some overlapping in the error bars is seen, the trend of decreasing salt rejection is apparent. In other words, selectivity decreased with an increase in the generation of the PAMAM dendrimers. As indicated in the previous section, PAMAM dendrimers react with TMC before the interfacial polymerization. This can have multiple effects on the formation of the selective layer. On the one hand, it likely leads to stronger interactions between the functionalized HNTs and the PA layer and better dispersion of HNTs [34]. On the other hand, it might reduce the available TMC to react with MPD during the interfacial polymerization and hence lowers the crosslinking and/or increases the number of dangling amine groups at the PA layer [58,59]. The excess NH_2 groups can be protonated and form NH_3^+, although it is less likely in a basic environment [60]. This may reduce the overall negative charge of the PA layer resulting in membranes' decreased ion repulsions and NaCl rejections [61–63]. It is well established that at neutral pH, PA-based composite membranes have a negative charge [58,63–65]. Since salt rejection decreases while the water flux stays relatively unchanged with the increasing generation of PAMAM dendrimers, the latter effects appear to surpass the former one. Nevertheless, even the lowest salt rejection of 94.5 ± 2.8% for TFN-HNT-G3 is within the range of TFN RO membranes with porous NPs [51].

The impact of chlorination on the permeate flux and salt rejection is

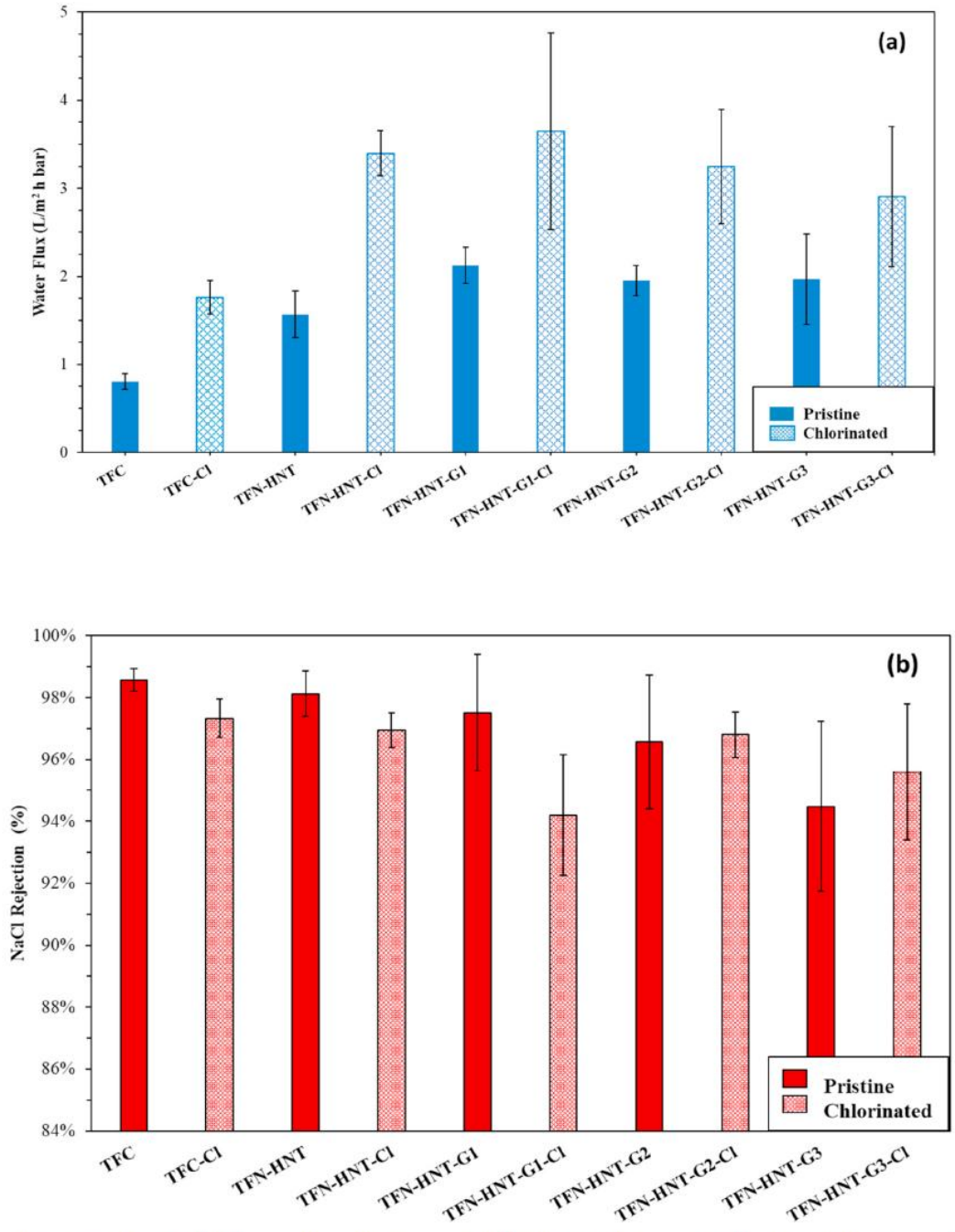

Fig. 8. Normalized permeate flux (a) and NaCl rejection (b) of the pristine (solid) and chlorinated (hashed) TFC and TFN membrane. Chlorine exposure: 12,000 ppm. h at pH 9.

also shown in Fig. 8. a and b, respectively. Chlorination increased membranes' water flux in all cases. TFN-HNT-G1-Cl had the highest average water flux of 3.64 ± 1.12 72.9 ± 22.4 L/(m^2 h bar). The largest increase in the average water flux, from 0.8 ± 0.09 to 1.76 ± 0.19 L/(m^2 h bar) (119%), was observed for the TFC membrane, while the smallest increase, from 1.96 to 2.9 ± 1.9 L/(m^2 h bar) (48%), was for the TFN-HNT-G3 membrane. Since the error bars overlapped for TFN-HNT-G3 and TFN-HNT-G3-Cl, both for water flux and salt rejection, it is safe to suggest that incorporating HNT-G3 led to the most stable membrane to chlorination. On the other hand, chlorination had a different effect on the average value of salt rejection of different membranes. The average value of salt rejection of the TFC and TFN-HNT membranes decreased

Table 1
Comparison of selected studies on chlorine resistance of RO membranes.

Membrane & Modification	RO Test Condition		Virgin Membrane		Chlorinated Membrane		Chlorination Conditions		Ref.
	Feed NaCl Concentration (ppm)	Pressure (bar)	J_w (LMH)	R (%)	J_w (LMH)	R (%)	exposure (ppm. h)	pH	
TFC	3000	20	16.1	98.6	35.2	97.3	12000	9	This
TFN-HNT-G2	3000	20	39	96.6	65	96.8	12000	9	Work
TFC	2000	15.5	15.1	98.6	16.9	80.4	10000	10.5	[28]
TFC/isophthaloyl chloride	2000	15.5	16.7	97.5	19.8	97.5	10000	10.5	
TFC BW30FR (Dow)	500	5	15.2	98.2	14.5	98.5	15000	9	[66]
TFC (Hangzhou Tianchuang)	500	5	26	98.1	42.9	95.9	15000	9	
TFC-g-poly(vinyl alcohol)	500	5	28.8	98.45	29.5	98.4	15000	9	
TFC	2000	15.5	9.18	99.3	32.5	91.1	48000	7	[67]
TFN-graphene oxide (GO)	2000	15.5	16.1	99.4	17.8	99.1	48000	7	
TFC RE4024-TL(Woongjin)	2000	15.5	105.8	97	124	93.7	1000	4	[68]
TFC RE4024-TL-g-imidazolidinyl urea [a]	2000	15.5	79.5	96.9	90	94.9	1000	4	
TFC BW30 (Filmtec)	2000	15	34.6	96.1[c]	7.9	92.3[c]	1000	4	[30]
TFC BW30-g-PAMAM	2000	15	32.3	95.2[c]	12.6	94.1[c]	1000	4	
TFC BW30-g-PAMAM-GO	2000	15	24.8	97.2[c]	10.2	96.3[c]	1000	4	
TFC	2000	15.5	15.1	98.6	25.8	62.5	10000	3.5	[28]
TFC/isophthaloyl chloride	2000	15.5	16.7	97.5	20.8	80	10000	3.5	
TFC	35000	55	22.1	98	48.6	67.1	500	–	[37]
TFC/aPES	35000	55	31.1	94.1	38.9	75.2	500	–	
TFN/aPES- HBP-g-silica [b]	35000	55	34.5	97.7	38.4	82.5	500	–	

[a] Grafted & regenerative, data after 1st chlorination cycle.
[b] Poly(arylene ether sulfone)/hyperbranched grafted silica NPs.
[c] Rejections based on the solution conductivity.

from 98.6 ± 0.4% to 97.3 ± 0.6% and from 98.1 ± 0.7% to 96.9 ± 0.6%, respectively. The TFN-HNT-G1-Cl membrane had an average salt rejection of 94.2 ± 1.9%, which was lower than that of the TFN-HNT-G1 membrane (97.5 ± 1.9%). Conversely, chlorination slightly increased the average value of salt rejection of the TFN-HNT-G2 and TFN-HNT-G3 membranes from 96.6 ± 2.2% to 96.8 ± 0.7% and from 94.5 ± 2.8% to 95.6 ± 2.2%, respectively. It should be noted that since the error bars of before and after chlorination largely overlapped for TFN-HNT-G2 and G3 membranes, they showed the highest stability in membrane selectivity. The greater the PAMAM dendrimer's generation, the more favourable the effect of chlorination on the respective TFN membrane's salt rejection. Considering the combination of the water flux and salt rejection before chlorination, the TFN-HNT-G1 membrane exhibited the best RO performance. However, after chlorination, it was the TFN-HNT-G2-Cl membrane that displays the best RO performance.

Table 1 shows a comparison between the results of this work with some of the recent studies on chlorine resistance of TFC RO membranes based on surface modification and/or incorporation of NPs. The table comprises both basic and acidic chlorination conditions. As evidenced by the table, chlorination in an acidic environment lowers the salt rejection more profoundly.

3.3. Chlorination mechanism

As discussed previously, it is the interplay of various simultaneous chlorination mechanisms that determines the overall RO performance of the membranes [15]. In the case of TFC and TFN-HNT membranes, the observed concurrent increase of the water flux and surface hydrophilicity suggests that chlorine-induced hydrolysis of the PA chain, Fig. 1, was the dominant chlorination mechanism. The corresponding decrease in salt rejection of TFC-Cl and TFN-HNT-Cl indicates the loosening of the selective PA layer's structure caused by reductions in its crosslinking [15,17,69]. In the case of the TFN-HNT-G1 membrane, an increase in the water flux and a decrease in salt rejection were associated with a decrease in surface hydrophilicity. It is possible that Cl was incorporated into the PA layer via N-chlorination. Hoffman's degradation of the PA layer could also take place. In basic conditions such as those used in this study, it has been shown that the secondary N-chlorinated amides can be decomposed to primary amines by a loss of carbonyl groups, which are converted to carbon dioxide [6,17,69]. Both above chlorination mechanisms would decrease the membrane's hydrophilicity while disrupting its intermolecular interactions resulting in higher water flux and lower salt rejection. An increase in the stability after chlorination was observed for TFN-HNT-G3 and a lesser extend for TFN-HNT-G2. The average value of the salt rejection for TFN-HNT-G3 even slightly increased after the chlorination. In fact, some research groups have proposed membrane chlorination as a post-treatment method to improve membrane selectivity [15,24,70–74]. A logical question arises; why the improvements in salt rejection after chlorination was observed for the TFN-HNT-G2 and TFN-HNT-G3 membranes, but not for the TFN-HNT-G1 membrane? In our work, chlorination was carried out in a basic environment with an identical ppm × hour exposure for all membranes. However, it is possible that despite the same bulk concentration, the effective chlorine concentration seen by the PA layer was inversely related to the generation of PAMAM dendrimers. As previously shown in Fig. 6, TMC reacts with dendrimer-functionalized HNTs forming amide groups, which then undergo hydrolysis when exposed to chlorine. Therefore, the number of amide groups that act as a "protective shield" increases exponentially with the dendrimers' generation. This could explain the different effects of chlorination on the RO performance of TFN-HNT-G1 from TFN-HNT-G2 and TFN-HNT-G3 membranes. This is in line with the findings of Do et al., who reported a simultaneous increase in the water flux and salt rejection in the basic environment and at low chlorine concentrations [14]. It is important to emphasize that the protective shield provided by the amine groups of dendrimers would not be permanent. It is likely that a greater concentration of HClO

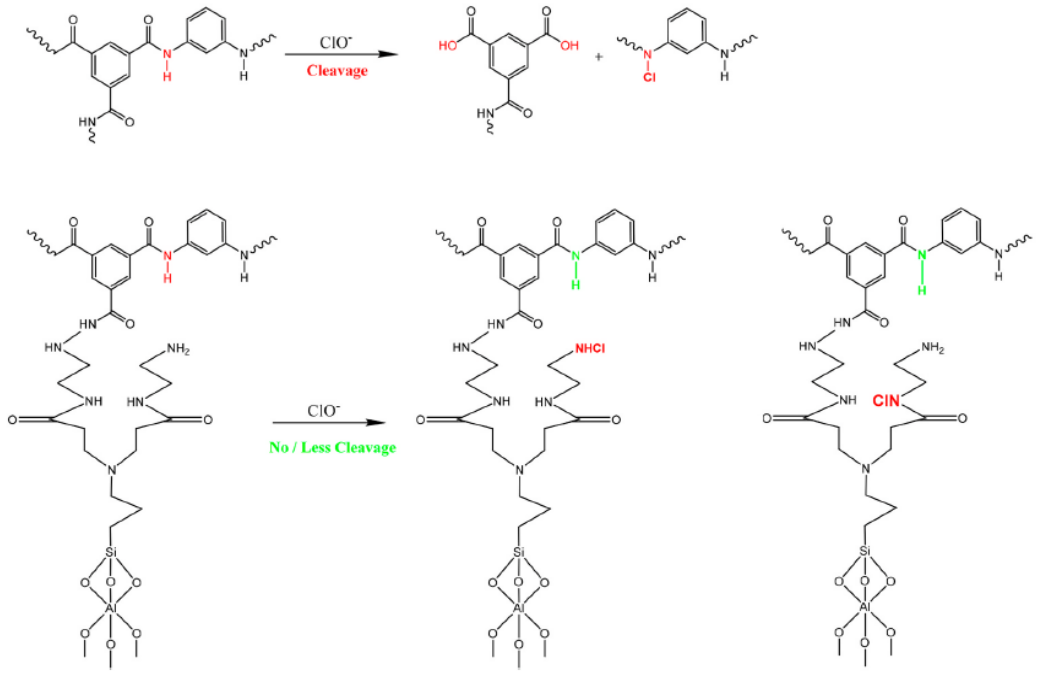

Fig. 9. Schematic representation of the chlorine scavenger role of PAMAM dendrimers in TFN membranes. In the absence of PAMAM functionalized HNTs (top reaction), chlorine directly accesses the amide bond in the PA chain. In the presence of PAMAM functionalized HNTs (bottom reaction), chlorine reacts with the amine and amide groups of PAMAM dendrimers.

and/or a longer exposure time of TFN-HNT-G2 and TFN-HNT-G3 would decrease their salt rejection in the same way as the chlorine exposure of 12,000 ppm.h affected the performance of the TFN-HNT-G1 membrane.

The role of chlorine scavenger played by the PAMAM dendrimer-functionalized HNTs can be explained by two distinct chemical reactions with ClO^- shown in Fig. 9. In the absence of PAMAM dendrimer-functionalized HNTs, the first reaction in Fig. 9 is likely the dominant mechanism, and the PA layer is essentially "defenceless" when exposed to chlorine. The incorporation of PAMAM dendrimer-functionalized HNTs can defend against the direct attack of chlorine on the PA layer, as shown by the second reaction in Fig. 9. However, it cannot prevent the first reaction from occurring. The balance between the two reactions depends on the number of amine groups controlled in this work by the generation of PAMAM dendrimers. This hypothesis may explain the effects of chlorination on the RO performance, particularly on the salt rejection of the TFN-HNT-G1, TFN-HNT-G2, and TFN-HNT-G3 membranes.

Another possible explanation for the observed increased chlorine resistance, a slight increase in the average value of the salt rejection of TFN-HNT-G2 and TFN-HNT-G3 after chlorination, is as follows. PAMAM functionalized HNTs react with TMC before the interfacial polymerization, leaving some aromatic amine end-groups of MPD unreacted. The excess MPD can be oxidized by chlorine to generate crosslinking by imine or azo-like bond groups [71,75]. In other words, chlorination of dendrimer-functionalized HNT-based TFN membranes could eventually help tighten the structure of the selective PA layer.

4. Conclusion

Chlorine intolerance of PA-based RO membranes is a severe challenge in desalination plants. We addressed this issue by incorporating poly(amidoamine) (PAMAM) dendrimers into the PA layer of TFN membranes via halloysite nanotubes (HNTs). The introduction of PAMAM grafted HNTs into the membranes doubled their water flux with a slight decrease in salt rejection. Chlorination tests and physicochemical characterizations confirmed that extra amine and amide groups in PAMAM dendrimers acted as chlorine scavengers. However, the exact mechanism of membrane chlorination should be a subject of further investigation. TFN membranes with the second and third generations of PAMAM dendrimers (TFN-HNT-G2 & G3) displayed a higher chlorination resistance as no statistically significant change in their water flux and salt rejection was observed after the chlorine exposure of 12,000 ppm.h at pH of 9. TFN-HNT-G2 membrane had the optimum overall desalination performance after chlorination with ~85.6% water flux improvement while maintaining its selectivity.

Author contributions

Farhad Asempour: design and coordination of experiments, synthesis of TFC and TFN membranes, membrane characterization (SEM, ATR-FTIR, contact angle), desalination performance tests and data analysis, manuscript writing. Somaye Akbari: functionalization of HNTs with different generations of PAMAM dendrimers, ATR-FTIR, TGA, XPS of NPs and membranes, AFT-FTIR data analysis and interpretation, manuscript writing. Mohammad Hassan Kanani-Jazi: functionalization of HNTs with different generations of PAMAM dendrimers, ATR-FTIR data analysis. Amirsajad Atashgar: desalination performance tests. Takeshi Matsuura: manuscript correction and redaction. Boguslaw Kruczek: coordination of the project, manuscript writing, correction, and redaction.

Declaration of competing interest

The authors declare that they have no known competing financial interests or personal relationships that could have appeared to influence the work reported in this paper.

Acknowledgements

The authors gratefully acknowledge the financial support provided by the Natural Science and Engineering Research Council (NSERC) Canada, Discovery Grant (DG), grant number: 04443.

Appendix A. Supplementary data

Supplementary data to this article can be found online at https://doi.org/10.1016/j.memsci.2020.119039.

References

[1] P.J.J. Alvarez, C.K. Chan, M. Elimelech, N.J. Halas, D. Villagrán, Emerging opportunities for nanotechnology to enhance water security, Nat. Nanotechnol. 13 (2018) 634–641, https://doi.org/10.1038/s41565-018-0203-2.
[2] M. Elimelech, W.A. Phillip, The future of seawater desalination: energy, technology, and the environment, Science 333 (2011) 712–717, https://doi.org/10.1126/science.1200488.
[3] X. Zhou, Z. Wang, R. Epsztein, C. Zhan, W. Li, J.D. Fortner, T.A. Pham, J.-H. Kim, M. Elimelech, Intrapore energy barriers govern ion transport and selectivity of desalination membranes, Sci. Adv. 6 (2020), https://doi.org/10.1126/sciadv.abd9045 eabd9045.
[4] W.J. Koros, C. Zhang, Materials for next-generation molecularly selective synthetic membranes, Nat. Mater. 16 (2017) 289–297, https://doi.org/10.1038/nmat4805.
[5] M. Al-Abri, B. Al-Ghafri, T. Bora, S. Dobretsov, J. Dutta, S. Castelletto, L. Rosa, A. Boretti, Chlorination disadvantages and alternative routes for biofouling control in reverse osmosis desalination, Npj Clean Water 2 (2019) 2, https://doi.org/10.1038/s41545-018-0024-8.
[6] R. Verbeke, W. Arts, E. Dom, M. Dickmann, W. Egger, G. Koeckelberghs, A. Szymczyk, I.F.J. Vankelecom, Transferring bulk chemistry to interfacial synthesis of TFC-membranes to create chemically robust poly(epoxyether) films, J. Membr. Sci. 582 (2019) 442–453, https://doi.org/10.1016/j.memsci.2019.02.016.
[7] M.L. Lind, A.K. Ghosh, A. Jawor, X. Huang, W. Hou, Y. Yang, E.M.V. Hoek, Influence of zeolite crystal size on zeolite-polyamide thin film nanocomposite membranes, Langmuir 25 (2009) 10139–10145, https://doi.org/10.1021/la900938x.
[8] W.J. Lau, S. Gray, T. Matsuura, D. Emadzadeh, J. Paul Chen, A.F. Ismail, A review on polyamide thin film nanocomposite (TFN) membranes: history, applications, challenges and approaches, Water Res. 80 (2015) 306–324, https://doi.org/10.1016/j.watres.2015.04.037.
[9] D.L. Zhao, S. Japip, Y. Zhang, M. Weber, C. Maletzko, T.-S. Chung, Emerging thin-film nanocomposite (TFN) membranes for reverse osmosis: a review, Water Res. 173 (2020), https://doi.org/10.1016/j.watres.2020.115557, 115557.
[10] H. Saleem, S.J. Zaidi, Nanoparticles in reverse osmosis membranes for desalination: a state of the art review, Desalination 475 (2020), https://doi.org/10.1016/j.desal.2019.114171, 114171.
[11] E.M.V. Hoek, M.T.M. Pendergast, A.K. Ghosh, Chapter 9 - nanotechnology-based membranes for water purification, in: A. Street, R. Sustich, J. Duncan, N. Savage (Eds.), Nanotechnol. Appl. Clean Water, second ed., 2014, pp. 133–154, https://doi.org/10.1016/B978-1-4557-3116-9.00009-3. William Andrew Publishing, Oxford.
[12] T.H. Lee, J.S. Roh, S.Y. Yoo, J.M. Roh, T.H. Choi, H.B. Park, High-performance polyamide thin-film nanocomposite membranes containing ZIF-8/CNT hybrid nanofillers for reverse osmosis desalination, Ind. Eng. Chem. Res. 59 (2020) 5324–5332, https://doi.org/10.1021/acs.iecr.9b04810.
[13] A. Shakeri, R. Razavi, H. Salehi, M. Fallahi, T. Eghbalazar, Thin film nanocomposite forward osmosis membrane embedded with amine-functionalized ordered mesoporous silica, Appl. Surf. Sci. 481 (2019) 811–818, https://doi.org/10.1016/j.apsusc.2019.03.040.
[14] J.R. Werber, C.O. Osuji, M. Elimelech, Materials for next-generation desalination and water purification membranes, Nat. Rev. Mater. 1 (2016), https://doi.org/10.1038/natrevmats.2016.18, 16018.
[15] R. Verbeke, V. Gómez, I.F.J. Vankelecom, Chlorine-resistance of reverse osmosis (RO) polyamide membranes, Prog. Polym. Sci. 72 (2017) 1–15, https://doi.org/10.1016/j.progpolymsci.2017.05.003.
[16] F. Asempour, Fabrication and characterization of novel environmentally friendly thin film nanocomposite membranes for water desalination, Thesis, 2017, https://doi.org/10.20381/ruor-21011. Université d'Ottawa/University of Ottawa.
[17] J.M. Gohil, A.K. Suresh, Chlorine attack on reverse osmosis membranes: mechanisms and mitigation strategies, J. Membr. Sci. 541 (2017) 108–126, https://doi.org/10.1016/j.memsci.2017.06.092.
[18] S.P. Chesters, N. Pena, S. Gallego, M. Fazel, M.W. Armstrong, F. del Vigo, Results from 99 seawater RO membrane autopsies, IDA J. Desalination Water Reuse 5 (2013) 40–47, https://doi.org/10.1179/2051645213Y.0000000006.
[19] R. Verbeke, A. Bergmaier, S. Eschbaumer, V. Gómez, G. Dollinger, I. Vankelecom, Elemental depth profiling of chlorinated polyamide-based thin-film composite membranes with elastic recoil detection, Environ. Sci. Technol. 53 (2019) 8640–8648, https://doi.org/10.1021/acs.est.8b07226.
[20] C. Liu, Y. Guo, X. Wei, C. Wang, M. Qu, D.W. Schubert, C. Zhang, An outstanding antichlorine and antibacterial membrane with quaternary ammonium salts of alkenes via in situ polymerization for textile wastewater treatment, Chem. Eng. J. 384 (2020), https://doi.org/10.1016/j.cej.2019.123306, 123306.
[21] R. Verbeke, V. Gómez, T. Koschine, S. Eyley, A. Szymczyk, M. Dickmann, T. Stimpel-Lindner, W. Egger, W. Thielemans, I.F.J. Vankelecom, Real-scale chlorination at pH4 of BW30 TFC membranes and their physicochemical characterization, J. Membr. Sci. 551 (2018) 123–135, https://doi.org/10.1016/j.memsci.2018.01.019.
[22] J. Powell, J. Luh, O. Coronell, Bulk chlorine uptake by polyamide active layers of thin-film composite membranes upon exposure to free chlorine—kinetics, mechanisms, and modeling, Environ. Sci. Technol. 48 (2014) 2741–2749, https://doi.org/10.1021/es4047632.
[23] D. Wu, J. Martin, J.R. Du, Y. Zhang, D. Lawless, X. Feng, Effects of chlorine exposure on nanofiltration performance of polyamide membranes, J. Membr. Sci. 487 (2015) 256–270, https://doi.org/10.1016/j.memsci.2015.02.021.
[24] J. Glater, M.R. Zachariah, A mechanistic study of halogen interaction with polyamide reverse-osmosis membranes, in: S. Sourirajan, T. Matsuura (Eds.), Reverse Osmosis Ultrafiltr, 1985, pp. 345–358, https://doi.org/10.1021/bk-1985-0281.ch026. American Chemical Society, Washington, D.C.
[25] Y.-N. Kwon, J.O. Leckie, Hypochlorite degradation of crosslinked polyamide membranes: I. Changes in chemical/morphological properties, J. Membr. Sci. 283 (2006) 21–26, https://doi.org/10.1016/j.memsci.2006.06.008.
[26] Y.-N. Kwon, C.Y. Tang, J.O. Leckie, Change of membrane performance due to chlorination of crosslinked polyamide membranes, J. Appl. Polym. Sci. 102 (2006) 5895–5902, https://doi.org/10.1002/app.25071.
[27] S. Gholami, A. Rezvani, V. Vatanpour, J.L. Cortina, Improving the chlorine resistance property of polyamide TFC RO membrane by polyethylene glycol diacrylate (PEGDA) coating, Desalination 443 (2018) 245–255, https://doi.org/10.1016/j.desal.2018.06.004.
[28] Y. Yao, W. Zhang, Y. Du, M. Li, L. Wang, X. Zhang, Toward enhancing the chlorine resistance of reverse osmosis membranes: an effective strategy via an end-capping technology, Environ. Sci. Technol. 53 (2019) 1296–1304, https://doi.org/10.1021/acs.est.8b06006.
[29] J. Wang, S. Zhang, P. Wu, W. Shi, Z. Wang, Y. Hu, In situ surface modification of thin-film composite polyamide membrane with zwitterions for enhanced chlorine resistance and transport properties, ACS Appl. Mater. Interfaces 11 (2019) 12043–12052, https://doi.org/10.1021/acsami.8b21572.
[30] V. Vatanpour, A. Sanadgol, Surface modification of reverse osmosis membranes by grafting of polyamidoamine dendrimer containing graphene oxide nanosheets for desalination improvement, Desalination 491 (2020), https://doi.org/10.1016/j.desal.2020.114442, 114442.
[31] G.-R. Xu, J.-N. Wang, C.-J. Li, Strategies for improving the performance of the polyamide thin film composite (PA-TFC) reverse osmosis (RO) membranes: surface modifications and nanoparticles incorporations, Desalination 328 (2013) 83–100, https://doi.org/10.1016/j.desal.2013.08.022.
[32] H. Huang, S. Lin, L. Zhang, L. Hou, Chlorine-resistant polyamide reverse osmosis membrane with monitorable and regenerative sacrificial layers, ACS Appl. Mater. Interfaces 9 (2017) 10214–10223, https://doi.org/10.1021/acsami.6b16462.
[33] F. Asempour, D. Emadzadeh, T. Matsuura, B. Kruczek, Synthesis and characterization of novel Cellulose Nanocrystals-based Thin Film Nanocomposite membranes for reverse osmosis applications, Desalination 439 (2018) 179–187, https://doi.org/10.1016/j.desal.2018.04.009.
[34] F. Asempour, S. Akbari, D. Bai, D. Emadzadeh, T. Matsuura, B. Kruczek, Improvement of stability and performance of functionalized halloysite nano tubes-based thin film nanocomposite membranes, J. Membr. Sci. 563 (2018) 470–480, https://doi.org/10.1016/j.memsci.2018.05.070.
[35] H. Wu, B. Tang, P. Wu, Optimizing polyamide thin film composite membrane covalently bonded with modified mesoporous silica nanoparticles, J. Membr. Sci. 428 (2013) 341–348, https://doi.org/10.1016/j.memsci.2012.10.053.
[36] S.Y. Park, S.G. Kim, J.H. Chun, B.-H. Chun, S.H. Kim, Fabrication and characterization of the chlorine-tolerant disulfonated poly(arylene ether sulfone)/hyperbranched aromatic polyamide-grafted silica composite reverse osmosis membrane, Desalination Water Treat. 43 (2012) 221–229, https://doi.org/10.1080/19443994.2012.672175.
[37] S.G. Kim, J.H. Chun, B.-H. Chun, S.H. Kim, Preparation, characterization and performance of poly(aylene ether sulfone)/modified silica nanocomposite reverse osmosis membrane for seawater desalination, Desalination 325 (2013) 76–83, https://doi.org/10.1016/j.desal.2013.06.017.
[38] G. Cavallaro, D.I. Donato, G. Lazzara, S. Milioto, Films of halloysite nanotubes sandwiched between two layers of biopolymer: from the morphology to the dielectric, thermal, transparency, and wettability properties, J. Phys. Chem. C 115 (2011) 20491–20498, https://doi.org/10.1021/jp207261r.
[39] Y. Joo, Y. Jeon, S.U. Lee, J.H. Sim, J. Ryu, S. Lee, H. Lee, D. Sohn, Aggregation and stabilization of carboxylic acid functionalized halloysite nanotubes (HNT-COOH), J. Phys. Chem. C 116 (2012) 18230–18235, https://doi.org/10.1021/jp3038945.
[40] M. Ghanbari, D. Emadzadeh, W.J. Lau, S.O. Lai, T. Matsuura, A.F. Ismail, Synthesis and characterization of novel thin film nanocomposite (TFN) membranes embedded with halloysite nanotubes (HNTs) for water desalination, Desalination 358 (2015) 33–41, https://doi.org/10.1016/j.desal.2014.11.035.
[41] Q. Zhao, D.L. Zhao, T.-S. Chung, Nanoclays-incorporated thin-film nanocomposite membranes for reverse osmosis desalination, Adv. Mater. Interfaces. 7 (2020), https://doi.org/10.1002/admi.201902108, 1902108.
[42] H. Dong, L. Wu, L. Zhang, H. Chen, C. Gao, Clay nanosheets as charged filler materials for high-performance and fouling-resistant thin film nanocomposite membranes, J. Membr. Sci. 494 (2015) 92–103, https://doi.org/10.1016/j.memsci.2015.07.049.

[43] R. Esfand, Poly(amidoamine) (PAMAM) dendrimers: from biomimicry to drug delivery and biomedical applications, Drug Discov. Today 6 (n.d.) 427–436.
[44] F.S. Fard, S. Akbari, E. Pajootan, M. Arami, Enhanced acidic dye adsorption onto the dendrimer-based modified halloysite nanotubes, Desalination Water Treat. 57 (2016) 26222–26239, https://doi.org/10.1080/19443994.2016.1160437.
[45] A. Sarkar, P.I. Carver, T. Zhang, A. Merrington, K.J. Bruza, J.L. Rousseau, S. E. Keinath, P.R. Dvornic, Dendrimer-based coatings for surface modification of polyamide reverse osmosis membranes, J. Membr. Sci. 349 (2010) 421–428, https://doi.org/10.1016/j.memsci.2009.12.005.
[46] Y. Li, S. Li, K. Zhang, Influence of hydrophilic carbon dots on polyamide thin film nanocomposite reverse osmosis membranes, J. Membr. Sci. 537 (2017) 42–53, https://doi.org/10.1016/j.memsci.2017.05.026.
[47] J. Xu, Z. Wang, X. Wei, S. Yang, J. Wang, S. Wang, The chlorination process of crosslinked aromatic polyamide reverse osmosis membrane: new insights from the study of self-made membrane, Desalination 313 (2013) 145–155, https://doi.org/10.1016/j.desal.2012.12.020.
[48] D. Emadzadeh, W.J. Lau, M. Rahbari-Sisakht, H. Ilbeygi, D. Rana, T. Matsuura, A. F. Ismail, Synthesis, modification and optimization of titanate nanotubes-polyamide thin film nanocomposite (TFN) membrane for forward osmosis (FO) application, Chem. Eng. J. 281 (2015) 243–251, https://doi.org/10.1016/j.cej.2015.06.035.
[49] C.Y. Tang, Y.-N. Kwon, J.O. Leckie, Effect of membrane chemistry and coating layer on physiochemical properties of thin film composite polyamide RO and NF membranes: II. Membrane physiochemical properties and their dependence on polyamide and coating layers, Desalination 242 (2009) 168–182, https://doi.org/10.1016/j.desal.2008.04.004.
[50] H.M. Park, K.Y. Jee, Y.T. Lee, Preparation and characterization of a thin-film composite reverse osmosis membrane using a polysulfone membrane including metal-organic frameworks, J. Membr. Sci. 541 (2017) 510–518, https://doi.org/10.1016/j.memsci.2017.07.034.
[51] D.L. Zhao, W.S. Yeung, Q. Zhao, T.-S. Chung, Thin-film nanocomposite membranes incorporated with UiO-66-NH_2 nanoparticles for brackish water and seawater desalination, J. Membr. Sci. 604 (2020), https://doi.org/10.1016/j.memsci.2020.118039, 118039.
[52] R.W. Baker, Membrane Technology and Applications, John Wiley & Sons, Incorporated, New York, UNITED KINGDOM, 2012.
[53] M. Safarpour, A. Khataee, V. Vatanpour, Thin film nanocomposite reverse osmosis membrane modified by reduced graphene oxide/TiO_2 with improved desalination performance, J. Membr. Sci. 489 (2015) 43–54, https://doi.org/10.1016/j.memsci.2015.04.010.
[54] G.N.B. Baroña, J. Lim, M. Choi, B. Jung, Interfacial polymerization of polyamide-aluminosilicate SWNT nanocomposite membranes for reverse osmosis, Desalination 325 (2013) 138–147, https://doi.org/10.1016/j.desal.2013.06.026.
[55] V.T. Do, C.Y. Tang, M. Reinhard, J.O. Leckie, Effects of chlorine exposure conditions on physiochemical properties and performance of a polyamide membrane—mechanisms and implications, Environ. Sci. Technol. 46 (2012) 13184–13192, https://doi.org/10.1021/es302867f.
[56] M. Stolov, V. Freger, Degradation of polyamide membranes exposed to chlorine: an impedance spectroscopy study, Environ. Sci. Technol. 53 (2019) 2618–2625, https://doi.org/10.1021/acs.est.8b04790.
[57] C. Xu, W. Chen, H. Gao, X. Xie, Y. Chen, Cellulose nanocrystal/silver (CNC/Ag) thin-film nanocomposite nanofiltration membranes with multifunctional properties, Environ. Sci. Nano. 7 (2020) 803–816, https://doi.org/10.1039/C9EN01367A.
[58] S. Romero-Vargas Castrillón, X. Lu, D.L. Shaffer, M. Elimelech, Amine enrichment and poly(ethylene glycol) (PEG) surface modification of thin-film composite forward osmosis membranes for organic fouling control, J. Membr. Sci. 450 (2014) 331–339, https://doi.org/10.1016/j.memsci.2013.09.028.
[59] A.A. Aziz, K.C. Wong, P.S. Goh, A.F. Ismail, I.W. Azelee, Tailoring the surface properties of carbon nitride incorporated thin film nanocomposite membrane for forward osmosis desalination, J. Water Process Eng. 33 (2020), https://doi.org/10.1016/j.jwpe.2019.101005, 101005.
[60] X. Bao, Q. Wu, W. Shi, W. Wang, H. Yu, Z. Zhu, X. Zhang, Z. Zhang, R. Zhang, F. Cui, Polyamidoamine dendrimer grafted forward osmosis membrane with superior ammonia selectivity and robust antifouling capacity for domestic wastewater concentration, Water Res. 153 (2019) 1–10, https://doi.org/10.1016/j.watres.2018.12.067.
[61] J. Meng, Z. Cao, L. Ni, Y. Zhang, X. Wang, X. Zhang, E. Liu, A novel salt-responsive TFC RO membrane having superior antifouling and easy-cleaning properties, J. Membr. Sci. 461 (2014) 123–129, https://doi.org/10.1016/j.memsci.2014.03.017.
[62] A.C. Sagle, E.M. Van Wagner, H. Ju, B.D. McCloskey, B.D. Freeman, M.M. Sharma, PEG-coated reverse osmosis membranes: desalination properties and fouling resistance, J. Membr. Sci. 340 (2009) 92–108, https://doi.org/10.1016/j.memsci.2009.05.013.
[63] E. Valamohammadi, F. Behdarvand, M.A. Tofighy, T. Mohammadi, Preparation of positively charged thin-film nanocomposite membranes based on the reaction between hydrolyzed polyacrylonitrile containing carbon nanomaterials and HPEI for water treatment application, Separ. Purif. Technol. 242 (2020), https://doi.org/10.1016/j.seppur.2020.116826, 116826.
[64] M. Ghanbari, D. Emadzadeh, W.J. Lau, T. Matsuura, M. Davoody, A.F. Ismail, Super hydrophilic TiO_2/HNT nanocomposites as a new approach for fabrication of high performance thin film nanocomposite membranes for FO application, Desalination 371 (2015) 104–114, https://doi.org/10.1016/j.desal.2015.06.007.
[65] Y. Mansourpanah, Z. Jafari, Efficacy of different generations and concentrations of PAMAM–NH_2 on the performance and structure of TFC membranes, React. Funct. Polym. 93 (2015) 178–189, https://doi.org/10.1016/j.reactfunctpolym.2015.04.010.
[66] Y. Hu, K. Lu, F. Yan, Y. Shi, P. Yu, S. Yu, S. Li, C. Gao, Enhancing the performance of aromatic polyamide reverse osmosis membrane by surface modification via covalent attachment of polyvinyl alcohol (PVA), J. Membr. Sci. 501 (2016) 209–219, https://doi.org/10.1016/j.memsci.2015.12.003.
[67] H.-R. Chae, J. Lee, C.-H. Lee, I.-C. Kim, P.-K. Park, Graphene oxide-embedded thin-film composite reverse osmosis membrane with high flux, anti-biofouling, and chlorine resistance, J. Membr. Sci. 483 (2015) 128–135, https://doi.org/10.1016/j.memsci.2015.02.045.
[68] J. Xu, Z. Wang, L. Yu, J. Wang, S. Wang, A novel reverse osmosis membrane with regenerable anti-biofouling and chlorine resistant properties, J. Membr. Sci. 435 (2013) 80–91, https://doi.org/10.1016/j.memsci.2013.02.010.
[69] J. Glater, S. Hong, M. Elimelech, The search for a chlorine-resistant reverse osmosis membrane, Desalination 95 (1994) 325–345, https://doi.org/10.1016/0011-9164(94)00068-9.
[70] M.J. Cran, S.W. Bigger, S.R. Gray, Degradation of polyamide reverse osmosis membranes in the presence of chloramine, Desalination 283 (2011) 58–63, https://doi.org/10.1016/j.desal.2011.04.050.
[71] N.P. Soice, A.C. Maladono, D.Y. Takigawa, A.D. Norman, W.B. Krantz, A. R. Greenberg, Oxidative degradation of polyamide reverse osmosis membranes: studies of molecular model compounds and selected membranes, J. Appl. Polym. Sci. 90 (2003) 1173–1184, https://doi.org/10.1002/app.12774.
[72] S. Yu, M. Liu, Z. Lü, Y. Zhou, C. Gao, Aromatic-cycloaliphatic polyamide thin-film composite membrane with improved chlorine resistance prepared from m-phenylenediamine-4-methyl and cyclohexane-1,3,5-tricarbonyl chloride, J. Membr. Sci. 344 (2009) 155–164, https://doi.org/10.1016/j.memsci.2009.07.046.
[73] X. Zhai, J. Meng, R. Li, L. Ni, Y. Zhang, Hypochlorite treatment on thin film composite RO membrane to improve boron removal performance, Desalination 274 (2011) 136–143, https://doi.org/10.1016/j.desal.2011.02.001.
[74] R. Verbeke, S. Eyley, A. Szymczyk, W. Thielemans, I.F.J. Vankelecom, Controlled chlorination of polyamide reverse osmosis membranes at real scale for enhanced desalination performance, J. Membr. Sci. 611 (2020), https://doi.org/10.1016/j.memsci.2020.118400, 118400.
[75] G.-D. Kang, C.-J. Gao, W.-D. Chen, X.-M. Jie, Y.-M. Cao, Q. Yuan, Study on hypochlorite degradation of aromatic polyamide reverse osmosis membrane, J. Membr. Sci. 300 (2007) 165–171, https://doi.org/10.1016/j.memsci.2007.05.025.